POLITECNICO DI MILANO

Research Doctorate Course in Bioengineering

XXV Cycle

Final dissertation

A bioengineering approach aimed at understanding the role of hemodynamic forces acting on human saphenous vein after coronary artery by-pass grafting

Marco PIOLA

Advisors
prof. Monica Soncini
prof. Gianfranco B. Fiore

Coordinator of the Research Doctorate Course
prof. Maria Gabriella Signorini

Tutor
prof. Alberto Redaelli

4 November 2013

Table of contents

Introduction

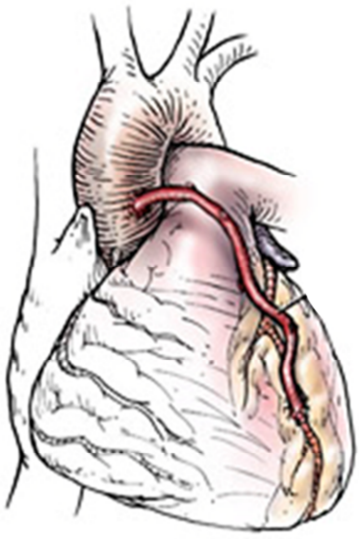

Adapted from (Rueda et al 2008)

Saphenous vein (SV) graft disease represents an unresolved problem in coronary artery bypass grafting (CABG). After CABG, a progressive remodeling of the SV wall occurs, possibly leading to the lumen occlusion. This process is termed intima hyperplasia (IH). The investigation of cellular and molecular aspects of IH progression is a primary endpoint toward the generation of occlusion-free vessels that may be used as 'life-long' grafts. While animal transplantation and *in vitro* models have clarified some of the remodeling factors, the human SV pathology is far from being completely understood.

In this scenario, the aim of the present doctoral project was to explore new tools and procedures to investigate *ex vivo* the effects of altered mechanical load experienced by the human SV after CABG surgery. The issue of the *ex vivo* mimicry of the pathologic arterialization mechanism, involved in SV graft disease, was addressed by a multidisciplinary approach. Advanced bioengineering/biotechnology modelling and prototyping tools, complying with biological methods and tissue engineering/regenerative medicine requirements, were applied. Furthermore, the application of principles and methods of life-science engineering were used for providing a reliable model system, facilitating the understanding of pathogenesis of vein graft IH. Particular focus was given to the control over the environmental conditions for tightly reproducing the essential stimuli involved in the pathological SV remodelling. The integration of these methodologies led to devising a novel laboratory-oriented culture platform, that was used for conducting extensive arterialization conditioning campaigns with human SVs, under strictly controlled hemodynamic conditions.

This doctoral project is part of a wider research, involving a biological laboratory partner, aimed at discovering molecular effectors involved in vein graft disease to be targeted by pharmacologic/gene expression interfering strategies, in view of a next generation treatments and protocols to be tested in preclinical and clinical models.

This interdisciplinary project was prominently experimental, supported by computer aided design and numerical modelling. The designing and prototyping of the *ex vivo* platforms were performed at the Laboratory of Experimental Micro and Biofluid-dynamics (*μBS Lab*) of the Dipartimento di Elettronica, Informazione e Bioingegneria of the Politecnico di Milano. The preliminary biological validation with human samples and the arterialization conditioning were performed at and in strict collaboration with the

Laboratory of Cardiovascular Tissue Engineering of the Centro Cardiologico Monzino in Milan.

Rationale of the doctoral project

CABG using autologous vessels is a standard surgical procedure to recover myocardial perfusion in patients with coronary artery disease (de Waard *et al.*, 2006; Parang and Arora 2009; Wallitt *et al.*, 2007). The two most represented coronary-compatible autologous vessels to be used in CABG are the inner mammary artery (IMA) and the saphenous vein (SV). Soon after introduction of CABG, it became evident that transplanted vessels undergo a series of structural modifications, leading, within few years, to a significant reduction of vessel patency. In a number of cases, this requires re-hospitalization with stent implantation in the grafts and, ultimately, re-intervention. Compared with artery-made bypasses, SV grafts show lower long-term patency; in fact, approximately 15-30% of vein grafts fail during the first year and more than 50% patients require re-intervention within 10 years after implantation (Goldman *et al.*, 2004; Tsui and Dashwood 2002), with high economic burden and consequences for the quality of the life of the patient. However, in most clinical cases, the use of a SV graft is unavoidable, since most patients need multiple bypass grafting procedures. In fact, the SV, due to its length and its superficial anatomical position, represents a preferred natural bypass conduit (Dashwood and Loesch 2009; Muto *et al.*, 2010; Severyn *et al.*, 2004; Surowiec *et al.*, 2000).

After CABG surgery, progressive structural modifications of the SV wall, due to IH, lead to the occlusion of the graft lumen (the so called vein graft disease, VGD). The beginning of the pathology occurs at much earlier stages after grafting (one week), with the activation of biomechanical- and inflammatory-driven cascades which prime vessel remodeling (Mitra *et al.*, 2006; Muto *et al.*, 2010). As a first factor, the surgical procedures used during SV grafts preparation cause major insults to the integrity of the vessel endothelium and adventitia. These insults promote inflammatory responses related to a direct exposure of the intima layer to pulsatile blood flow and to a significant decrease in Nitric Oxide (NO) synthesis, with consequence for enhanced vasospasm and lower atheroprotection. The evolution of surgical techniques to harvest SV segments to be used for CABG surgery, has led to the devise of “no-touch” techniques, which preserve the

structure of the endothelium and the adventitia with slower progression of intima IH and enhanced vessel patency (Ahmed *et al.,* 2004; Dashwood *et al.,* 2005; Rueda *et al.,* 2008; Souza *et al.,* 2006). However, while the use of these surgical strategies lead to the maximization of vessel integrity prior to vein implantation into arterial position, an un-avoidable mechanical stimulation due to changes in pressure load and flow, appears to have prime role in VGD (Berceli *et al.,* 2009; Hwang *et al.,* 2011; John 2009; Tran-Son-Tay *et al.,* 2008). In fact, immediately after grafting, SV segments are exposed to a variety of hemodynamic stimuli (vascular wall strain and stress and lumen shear stress activation) activating several cellular pathways and responses in the venous vessel wall. The new hemodynamic conditions experienced by the vein after transposition into the coronary circulation are similar to those experienced by coronary arteries. In particular, in the coronary artery circulation, the blood flow is characterized by a high pulsatile pressure, oscillating between 80 and 120 mmHg, and a pulsatile flow (with mean flow rate of 250 ml/min), which results in an elevated shear stress (1 - 7 Pa) (Bouten *et al.,* 2011; Dummler *et al.,* 2011). Such forces have antagonistic effects on disease progression: elevated shear stresses may have an atheroprotective role due to hemodynamic-related increase of NO release by endothelial cells (EC) while a non-physiologic mechanical loading of the vein wall may have a pro-pathologic effect due to mechanical ruptures in the endothelial layer and abnormal wall strain/stress of smooth muscle cells (SMCs) sheets (John 2009).

The major cause of SV graft failure is an over-proliferation of SMCs into the vessel intima layer leading to IH after few months (Lemson *et al.,* 2000; Motwani and Topol 1998; Muto *et al.,* 2010). SMCs proliferation begins quite shortly after CABG surgery, and precedes the later development of graft atherosclerosis that concurs to further reduce vessel patency at later times (Parang and Arora 2009; Wallitt *et al.,* 2007). *In vitro* and *in vivo* (animal models) investigations have established that uncontrolled SMCs proliferation/IH phenomena is induced by inflammatory response, vein de-endothelialization and modified wall stress/strain (Wallitt *et al.,* 2007). In these conditions, SMCs respond with apoptosis (Morrow *et al.,* 2005), modified proliferation, as well as enhanced/reduced migratory activity (Qi *et al.,* 2010). In addition, after vein implantation into arterial position, SMCs loose their typical contractile phenotype and start to proliferate and to invade the intima layer, thus reducing the vascular lumen. Furthermore, various animal models have been devised to address the pathologic evolution of the arterialized veins. These studies have

highlighted the relevance of different cell types and signal transduction pathways involved in the initiation of the phenomena leading to IH (Hoglund *et al.,* 2010; Torsney *et al.,* 2005). The parallel evolution of preclinical models mimicking human vein arterialization in mice and rabbits such as vena cava or jugular veins into carotid interposition (Hu and Xu 2002; Jiang *et al.,* 2004), have allowed investigating the role of intrinsic and extrinsic cellular compartments and altered hemodynamics in intima thickening associated to vein arterialization. However, the establishment of IH in human arterialized veins is still far from being completely understood.

The use of bioengineering approaches is an option to study VGD. Several organ culture system were designed to recapitulate arterialization in cultured human veins for studying the physiopathology of VGD consequent to SV exposure to coronary artery-mimicking flow and pressure. As recently discussed, various devices, tailored to perform *ex-vivo* culture of human SVs for a period of time spanning from 4 to 14 days and under dynamic conditions, have been developed (Piola *et al.,* 2012). The platforms that have been devised to this aim appeared insufficiently refined to maintain a tight control of vessels biological conditions for global molecular profiling (Piola *et al.,* 2012). In particular, the design philosophy of the state-of-the art devices did not allow the simultaneous replication of all the main biophysical conditions acting *in vivo* during human vein arterialization. These lacks preclude the obtainment of reliable information on the activation of bio-mechanically stimulated molecular pathways or the possible interaction of vein-resident cells with circulating cells.

Novel *ex vivo* models are necessary in order to: *i)* tightly replicate the altered hemodynamic conditions, especially the raise in wall strain and shear stress, *ii)* obtain *ex vivo* arterialized SV segments for investigating the mechano-biological basis of the early events leading to IH at global molecular level, and *iii)* in perspective, attempt therapeutic strategies by pharmacological conditioning of the dynamically cultured vein segments.

The strategy adopted in the present doctoral project consists of devising and biologically testing a novel *ex vivo* model of human vein arterialization, applying bio-and tissue-engineering methods. The resulting *ex vivo* platform tried to overcome some of the limitations of the state-of-the-art models, focusing onto the control of the hemodynamic and biochemical microenvironments. In our view, this is crucial to obtain a global comprehension of VGD progression, and in perspective to perform comparative studies of

drug administration or gene expression modulation (*gene therapy, siRNA and antagomir approaches*), to devise preconditioning protocols and/or regenerative medicine strategies that reduce the clinical impact of VGD pathology.

Outline of the thesis

The dissertation is structured into 4 main chapters, that describes the various steps of the process that lead to manufacture of a novel EVCS for the *in vitro* mimicking of the hemodynamic forces acting on human saphenous vein after CABG surgery.

In Chapter 1, the current strategies, applied for studying the physiopathology of VGD consequent to SV exposure to coronary artery-compliant flow and pressure, are presented. The chapter is based on a published article where the state of the art of the *ex vivo* arterialization models, and also the products and the related patents, is revised. The published article is: M. Piola, M. Soncini, F. Prandi, G. Polvani, G.B. Fiore, M. Pesce. *Tools and Procedures for Ex Vivo Vein Arterialization, Preconditioning and Tissue Engineering: A Step Forward to Translation to Combat the Consequences of Vascular Graft Remodeling* on Recent Patents On Cardiovascular Drug Discovery, 2012, 7 (3): 186-195.

In Chapter 2, the design of a novel *ex vivo* vein culture system (EVCS), aimed at replicating *ex-vivo* arterialization conditions experienced by SV after CABG for studying the biological mechanisms activated by SV exposure to arterial-like conditions, is presented. This version of the EVCS is conceived as pressure-driven vessel straining system for studying the early remodeling events caused by pure pulsatile arterial-like pressure. These activities were mainly carried out at the Laboratory of Experimental Micro and Biofluid Dynamics of the Dipartimento di Elettronica, Informazione e Bioingegneria of the Politecnico di Milano; preliminary functional testing of the designed device was also carried out at the Laboratory of Cardiovascular Tissue Engineering of the Centro Cardiologico Monzino. The chapter is partially based on a manuscript: “M. Piola, F. Prandi, N. Bono, M. Soncini, E. Penza, M. Agrifoglio, G. Polvani, M. Pesce, and G. B. Fiore. *A compact and automated ex-vivo vessel culture system for the pulsatile pressure conditioning of human saphenous veins*. Journal of Tissue Engineering and Regenerative Medicine, [*Epub ahead of print*] doi:10.1002/term.1798”.

In Chapter 3, the effects induced by different dynamic conditions on the human SV early events associated to vascular remodeling are presented. These activities were carried out at the Laboratory of Cardiovascular Tissue Engineering of the Centro Cardiologico Monzino. The chapter is partially based on a technical manuscript: "M. Piola, F. Prandi, N. Bono, M. Soncini, E. Penza, M. Agrifoglio, G. Polvani, M. Pesce, and G. B. Fiore. *A compact and automated ex-vivo vessel culture system for the pulsatile pressure conditioning of human saphenous veins*. Journal of Tissue Engineering and Regenerative Medicine, [*Epub ahead of print*] doi:10.1002/term.1798".

In Chapter 4, the evolution of the bioreactor configuration from a simple pressure-driven vessel straining system to an *ex vivo* SV preconditioning system in the presence (or not) of controlled chemical conditions *(i.e., hypoxia*), arterial-like pressure, and flow patterns, is proposed. The bioreactor was upgraded to better replicate the full biomechanical stimuli involved in CABG arterialization, *i.e.* pulsatile wall stretch and wall shear stresses applied synchronously and with the correct phasing.

Finally in the Conclusive remarks chapter, a discussion of the overall results obtained during the development of the doctoral project is presented.

1

Tools and procedures for ex vivo vein arterialization, preconditioning and tissue engineering

This chapter is based on: M. Piola, M. Soncini, F. Prandi, G. Polvani, G.B. Fiore, M. Pesce. *Tools and Procedures for Ex Vivo Vein Arterialization, Preconditioning and Tissue Engineering: A Step Forward to Translation to Combat the Consequences of Vascular Graft Remodeling*. Recent Patents On Cardiovascular Drug Discovery, 2012, 7 (3): 186-195.

Introduction

Coronary artery bypass grafting (CABG) has been introduced in vascular surgery more than 50 years ago to combat the consequences of myocardial ischemia (Owens 2010; Parang and Arora 2009; Wallitt *et al.,* 2007). Although the use of modern tissue engineering (TE) techniques has demonstrated the feasibility of *ex vivo* vessels fabrication (L'Heureux *et al.*, 2006), the use of autologous vessels from the patients themselves is, still today, the unique option accessible to surgeons. The two most represented coronary-compatible autologous vessels to be used in CABG are the inner mammary artery (IMA) and the saphenous vein (SV). Soon after introduction of CABG, it became evident that the transplanted vessels are liable to undergo a series of structural modifications, leading to significant patency reduction, with the need for patient re-hospitalization, stent implantation or, ultimately, re-intervention (Parang and Arora 2009; Wallitt *et al.*, 2007). The clinical impact of graft disease is different, depending on the origin of the vessels employed. It is estimated mammary artery grafts maintain an 85% patency after a 10-years while patency of SV grafts drops to 50%-60%, at a comparable time.

Basic investigations have clarified the potential contribution of vascular-resident or recruited cells (e.g., smooth muscle cells and monocytes), or of intracellular signaling activation pathways in the establishment of vein graft disease (VGD). On the other hand, a "system" level understanding of the disease progression as a whole is still unavailable. In fact, it is unclear which is the role of biomechanics on the response of vessel-resident cells, and whether changes in the global gene expression and (epi)genetic circuitries occur as a result of modified flow conditions.

In this context, the use of bioengineering approaches to reproduce arterialization in cultured human veins is likely to provide valuable tools for studying the physiopathology of VGD consequent to SV exposure to coronary artery-compliant flow and pressure. This may also help to dissect the contribution of different cellular populations in the progression of intima hyperplasia in the graft, and assess vessel responses to novel *ex vivo* pharmacological treatments. Finally, the conception of vessel perfusion systems may concur to establish tissue engineering (TE) protocols to obtain artificial vessels (Niklason *et al.,* 1999; Seliktar *et al.,* 2003) which may be prospectively used as a novel and standardized resource for CABG.

The first section of the present chapter provides an overview of the vessel perfusion systems designed and patented to study the vein arterialization process, while the second part discusses some of the bioreactor-based strategies (and the relative patented technologies) that have been devised to produce fully engineered vessels.

1.1 Vessel perfusion systems

SV segments used for CABG undergo mechanical damages and flow/pressure loads, which are believed to activate pathways causing intima hyperplasia (IH). A crucial component contributing to VGD is the change in the pressure load and cyclic strain consequent to arterialization. In fact, in normal conditions SVs are subjected to quasi-steady flow patterns and are exposed to very low shear stresses (0.1-0.6 Pa) [7] and pressure loads (5-10 mmHg) [7]. By contrast, after CABG, SV segments are subjected to fast pulsatile flow, which is supposed to cause adaptive remodeling in the SV wall, leading to progressive bypass occlusion. The new hemodynamic stimuli are similar to those experienced by coronary arteries; namely, a mean flow rate up to 250 ml/min, a high wall shear stress in the range of 0.75-2.25 Pa [8], a systolic/diastolic pressure of approximately 120/80 mmHg with a circumferential strain of 10-15% [8].

Several attempts have been made at mimicking these conditions and characterize molecular pathways implicated in SVs arterialization. To achieve this goal, *ex-vivo* vessel perfusion culture systems (EVPCS) have been developed, where the survival of animal- or human-derived vessel segments is ensured by immersion into culture media, and vessel mechanical stimulation is performed by an appropriate arterial-like circulation inside the vessel lumen. This approach has been inspired by the pioneer investigation of Lindberg and Carrel (Carrel and Lindbergh 1935), proposing, for the first time, the use of *ex vivo* perfusion systems for studying the function of isolated organs outside the body.

In this context, despite only one EVPCS has been patented (Clerin *et al.*, 2010) (Table 1.1), several studies have been conducted using various devices able to expose intact vessels to steady flow perfusion.

Patent Number	Publication Date	Author	Title	Brief description	Novel aspects
US20100331964A1	30/12/2010	Clerin et al. (Clerin *et al.*, 2010)	*Ex-vivo* remodeling of excised blood vessel for vascular grafts	*Ex vivo* method and System where excised small diameter blood vessels can be harvested and cultured to provide viable vascular grafts	A modeled excised small vessel, having increased diameter, length, and wall thickness produced by physically remodeling a small blood vessel

***Table 1.1**. A relevant patent involving the use of a bioengineering approach to study vein adaptation to arterial- like conditions: a brief description and the novel aspects of the patent content are provided.*

In the attempt at studying the biology of vein arterialization, flow perfusion systems were initially designed to assess basic survival and perform pharmacological treatment of SV segments *ex vivo*. These systems allowed culturing SV segments for different periods of time; however, they had the limitation of not including a pressure control, which is crucial to mimic the pulsatile arterial-like flow, recognized as one of the primary cause of vessel patency reduction. Therefore, these systems were only able to elicit biological responses associated to vessel perfusion with constant flows, and, paradoxically, demonstrated the role of laminar shear stress on IH inhibition (Porter *et al.*, 1996; Rey *et al.*, 2004). In a first example, 0.5 cm-length longitudinal-sliced segments of human SV were pinned to the inside of a silicone tube and perfused for 14 days with venous (a flow rate of 70 ml/min resulting in a low shear stress of 0.1 Pa, and a pressure of 15 mmHg) and arterial (a flow rate of 500 ml/min resulting in an high shear stress of 0.9 Pa, and a pressure of 85 mmHg) flow patterns (Porter *et al.*, 1996). The result of this study was that high-pressure constant flow inhibits IH, likely as a consequence of high shear stress. In another study by Surowiec and colleagues (Surowiec *et al.*, 2000) a vascular perfusion culture system enabling culture of intact vessels for a period up to 96 hours was developed. This bioreactor was designed with a tightly-controlled perfusion rate in order to expose SV segments to 100 ml/min flow with a 40 mmHg intraluminal pressure and assess the effect of pharmacologic stimulation on vascular contractility. Using a similar system, Rey and colleagues (Rey *et al.*, 2004) extended the observation time to 14 days and concluded that *ex vivo* conditioning with a constant flow (resulting in low shear stresses in the range of 0.2-0.6 Pa) inhibits the formation of neointima, through a generalized cytostatic effect on all the cells of the vein.

A significant advancement toward the development of EVPCSs as tools to mimic SV arterialization has been the inclusion of controllers able to elevate the SV intraluminal pressure. A first example of this novel approach was reported by Miyakawa and colleagues, who developed a flow perfusion system tailored to culture human SV under venous (flow rate of 5 ml/min) or arterial conditions (flow rate of 50 ml/min and constant pressure of 80 mmHg) up to 4 days (Miyakawa *et al.,* 2008). In this bioreactor, the effect of pressure on the IH was evident: enhanced apoptosis and vascular remodeling were observed, closely resembling early events of vein arterialization observed in animal models. In another report, Gusic and co-workers (Gusic *et al.,* 2005a; Gusic *et al.,* 2005b) were able to discriminate between the effects induced by flow shear stress and those elicited by mechanical wall stress, using different pressure and flow-patterns. Finally, *ex-vivo* stimulation of porcine SVs was performed by adapting a previously developed system patented by Clerin et al. ((Clerin *et al.,* 2010; Clerin *et al.,* 2002; Clerin *et al.,* 2003), Tab. 1), to comply with vessel stimulation with different flow rates (5-85 ml/min), shear stress (0.26-5.6 Pa) and pressure (25-90 mmHg) amounts. Interestingly, in these reports SVs were perfused with culture medium added with Dextran in order to mimic blood viscosity (~4 cP). The main result of these studies showed that increases in laminar shear stress neutralized intimal thickening, while ramped perfusion pressures induced IH in a dose-dependent manner.

The latest development in EVPCS design to mimic arterialization conditions has been the inclusion of perfusion systems, allowing the stimulation of vessel segments with sine-like pressure patterns at defined frequencies. In a first example, Saucy and colleagues (Saucy *et al.,* 2010) investigated the impact of high flow pulsatile perfusion (resulting in high shear stresses in the range of 0.9-1.5 Pa) obtained by applying a flow rate of 120±15 ml/min, a pulse rate of 60 pulse/min, and a systolic/diastolic pressure of 80±10/40±10 mmHg on human SV segments for 14 days. By this, the authors were able to establish an important correlation between the expression level of urokinase and tissue-type plasminogen activators and the applied mechanical stress, thus linking expression of extracellular matrix remodeling enzymes and a biomechanical stimulus. In a second example, Voisard and colleagues developed a pulsatile system able to stimulate up to 5 SV segments in parallel and generate arterial-like conditions (a mean flow perfusion of 5000 ml/min, a pulsatile flow with a rate of 80 bpm and a systolic/diastolic pressure of 130/80

mmHg) (Voisard *et al.*, 2010). Using this system, the Authors observed elevation of cellular proliferation in the vein wall as early as at 4 days after the beginning of mechanical conditioning. The most advanced perfusion system devised so far was, finally, the platform devised by Dummler and colleagues (Dummler *et al.*, 2011). These Authors developed an EVPCS to perform pulsatile *ex-vivo* stimulation of SVs under venous (a flow rate of 5 ml/min and a pressure of 10 mmHg) or arterial (a flow rate of 50 ml/min and a pressure of 100 mmHg) conditions. The biological results obtained using this device showed a relatively rapid occurrence of morphological changes in the vein structure, especially in the media and in the intima layers. These morphological changes were also associated with an increase in the expression of matrix metalloprotease-2 (MMP-2).

Despite a variety of systems able to expose vein segments to arterial-like flow patterns have been devised and reported in the literature, the lack of a systematic approach at investigating the global molecular changes associated to vessel arterialization still precludes a complete understanding of the arterialization process as a *pro*-pathological condition in CABG. In this framework, it might be relevant to design new bioreactor-based platforms with vessel stimulation circuits containing minimized volumes, to allow the outer and the inner vein layers to be exposed to controlled amounts of small molecules and drugs while in motion. In this way, for example, the effect of novel therapeutic agents such as small molecules, gene-transferring vectors, small interfering RNAs (siRNAs) or even antagomirs (McDonald *et al.*, 2012; Wiedemann *et al.*, 2012) might be studied for their beneficial effects on IH inhibition directly in human samples, to be compared to those achieved in normally used animal-based methods (Thomas 2012). Another advantage of perfusion systems miniaturization might be the option to add in the inner and/or the outer stimulation circuits living cells (e.g. endothelial progenitor cells and monocytes), which are known to dynamically interact with the inner vein wall at early stages of vein arterialization, and assess their contribution to the IH prevention/progression. This may also open the way to novel tissue engineering approaches using circulating EPCs to perform grafts “pre-endothelialization” (Griese *et al.*, 2003), or to test novel treatments aimed at minimizing homing of cells directly involved in graft inflammatory reaction and neointima accumulation.

1.2 Bioreactor-based approaches for vascular tissue engineering

One of the major goals in tissue engineering is the derivation of artificial tissues and organs to be used as replacements of conventionally implanted prostheses. Paradigmatic is, for example, the development of decellularization protocols of entire organs such as the heart, the lung, the windpipe, and the liver (Bader and Macchiarini 2010; Jungebluth *et al.,* 2012; Ott *et al.,* 2010; Ott *et al.,* 2008; Uygun *et al.,* 2010), followed by cellular reseeding. Given the elevated demand of CABG implantations worldwide, the engineering of vascular substitutes of IMA and SV with higher compatibility and lower patency reduction is therefore actively pursued.

In order to replace natural coronary arteries, artificial vessels for CABG require to be designed with vessel-like structure, physiology and mechanical resistance. To obtain this, an optimal combination of vascular cells (namely endothelial cells, interstitial cells and smooth muscle cells), biomaterials and mechanical stimulation must be found (Barron *et al.,* 2003; Dermenoudis and Missirlis 2010; Martin *et al.,* 2004). Thus, as in the case of the *ex vivo* organ culture systems used for mimicking vein arterializations (see before), bioreactors used to generate tissue-engineered blood vessels (TEBV) consist of components necessary to actuate a mechanical control of the growing vessels. These are: *i*) housing tools, hosting the vessel substitute, *ii*) sterile culture chambers and fluidic circuits for media recirculation, and *iii*) active systems able to stimulate the vessel substitute. In order to generate artificial vessels to be clinically used, these systems must comply with the good manufacturing practice (GMP) requirements. Therefore, they have to be customized to perform scaffold cell seeding, growth and release of artificial vessels with simple and traceable procedures (Arrigoni *et al.,* 2008; Banes *et al.,* 2009; Dunkelman *et al.,* 1998; Elizondo *et al.,* 1999; Seifalian *et al.,* 2002; Villalona *et al.,* 2010). In addition to GMP compliance, TEBV properties must finally comply with the ANSI/AAMI/ISO 7198:1998/2001 standards for tubular vascular prostheses. These regulations establish that mechanical properties, volume compliance, suture retention strength, viscoelasticity and burst pressure must be comparable to those of native vessels such as saphenous vein and internal mammary artery (IMA); e.g. a mean value of suture retention strength around 138 grams (IMA) and mean burst pressures of 1600 mmHg (Konig *et al.,* 2009; L'Heureux *et al.,* 1998) and 3000 mmHg (Konig *et al.,* 2009) (SV and IMA, respectively). The bio-artificial prostheses should elicit neither inflammatory nor immunogenic responses and

should not undergo uncontrolled remodeling after implantation (Campbell and Campbell 2007; Nerem 2000; Sarkar *et al.*, 2007; Thomas 2003).

1.2.1 Vascular tissue engineering using cell seeding techniques

1.2.1.1 Cell seeding into bio-artificial polymer scaffolds

The first attempt at generating *native-like* blood vessels using a simple bioreactor-assisted TE approach and a combination of endothelial cells (ECs), smooth muscle cells (SMCs), and fibroblasts (FBs) was reported in the pioneer investigation of Weinberg and Bell in 1986 (Weinberg and Bell 1986). In this study, based on a previously patented system by Bell (Bell 1985) (Table 1.2), a method for producing living blood vessels by exploiting a cell-seeded collagen gel was described for the first time. In this report, the fabrication of a multilayered blood vessel equivalent was obtained by sequential seeding different cells types into bio-artificial scaffolds. A SMC layer was first generated culturing SMCs into a collagen gel around a cylindrical mandrel. FBs were then added by adding a FB-containing cell suspension around the outer SMCs layer up to 7 days. Finally, ECs were let home to the inner layer, by perfusion-assisted seeding through the artificial vessel lumen. The final structure consisted of a vessel-like structure with ECs lining the lumen, surrounded by SMCs and FBs layers. When assessed for mechanical compliance, these bio-artificial vessels were unable to withstand physiological arterial pressures. In fact they had a burst pressure of 10 mmHg. To ameliorate the mechanical resistance of the engineered vessel, a Dacron® mesh was then used providing a final burst pressure up to 70 mmHg.

A similar method was used by McAllister and L'Heureux. These Authors attempted to produce vascular grafts using a sheet-based cell-self-assembly technique (Auger *et al.*, 1997; L'Heureux *et al.*, 2006; L'Heureux *et al.*, 1993; L'Heureux *et al.*, 1998). The same authors patented an automatic method involving the use of a rotating mandrel for the fabrication of multilayered TEBVs (McAllister and l'Heureux 2002) (Table 1.2). The resulting artificial vessels showed a structure resembling that of native arteries and a burst pressure of 2000 mmHg; however, they were not compliant as native vessels. A similar method was finally patented by Tranquillo (Tranquillo *et al.*, 2007) (Table 1.2) for creating TEBVs including an intimal layer surrounded by a SMCs media layer constructed around a

tubular support. Table 1.2 resumes the patents involving the use of bioreactor-based approaches for vascular TE using sheets-based techniques.

Patent Number	Publication Date	Author	Title	Brief description	Novel aspects
US4546500	15/10/1985	Bell (Bell 1985)	Fabrication of living blood vessels and glandular tissues	Apparatus for producing a vessel equivalent prosthesis	First method of producing *in vitro* a living multilayered tubular structure
US5618718	08/04/1997	Auger et al. (Auger *et al.*, 1997)	Production of a contractile smooth muscle	*In vitro* production of three-dimensional construct starting from smooth muscle cells	Fully biological and autologous human TEBV using SMCs
US20020188349A1	12/12/2002	McAllister et al. (McAllister and l'Heureux 2002)	Tissue engineered blood vessels and apparatus for their manufacture	Bioreactor with an enclosed chamber, a sheet growth module, a rotating mandrel for the manufacture of TEBV whit burst strength withstanding physiological blood pressure	Improvement and automation of TEBV fabrication process using autologous FBs and ECs
US20070128171	07/06/2007	Tranquillo (Tranquillo *et al.*, 2007)	Engineered blood vessel	Methods for the fabrication of engineered blood vessels using matrices comprising ECs and SMCs.	Formation of tubular vascular constructs by means of fibrin gel circumferentially positioned around a porous mandrel

Table 1.2*. List of relevant patents involving the use of bioreactor-based approaches for vascular tissue engineering using sheets-based techniques: a brief description and the novel aspects of the patent content are provided.*

1.3.1.2 Cell seeding into synthetic polymer scaffolds

Several biomaterials have been used for supporting and guiding cells during vascular tissue formation. Among the synthetic polymers applied in vascular engineering (Bouten *et al.*, 2011; Gong and Niklason 2006; Naito *et al.*, 2011), the most widely used are biodegradable polymers, such as polycaprolactone (PCL), polylactic acid (PLA), polyglycolic acid (PGA), and their copolymer polylactic-co-glicolic acid (PLGA) (Hoerstrup 2006; Hoerstrup *et al.*, 2001; Wang *et al.*, 2010). In this context, crucial are the reports of Shin'oka (Shin'oka *et al.*, 2001; Shin'oka *et al.*, 2005), Niklason (Niklason *et al.*, 1999), and Hoerstrup (Hoerstrup 2006; Hoerstrup *et al.*, 2001). While the approach of Niklason and Hoerstrup made use of biomimetic perfusion systems for scaffold

conditioning (see section 2.2), Shin'oka and colleagues derived TEBVs by seeding vein derived cells onto a biodegradable polymer graft composed of PCL and PLA, reinforced with PGA (1:1, w/w) with internal diameter of 10 mm, length of 20 mm, and thickness of 1 mm. After 10 days of culture, TEBVs were used to reconstruct the occluded pulmonary artery (Shin'oka *et al.,* 2001). 42 pediatric patients were treated with this procedure; no complications occurred after a 32-months follow-up and all TEBVs were patent (Shin'oka *et al.*, 2005).

1.2.1.3 Re-engineering of natural vessels

An alternative strategy to the use of bio-artificial or synthetic scaffolds to produce artificial blood vessels is to "re-engineer" human- or animal-derived vessels. This strategy offers the advantage of maintaining the normal three-dimensional tissue architecture and the native extracellular matrix (ECM) composition. For this reason re-engineered vessels may have a superior mechanical performance compared with artificially fabricated vessels (Badylak *et al.*, 2009; Fomovsky *et al.*, 2010; Quint *et al.*, 2011). A potential disadvantage, at least in the case of animal-derived vessels, is the possible permanence of "xeno-antigens" (e.g. α-GAL (Galili 2005)), which may preclude a full graft biological compatibility, even after recellularization.

Different strategies to perform re-engineering of allogenic or xenogenic grafts have been set up. In a first one, named "transdifferentiation", collected donor native tissues are seeded (without prior decellularization) with recipient-specific autologous cells (such as SMCs, ECs, FBs and macrophages) followed by continuous exchange of the medium. In this way they are converted into an immunologically tolerable tissue for the recipient. This method was established and patented by Orton in 1993 (Orton 1993) and more recently, was used by Bader to transform donor-derived veins and xenogenic arteries into autologous vessels *in vitro* ((Bader 2012), Tab. 3). The second strategy consists in a recellularization process into a cell-free tissue obtained by means of decellularization (Brendel and Duhamel 1989). Decellularization is achieved by chemical (e.g., acids and bases, hypotonic and hypertonic solutions, ionic and non-ionic detergents, and alcohols), enzymatic (e.g., nuclease, trypsin, and collagenase) and physical (e.g. temperature, pressure and mechanical forces) methods, which can be also combined in order to disrupt

cells and remove cellular and nuclear material (Crapo *et al.,* 2011; Gilbert *et al.,* 2006; Soma and Kotturathu 2009). Different techniques are used for enhancing the efficiency of the decellularizing agents: perfusion (Montoya and McFetridge 2009; Ott *et al.,* 2008), immersion and agitation (Pellegata *et al.,* 2012) are the most utilized tools. After decellularization, cell removal assessment is performed using different methods, such as staining with fluorescent dyes (DAPI/ Hoechst), and standard histological staining (Hematoxylin/Eosin, Masson's Tricrome, and Movat's Pentachrome). Finally, in order to form a non-thrombogenic ECs barrier within the graft lumen, different strategies have been suggested. An example is the direct implantation in the patient (*in situ* approach) in order to to recruit circulating endothelial progenitors directly from the surrounding tissue, or to seed the decellularized vessel with autologous ECs (*in vitro* approach), prior to the implantation (Bischoff *et al.,* 2004; Wolfinbarger 2003).

Decellularized natural tissues, such as human veins (Schaner *et al.,* 2004; Soma and Kotturathu 2009; Squillace 2010; Teebken *et al.,* 2009), human and animal arteries (Amiel *et al.,* 2006; Bischoff *et al.,* 2004; Dahan *et al.,* 2012; Kaushal *et al.,* 2001), umbilical cord vessels (McFetridge 2005), and small intestinal submucosa (Badylak *et al.,* 2002; Lantz *et al.,* 1993) have been used as matrices, allowing repopulation with donor-derived cells by means of *in situ* or *in vitro* approach. In table 1.3 a list of patents relevant to the use of these approaches is shown.

Patent Number	Publication Date	Author	Title	Brief description	Novel aspects
US4801299	31/01/1989	Brendel et al (Brendel and Duhamel 1989)	Body implants of extracellular matrix and means and methods of making and using such implants	Earliest patent describing decellularization process for TEBV application	First method for forming a body implant starting from a tissue which has been treated with denaturing detergent to obtain acellular matrix
US5192312	09/03/1993	Orton (Orton 1993)	Treated tissue for implantation and methods of treatment and use	Method for treating bioprosthetic graft prior to transplant	Colonization process to make non-immunogenic an allogenic or xenogenic matrices
US20030219417A1	27/11/2003	Wolfinbarger (Wolfinbarger 2003)	Bioreactor mediated recellularization of natural and tissue engineered vascular grafts	Process for repopulating an acellular tissue graft using tissue engineering methodologies	Bioreactor approach for generating and conditioning a recellularized and re-endothelialized vascular graft using perfusion
US20040044403A1	04/03/2004	Bischoff et al. (Bischoff *et al.*, 2004)	Tissue-engineered vascular structures	Method for making small diameter vessels to replace clogged or damaged coronary blood vessels	Use of endothelial progenitors cells as source of EC for vascular tissue engineering
US20050203636A1	15/09/2005	McFetridge (McFetridge 2005)	Decellularized grafts from umbilical cord vessels and process for preparing and using same	A method and process for preparing vascular tissue graft starting form decellularized umbilical cord vessel.	Use of decellularized umbilical cord vessel as acellular matrix for vascular tissue graft
WO2009044407A1	09/04/2009	Soma et al. (Soma and Kotturathu 2009)	Small diameter vascular graft from processed cadaver saphenous vein	Decellularization techniques, including chemical, enzymatic and mechanical means for removing cellular components in order to obtain a material composed essentially of ECM components.	Process for diminishing the antigenicity and calcification of decellularized cadaver saphenous veins
US7658706B2	09/02/2010	Squillace (Squillace 2010)	Vascular graft sterilization and decellularization	Method for sterilization and decellularization of allografts or xenografts to create grafts suitable for implantation in humans.	Optimization of sterilization and decellularization procedures to reduce immune reaction of vascular grafts
US20120009677A1	12/01/2012	Bader (Bader 2012)	Method for producing a bio-artificial transplant	Method for transforming *in vitro* a biological donor tissue	Trans-differentiation of allogenic vein and xenogenic artery into autologous arteries

Table 3.1. *List of patents involving the use of approaches for vascular tissue engineering using decellularize-and-recellularize techniques of biological tissue: a brief description and the novel aspects of the patent content are provided.*

1.2.2 Biomechanical mimicking in vascular tissue engineering

Mechanical stimulation is an integral component of the cardiovascular developmental process. For example, it has been hypothesized that the beginning of pulsatile flow in the primary vascular system is a trigger of vascular and cardiac development, likely due to biomechanical effects on differentiation of cardiac and vascular progenitors. Although the global effect of the mechanical stretching in mature vessels has not been sufficiently addressed with bioreactor-assisted stimulation (see before), several studies have highlighted the role of mechanical stimulation in eliciting various responses in individual vascular cell types. For this reason, mechanical conditioning of *ex vivo* growing vessels is likely a crucial conditioning strategy to obtain fully functional TEBVs.

In vivo, vascular tissues are subjected to *i*) shear stress, acting on ECs and influencing their orientation in the direction of flow, *ii*) luminal pressure, *iii*) stretch, mainly in the circumferential direction, and *iv*) longitudinal tension. Clearly, all these stimuli may have important effects on the structure of the artificially assembled vessels and may determine also their mechanical properties after the end of the preparation procedure (Niklason *et al.*, 1999). In addition, mechanical stimuli have been shown to promote cellular responses such as the deposition of ECM components, and to cause changes in the (epi)genetic programming and the phenotype of vascular cells (Shi and Tarbell 2011).

To address this issue, several groups of researchers have developed dynamic culture systems suitable for applying, with a controlled manner, single (Dunkern *et al.*, 1999; Hoerstrup *et al.*, 2001; Tschoeke *et al.*, 2008; Williams and Wick 2004) or combined biomechanical stimuli (Bilodeau *et al.*, 2005; Dancu 2011; Fan *et al.*, 2009; McCulloch *et al.*, 2004; Niklason *et al.*, 2003; Vilender and Nickel 2008) to bio-synthetic vessels, such as shear stress, pressure, and axial, bending and torsional loads.

In early studies, flow perfusion was used to promote the endothelialisation of polytetrafluoroethylene grafts (Dunkern *et al.*, 1999) and to produce impermeable vascular substitutes using polyester grafts as described by Sauvage (Sauvage and Kaplan 1990). More recently, the implication of applying a 0.5-Pa shear stress (resulting from applying a steady state flow of 50 ml/min) on the properties of an engineered vascular graft was elucidated using the ElectroForce® Biodynamic™ Test Instrument (Bose Corp., Electroforce System Group, MI, USA) (Boccafoschi *et al.*, 2012) Further Tschoeke (Tschoeke *et al.*, 2008) developed a flow perfusion bioreactor for applying a 250 ml/min

fluid flow to a fibrin-based vascular graft (internal diameter of 5 mm) reinforced with a polyvinylidenefluoride mesh (with a pore size of 1-2 mm), and seeded with ovine myofibroblasts. After a stimulation period of 14 days, the graft tissue had a suture retention strength of 642 grams (similar to that of native carotid arteries, which reaches 753 grams (Cho *et al.,* 2005)) and a burst pressure of 236 mmHg.

A biomimetic pulsatile flow is necessary to properly simulate the physiologic arterial hemodynamics in TEBV bioreactors. Pulsatile physical forces allow vascular graft performance to be enhanced by increasing ECM deposition and reinforcing mechanical resistance of PGA synthetic grafts. For example, Niklason et al. (Niklason *et al.,* 1999), after 8 weeks of pulsatile stimulation (5% of radial distension at a rate of 165 pulse/minute), obtained an engineered vessel with a burst pressure of about 2000 mmHg, and a suture retention strenght of 90 grams, while Hoerstrup and colleagues (Hoerstrup *et al.,* 2001; Sodian *et al.,* 2002) used a novel *in vitro* pulse duplicator system for generating a biomimetic microenvironment supporting tissue formation. Using this apparatus, these Authors found that the mechanical properties of PGA seeded grafts increased with respect to static controls at 28 days of pulsatile culture. Analogously, Iwasaki (Iwasaki *et al.,* 2008) developed a hemodynamic-equivalent pulsatile bioreactor consisting of a ventricular model, two synthetic polymer-made valves, a compliant silicone tube, a peripheral resistive unit, a gas exchange unit, and a housing for mounting the vessel. This complex system enabled the formation of elastic vessel grafts with mechanical properties comparable to those of native arteries after a 2-week stimulation under a constant pulse rate of 70 bpm and a gradual increase in mean flow and pressure up to 600 ml/min and 100 mmHg, respectively. Finally, Thompson and colleagues (Thompson *et al.,* 2002) developed a bioreactor using a mechanical ventilator to induce pulsatile flow, while Narita (Narita *et al.,* 2004) adapted an intra-aortic-balloon pump system to develop a bioreactor able to produce a wide range of pulsatile stimuli on a tubular PLA scaffold (flow rate spanning from 0 to 3000 ml/min, systolic and diastolic pressures ranging from 10 to 200 mmHg and from 0 to 100 mmHg, respectively).

Bioreactors can also provide very complex mechanical conditioning including axial bending and torsional stimuli. For example, Seliktar (Seliktar *et al.,* 2000) applied cyclic strain at a frequency of 1 Hz up to 8 days to a collagen-based blood vessel construct. The results showed significant enhancement of the mechanical properties and cell organization

with respect to the static incubated constructs and depended on an active remodeling process. In another report (Bilodeau *et al.*, 2005), a perfusion bioreactor equipped with a pump for applying continuous or pulsatile flow (beat rate range 50-200 bpm) and a pneumatic cylinder to stretch and twist the vessel was devised. This approach was similar to that followed in a patented method to produce a human hybrid bypass graft using a bioreactor allowing a tight control of hemodynamic forces such as pressure, flow and stretch (Dancu 2011), and that described in another patent (Niklason *et al.*, 2003) claiming a method to perform pulsatile stretching of tubular constructs in order to align SMCs circumferentially (Table 1.4). An overview of the relevant patents regarding bioreactor-based approaches providing biomechanical stimuli to vascular TE constructs is summarized in table 1.4.

Patent Number	Publication Date	Author	Title	Brief description	Novel aspects
US4911713	27/03/1990	Sauvage et al. (Sauvage and Kaplan 1990)	Method of making vascular prosthesis by perfusion	A method for fabricating an impermeable vascular prosthesis perfusing the lumen of the textile conduit	Method for making vascular textile prosthesis impermeable, combining perfusion and chemical treatments
US005792603A	08/11/1998	Dunkelman et al. (Dunkelman *et al.*, 1998)	Apparatus and method for sterilizing, seeding, culturing, storing, shipping and testing tissue, synthetic or native, vascular grafts	Bioreactor that provide a dynamic environment for seeding, culturing and testing vascular grafts	Dynamic environment for culturing vascular grafts of any length and diameter applying shear and radial stresses
US005916800A	29/06/1999	Elizondo et al. (Elizondo *et al.*, 1999)	Cardiovascular bioreactor apparatus and method	Methods and apparatus for processing and shipping cardiovascular products, within sterile and aseptic environment	New mounting system for biological materials such as heart valves and vascular grafts
US6537567B1	25/03/2003	Niklason et al. (Niklason *et al.*, 2003)	Tissue-engineered tubular construct having circumferentially oriented smooth muscle cells	Methods for the production of organized tissue engineered constructs	Use of distensible bodies to impart pulsatile stretching force to the lumens of constructs during growth
US7348175B2	25/03/2008	Vilender et al. (Vilender and Nickel 2008)	Bioreactor with plurality of chambers for conditioning intravascular tissue engineered medical products	A microprocessor controlled and instrumented bioreactor for conditioning tissue engineering medical product. This system allows the control of fluid flow and tissue displacement and allows the measurements of the material properties.	Possibility of growing and conditioning vascular tissues within a controlled and strictly reproducible environment
US20090123993A1	14/05/2009	Banes et al. (Banes *et al.*, 2009)	Bioreactor for development of blood vessels	Blood vessel bioreactor developed for harvest, maintain, transport and produce vascular vessels	Vessel attachment/ engagement cuff connectors and clamps
US2009181448A1	16/07/2009	Fan et al. (Fan *et al.*, 2009)	Perfusion type vascular tissue bioreactor with rotary and stretching functions	Multi-module bioreactor for vascular construct able to generate physiological pulsatile flow	Generation of physiological pulsatile flow perfusion and multi-mechanical stimulation; mimicking vascular compliance, inertia, and resistance
US20110014597A1	20/01/2011	Frerich (Frerich 2011)	Perfusable Bioreactor for the Production and/or Cultivation of a	Bioreactor with elastic walls designed for the production of	Possibility of study the interactions between the vessel and the stromal

			Human or Animal Blood Vessel and/or a Human or Animal Tissue	human vessel	tissue
US7968329B2	21/06/2011	Dancu (Dancu 2011)	Method of conditioning a hybrid synthetic tubular structure to yield a functional human hybrid coronary bypass graft	Method for producing a human hybrid coronary by-pass graft conditioning a synthetic tubular matrix	Possibility of controlling, simultaneously and independently, hemodynamic forces in order to recapitulate *in vivo* vascular hemodynamic environments

Table 1.4*. List of patents involving the use of bioreactor-based approaches for vascular tissue engineering using biomechanical stimulation: a brief description and the novel aspects of the patent content are provided.*

1.3 Conclusions

The use of bioreactor-assisted culture of vascular grafts and substitutes has been confined, thus far, to simple preconditioning strategies to assess basic cellular responses to arterial-like mechanical forces, or to attempt vessel engineering. In our view, the use of these systems in the context of a wider molecular comprehension of vessel response to biomechanical stimulation will lead to dissection of mechanisms governing graft failure in patients.

A first area of interest appears the application of "omics" molecular investigation to assess the biomechanics-associated changes in the vascular global gene expression pattern. This is of interest in the recent view that vein graft disease involves a possible cross-talk between various cellular components of the vessels exposed to mechanical load (Hu *et al.*, 2004; Torsney *et al.*, 2005), or their interaction with cells recruited in the graft by the circulation (Zhang *et al.*, 2004). In this scenario, segments of human vessels exposed to differential mechanical loads in refined bioreactor platforms may be studied for changes in their transcriptome signature to assess the differential activation of *pro-* vs. *anti-*remodeling gene expression "modules" (Segal *et al.*, 2003). In addition, the customization of the platforms to allow injection of defined amounts of circulating cells such as monocytes or endothelial progenitor cells (EPCs), may help dissect the molecular mechanisms underlying homing of cells participating (Hu *et al.*, 2002), or potentially inhibiting restenosis (Brown *et al.*, 2010; Zhu *et al.*, 2010).

Another area of interest pertains to the role of recently identified vessel-resident progenitors (Ergun *et al.,* 2011; Majesky *et al.,* 2011; Torsney and Xu 2011) in VGD progression. These cells have been also found in human SV and have thereby named saphenous vein progenitors (SVPs) (Campagnolo *et al.,* 2010); they are adventitial pericyte-like cells that may be activated, directly or indirectly, to differentiate into proliferating SMCs as a result of vein arterialization. This hypothesis, in line with investigations highlighting the role of adventitia cells in the progression of transplant arteriosclerosis in animal models (Hu *et al.,* 2004; Torsney *et al.,* 2005), may be optimally addressed using pulsatile perfusion systems where segments of human SV are exposed to arterial flow conditions, followed by immunofluorescence studies to assess SVPs mitogenic activation and differentiation. This latter approach may be finally helpful also to uncover possible changes in the epigenetic signatures associated to mechanical stress in various cell types resident in the vein, and thus to understand the involvement of chromatin and histone code (Berger 2007; Kouzarides 2007) modifications following arterialization.

In summary, while significant advancements have been made in the design and construction of bioreactor platforms to replicate arterial-like conditioning, the conception of integrated approaches to understand the biology of the vessels “as a whole” in response to alteration of mechanical conditions is only at its early stages. In our view this is crucial to obtain a global comprehension of vein graft disease progression, to perform comparative studies of drug administration or gene expression modulation (gene therapy, siRNA and antagomir approaches), to devise preconditioning protocols and/or tissue engineering strategies that reduce the clinical impact of this pathology.

2

Design of a novel ex vivo vessel culture system

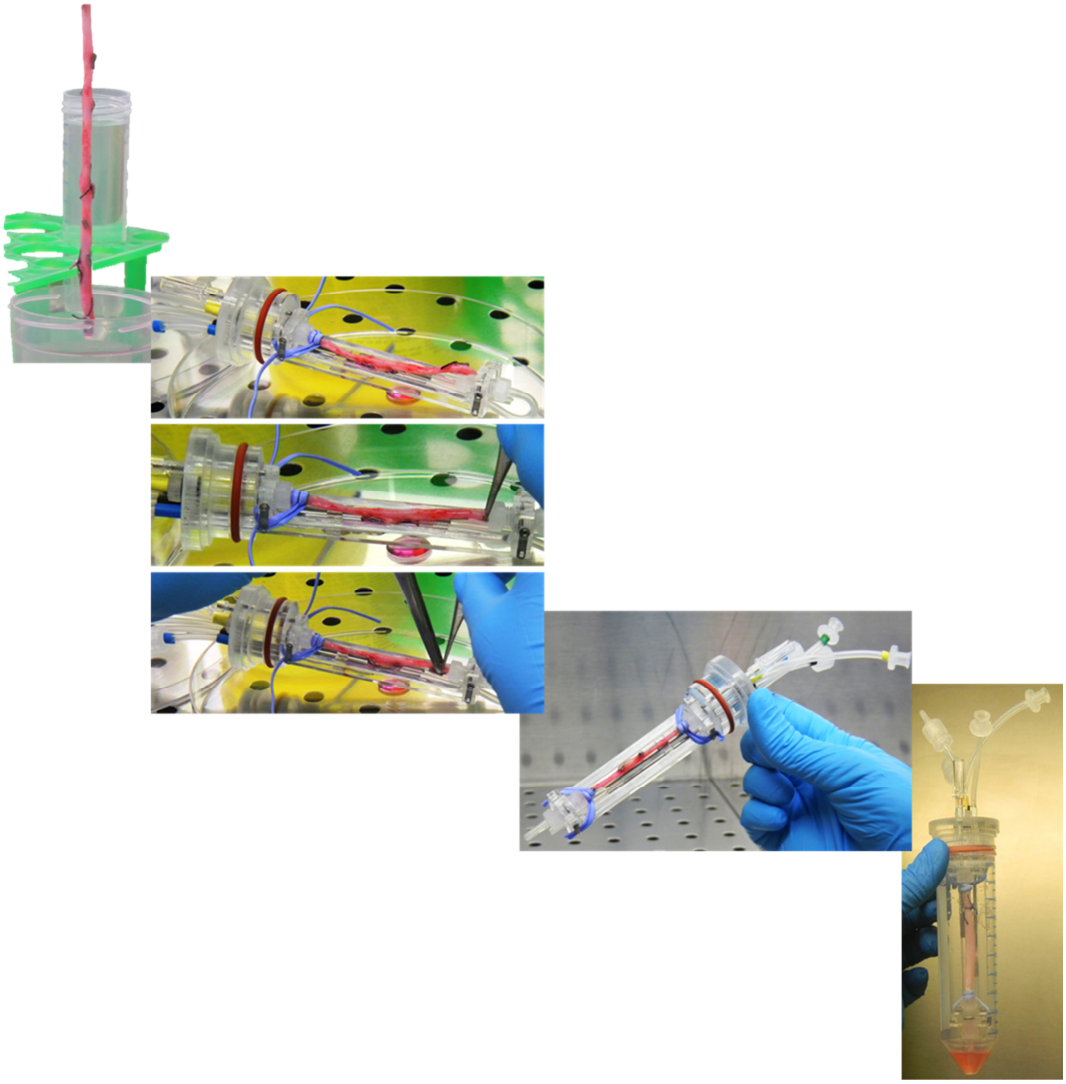

This chapter is partially based on*:* "M. Piola, F. Prandi, N. Bono, M. Soncini, E. Penza, M. Agrifoglio, G. Polvani, M. Pesce, and G. B. Fiore. *A compact and automated ex-vivo vessel culture system for the pulsatile pressure conditioning of human saphenous veins*. Journal of Tissue Engineering and Regenerative Medicine, [*Epub ahead of print*] doi:10.1002/term.1798".

Introduction

Saphenous vein (SV) graft disease represents an unresolved problem in coronary artery bypass grafting (CABG). After CABG, a progressive remodeling of the SV wall occurs, possibly leading to the lumen occlusion, a process termed intima hyperplasia (IH). The investigation of cellular and molecular aspects of IH progression is a primary endpoint toward the generation of occlusion-free vessels that may be used as 'life-long' grafts. While animal transplantation models have clarified some of the remodeling factors, the human SV pathology is far from being understood. This is also due to the lack of devices able to reproduce the altered mechanical load encountered by the SV after CABG.

In this chapter we propose the design of a compact and automated *ex-vivo* vessel culture system (EVCS) able to artificially produce the effects of the arterial pressure-related cyclic wall distention, one of the major biomechanical causes of IH in venous CABGs together with the pulsatile wall shear stress (Anwar *et al.,* 2012; Berceli *et al.,* 1990; John 2009; Muto *et al.,* 2010; Owens 2010; Stigler *et al.,* 2012). This aim is achieved by the development and functional assessment of a low-volume, reliable and user-friendly device, capable to replicate automatically the pulsatile pressure patterns of the physiological coronary environment. In perspective, the present EVCS could be used as tool to carry out molecular and cellular studies in order to better understand the impact of modified hemodynamic conditions on *in vivo* SV remodeling.

The approach applied for the design and manufacture of the device entailed a first phase of literature research, and interaction with the final user of the device; on these bases, the general and functional requirements of the bioreactor were identified, and a preliminary design of the system proposed. Subsequently, different culture chamber prototypes were designed, manufactured, and tested to define a final optimized configuration of the system. The design of the dynamic culture system made use of the 3D CAD software Pro/Engineering Wildfire 4.0 (Parametric Technology Corporation, PTC, Needham, MA), while the prototypes were manufactured using a parallel lathe (OPTI D 240x500 G-Vario, Optimum, DE), a numerical control machine (Roland MDX-40, Roland Corporation, Tokyo, JP), and a laser cutting (Versalaser VSL2.30, SK Laser, Germany), plus additional manual finishing. These activities were carried out at the Laboratory of Experimental Micro and Biofluid-Dynamics (μBS Lab) of the Dipartimento di Elettronica, Informazione e Bioingegneria of the Politecnico di Milano.

2.1 Design of the EVCS

2.1.1 Design specifications

The design of the EVCS took into account the general specifications of a bioreactor for tissue engineering application (Martin *et al.*, 2004), with particular emphasis on the ease of assembly under laminar flow hood, and the safety of use in a cell culture laboratory. Specifically, the following basic requirements were addressed: *i)* biocompatibility of materials, *ii)* transparency, to ensure visual inspection for air bubble and/or medium color changes, *iii)* compatibility with sterilization processes, e.g., via autoclaving and/or ethylene-oxide (EtO), *iv)* minimization of priming volume, in order to limit the cost of soluble culture medium compounds, and *v)* easiness of vessel accommodation and handling during the EVCS assembly.

2.1.2 Architecture of the ex-vivo vessel culture system

The EVCS is designed to apply a CABG-like pressure stimulation (CABG-PS), *i.e.* a pulsed pressure oscillating between a diastolic minimum and a systolic maximum (*e.g.*, 80-120 mmHg), or a steady flow perfusion, *i.e.*, a physiological venous perfusion condition (VP, *e.g.*, 5 mmHg) within a controlled and strictly reproducible mechanical environment. A schematic representation of the system's layout is shown in Figure 2.1. During culture, SV grafts are hosted in a culture chamber accommodated inside an incubator. The culture chamber is connected to a hydraulic circuit and actuators (pump and solenoid pinch-valve) to apply pressure stimulation to the human vessels or to allow the medium recirculate within the vessel. The hydraulic actuators are managed by a programmable monitoring and control (M/C) system, which operates via a pressure-based feedback loop.

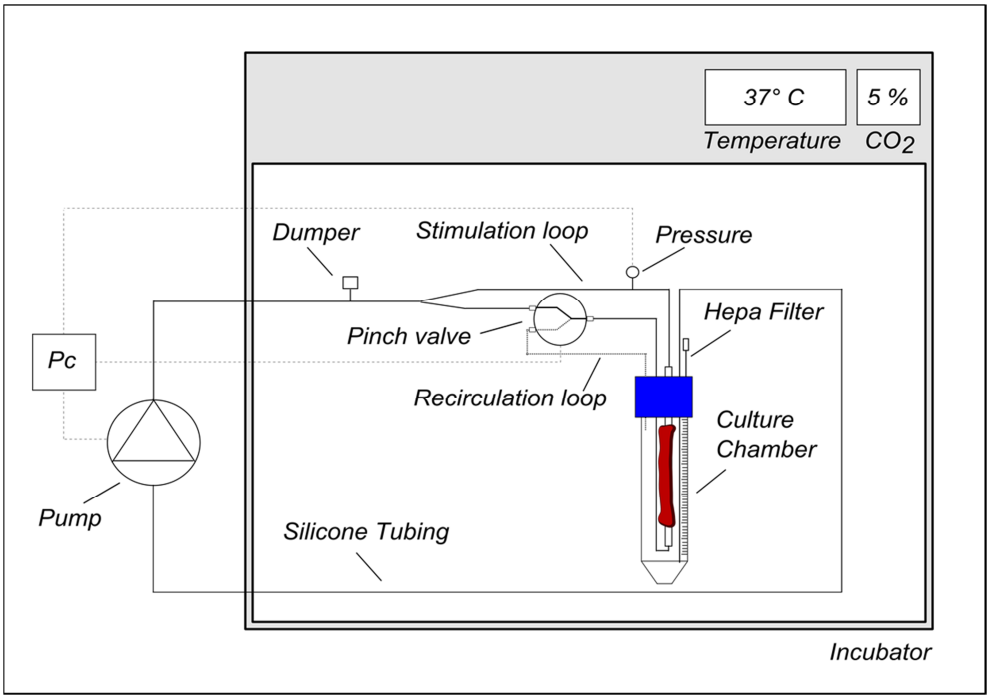

Figure 2.1. *Design of the EVCS. (A) Layout of the EVCS: thick lines represent the hydraulic circuit; thin lines represent the monitoring and control (M/C) signals. In particular, the M/C system manages the hydraulic actuators (a pump and a solenoid pinch-valve) via a pressure-based signal registered by the pressure sensor.*

2.1.3 SV culture chamber

The culture chamber (Figure 2.2) includes a commercial reservoir and a purpose-developed vessel housing which is integrated with the reservoir cap. All the culture chamber parts built in house were designed with 3D-CAD Pro/Engineer Wildfire 4.0 (PTC, Needham, MA), and manufactured by laser cutting (Versalaser VSL2.30, SK Laser, Germany), and/or computer numerical control machining (Modela MDX-40, Japan) from polymethylmethacrylate blocks (PMMA, Plasting S.r.l., Segrate, Italy). All the utilized materials are suitable for EtO sterilization. The vessel housing allows hosting SV samples up to 5.5 cm in length. The hosted vessel segment is cannulated at both ends using polypropylene (PP) barbed fittings (Cole Parmer, IL, USA), and secured using an extensible vessel loop (Esafarma S.r.l., Italy) as an elastic tourniquet. A standard 50-ml falcon tube (International PBI S.p.A, Italy) acts as a medium reservoir. The reservoir and the housing are coupled trough a silicone O-ring.

Five ports through the cap ensure the chamber's connection to the outside. Two ports ensure injection/removal of the culture medium to/from the vessel (Figure 2.2, port a and b). Two other ports provide connection for recirculation of the reservoir medium, *i.e*. the

medium external to the hosted SV (Figure 2.2, port c and d). One additional port provides communication with the incubator environment through a HEPA filter, to guarantee a sterile gas exchange while keeping the pressure inside the culture chamber atmospheric (Figure 2.2, port e).

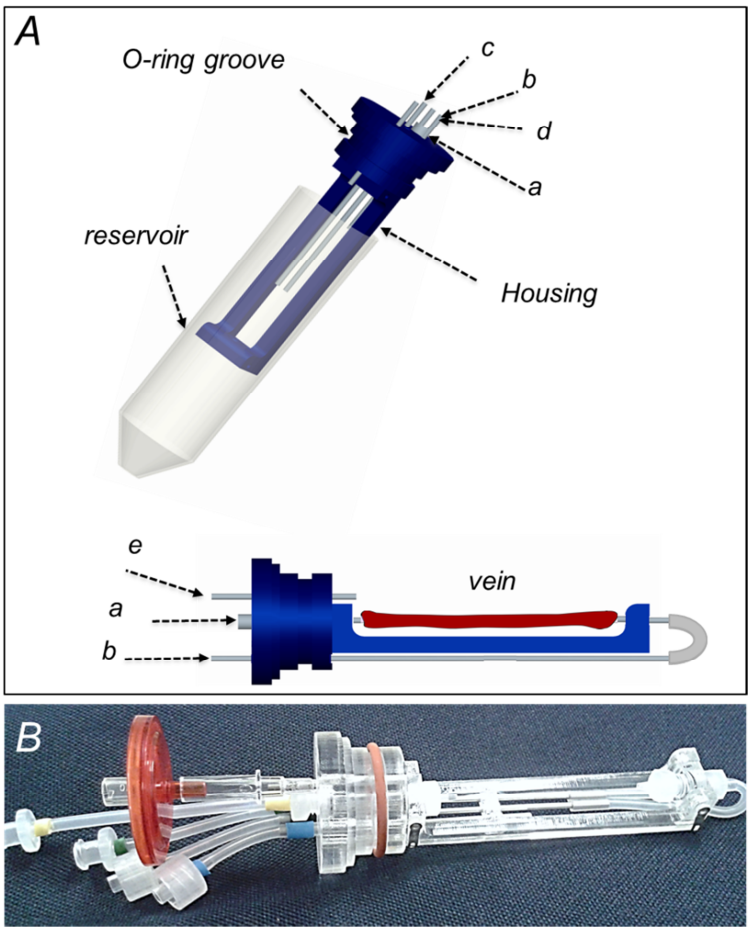

***Figure 2.2**. 3D CAD model of the SV culture chamber. The chamber consists of the SV housing inserted into a 50-ml falcon tube which acts as a reservoir; a and b are the ports for the vessel connection sites; c and d are the ports for connecting the culture chamber to the hydraulic circuit; e is the port for HEPA filter. (B) Prototype of the EVCS chamber realized in PMMA.*

2.1.4 The hydraulic circuit

The hydraulic circuit consists of silicone tubing (Platinum Cured, Cole Parmer, IL, USA) and PP-based pump tubing (PharMed BPT®, Carlo Erba Reagenti, Milano, Italy). PP luer connectors (Cole Parmer, Cole Parmer, IL, USA) are used to guarantee leak-free connections, and facilitate circuit assembly under laminar flow hood. A 5-ml syringe, filled with 1.6 ml of culture medium and 3.4 ml of air, acts as a compliance chamber for damping pump disturbances.

2.1.4.1 Dimensioning of the fluidic circuit

Gaseous exchange between the culture and the incubator environments occurs via the free surface of the medium in the SV culture chamber, via the oxygen-permeable silicone tubing and via the vessel segment (Figure 2.3). In the present paragraph, the dimensioning of the fluidic circuit, allowing for a proper oxygenation of the culture medium, is carried out basing on a mathematical model of oxygen transfer adapted from literature (Orr and Burg 2008).The tubing length was dimensioned in order to minimize the head loss along the hydraulic circuit during the vessel stimulation period. Further, the silicone tubing length was dimensioned according to an analytical model (Orr and Burg 2008) based on the balance between oxygen depletion (vessel cell metabolism) or replenishment (silicone tubing and free surface of the reservoir) in order to guarantee appropriate vessel oxygenation. Specifically, the mathematical model of oxygen transfer used for the determination of the tubing length took into account the sole silicone tubing and the SV vessel (Figure 2.3), whereas the reservoir was considered to be not oxygenating. This assumption is in favor of safety.

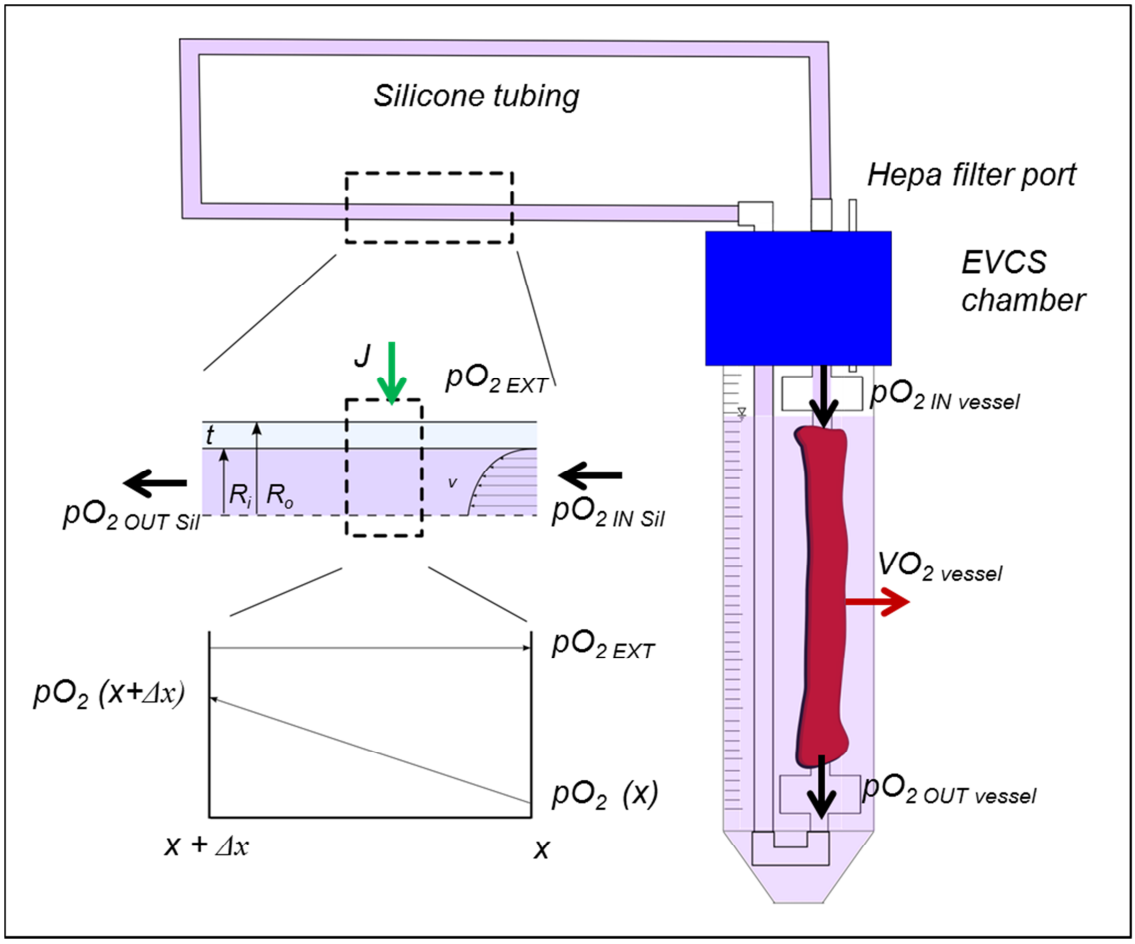

Figure 2.3. *Schematic representation of the oxygen transfer in the silicone tubing and in the SV vessel; the reservoir is considered to be not oxygenating. With regard to the vessel, $pO_{2\_IN\_vessel}$ and $pO_{2\_OUT\_vessel}$ represent the oxygen partial pressures at the inlet and at the outlet of the vessel, and VO_{2_vessel} is the global oxygen consumption due to cell metabolism (red arrow). With regard to the tubing, J is the local oxygen transfer per unit length crossing the tubing wall by diffusion (green arrow), t is the tubing thickness, R_o and R_i are the outer and inner radius respectively; v is the fluid velocity through the tubing; $pO_{2\_IN\_Sil}$ and $pO_{2\_OUT\_Sil}$ represent the oxygen partial pressures at the inlet and at the outlet of a silicone tubing of length L, pO_{2_x} and $pO_{2\_x+\Delta x}$ are the oxygen partial pressures at the inlet and at the outlet of a generic infinitesimal tubing element of length Δx; pO_{2_EXT} is the oxygen partial pressure within the incubator.*

The global oxygen transfer across the length of the silicone tubing ($VO_{2\ Silicone\ tubing}$) was expressed by the following equation:

$$VO_{2\ \text{Silicone tubing}} = \alpha Q\ (pO_{2\ \text{OUT Sil}} - pO_{2\ \text{IN Sil}}) \qquad (1)$$

where α represented the solubility coefficient of oxygen in the culture medium (considered equal to the one in water, 9.8 10^{-6} mmol/ml kPa), Q the flow rate of medium, $pO_{2\ IN\ Sil}$ and $pO_{2\ OUT\ Sil}$ the oxygen partial pressures at the inlet and at the outlet of the silicone tubing. Local oxygen transfer across the area of the silicone tubing wall ($J\Delta x$) was driven by the

differential in oxygen partial pressure between the constant incubator partial pressure $pO_{2\,EXT}$ (141 mmHg, considering an incubator atmosphere composed by air with a 5% CO_2 percentage) and the oxygen partial pressure of the medium $pO_2(x)$ at a distance x from the inlet of the silicone tubing, according to the following equation:

$$J\Delta X = UW\Delta X\,(pO_{2\,EXT} - pO_2(x)) \tag{2}$$

where J was the volumetric transport rate of oxygen per unit length transferred towards the medium within the tubing across the area $W\Delta x$ (W was the log mean of the inner and outer tubing circumference), U the overall mass transfer coefficient of the silicone tubing, and Δx the length of an infinitesimal tubing element (Figure 2.3). The log mean of the inner and outer tubing circumference (W) was defined as follows:

$$W = \frac{2\pi(R_o - R_i)}{\ln\frac{R_o}{R_i}} \tag{3}$$

where R_o and R_i were the outer and inner tubing radii, respectively (Figure 2.3); the overall mass transfer coefficient was computed as:

$$U = \frac{1}{\frac{W}{(k_o/RT)W_o} + \frac{t}{\rho_{STP}K_{Sil}} + \frac{W}{k_i\,\alpha W_i}} \tag{4}$$

where W_i and W_o were the inner and outer tubing circumferences, t is the tubing thickness, k_i and k_o the inner and outer local mass transfer coefficients (Orr and Burg 2008), K_{Sil} the permeability coefficient of oxygen through silicone (6.2 10^{-8} cm^3(STP) cm/s cm^2 cmHg) (Robb 1968), R the gas constant (82.06 cm^3 atm/mol K), T the incubator temperature (310 K), and ρ_{STP} the gas density at standard temperature and pressure (4.46 10^{-5} mol/cm^3). The overall mass transfer coefficient U accounted for the various resistances that oxygen encountered while diffusing from the incubator environment into the tubing: a resistance due to the diffusion through a stagnant gas film region at the exterior of the tubing, represented by the outer local mass transfer coefficient k_o; a resistance due to the diffusion through the tubing wall, represented by the permeability coefficient K_{Sil}; and a resistance

due to the diffusion of oxygen through the medium itself, represented by the inner local mass transfer coefficient k_i (Orr and Burg 2008).

Taking into account the following relationship between the global oxygen transfer ($VO_{2\ Silicone\ tubing}$) and the local transfer:

$$V0_{2\ Silcone\ tubing} = \int_0^L J\Delta x \tag{5}$$

the equation (1) was solved for the partial pressure at the outlet of the tubing $pO_{2\_OUT\_Sil}$ and combined by the equations (2) and (5), solved for the global oxygen transfer across the length of the silicone tubing ($VO_{2\ Silicone\ tubing}$). The resulting relation was:

$$pO_{2\ OUT\ Sil} = pO_{2\ EXT} - (pO_{2\ EXT} - pO_{2\ IN\ Sil})\, e^{-\frac{UWL}{\alpha Q}} \tag{6}$$

This equation express the partial pressure at the end of the silicone tubing ($pO_{2\ OUT\ Sil}$) as a function of the oxygen level in the medium entering the tubing ($pO_{2\ IN\ Sil}$), of the constant incubator partial pressure of oxygen ($pO_{2\ EXT}$), and of the silicone tubing length L.

The other component needed to model the oxygen transport requirements within the bioreactor circuit was the cellular oxygen consumption within the SV vessel, $VO_{2\ vessel}$ (Figure 2.3):

$$VO_{2\ vessel} = \alpha Q\ (pO_{2\ IN\ vessel} - pO_{2\ OUT\ vessel}) \tag{7}$$

where $pO_{2\ IN\ vessel}$ and $pO_{2\ OUT\ vessel}$ represented the oxygen partial pressures at the inlet and at the outlet of the vessel segment (Figure 2.3). Briefly, the oxygen consumption of native vascular tissue was set equal to 3.57×10^{-3} mlO_2/min, assuming an oxygen demand of $3\times57\ 10^{-6}$ mlO_2/(min kg) and considering the mass of a SV graft to be about 1 g (Hoenicka *et al.*, 2010).

In addition, the following entrance and exit relationships relating the oxygen partial pressure of the medium entering and exiting each component (vessel and silicone tubing) were written:

$$pO_{2\ OUT\ Sil} = pO_{2\ IN\ vessel} \tag{8}$$

$$pO_{2\ IN\ Sil} = pO_{2\ OUT\ vessel} \tag{9}$$

This mathematical description of the oxygen transfer within the fluidic circuit of the bioreactor system was used to determine the minimum tubing length *L* required to guarantee oxygen replenishment in the culture medium after depletion caused by cell metabolism within the vessel. Hence, combining the (6), (7), (8), and (9), the silicone tubing length *L* was calculated according with:

$$L = -\frac{\alpha Q}{UW} ln \frac{pO_{2\ EXT} - pO_{2\ OUT\ Sil}}{pO_{2\ EXT} - pO_{2\ OUT\ Sil} + \left(\frac{VO_{2\ vessel}}{\alpha Q}\right)} \tag{10}$$

Figure 2.4 shows the trend of L as a function of *Q* for a silicone tube with an inner diameter equal to 0.8 mm and wall thickness of 0.8 mm. In the graph, *L* is parameterized for different values of the desired $pO_{2\ OUT\ Sil}$.

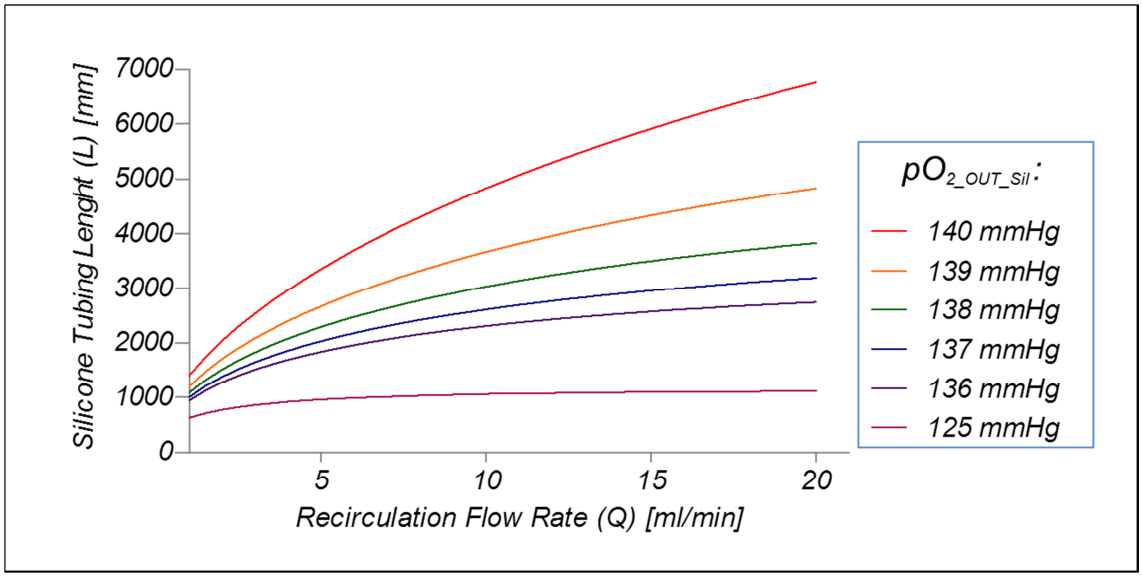

Figure 2.4. *Length of the silicone tubing as a function of the flow rate, Q. The tubing length is parameterized for different values of the desired oxygen partial pressure at the outlet of the silicone tubing ($pO_{2\ OUT\ Sil}$). In the graph, y-axis intersects the x-axis at 1 ml/min.*

On the basis of the data emerging from the dimensioning of the silicone tubing appeared evident that as the flow rate increases the tubing length increases too. The length of the tubing represents a crucial point. Practical reasons impose to limit the pressure losses and to minimize the overall priming volume. In addition, a $pO_{2\ OUT\ Sil}$ range of 137-139 mmHg is considered to be acceptable in order to maintain the viability of the vessel segment. Thus, considering a suitable flow rate lower than 10 ml/min (to limit head losses), the necessary silicone tubing size results to be at least 250 cm long.

2.1.5 Monitoring and control system

The M/C system is able to automatically apply the CABG-PS to the SV segments or the SV perfusion by automated control of a peristaltic pump (Watson Marlow 323D with 314D pumping head, Watson Marlow Group, UK) and a solenoid pinch-valve (S305-09, SIRAI® Elettromeccanica, Italy) (Figure 3.1). The solenoid pinch-valve enables switching between the vessel stimulation loop and the recirculation loop (Figure 2.5 B). The hydraulic actuators are connected to a PC equipped with a I/O board (NIDAQCard-6036E, National Instruments Corp.) and are managed via a customized LabView software (National Instruments Corp., TX, USA) adapted from Vismara and colleagues (Vismara *et al.*, 2009). The pressure sensor Press-S-000 (PendoTECH, NJ, USA) provides the intraluminal pressure feedback signal to the software (Figure 2.1).

The CABG-PS program consists of a cyclical alternation of a pulsatile stimulation period and a recirculation period. Particularly, the single cycle is composed of four steps (Figure 2.5A): *i)* the loading step, in which the culture medium is delivered through the vessel until the intraluminal pressure reaches a lower pressure limit (P_{min}); *ii)* the pulsatile stimulation step, during which the vessel is inflated and deflated in order to apply a controlled CABG-PS within the pre-defined pressure ranges (P_{min} - P_{max}) and for a pre-defined time and number of pulses per minutes; *iii)* the unloading step, in which the intraluminal pressure within the vessel is lowered again to zero (P_0) by inverting the medium flow direction; and finally, *iv)* the recirculation step, characterized by a constant flow rate allowing a metabolic supply to the vessel for a predefined recirculation period. The user can set all the specific parameters via the software interface, namely P_{min} and P_{max}, the pulse frequency (f) and the number of pulses (# pulse) for the pulsatile stimulation period; the duration (T_R) and the medium flow rate (Q_R) for the recirculation period.

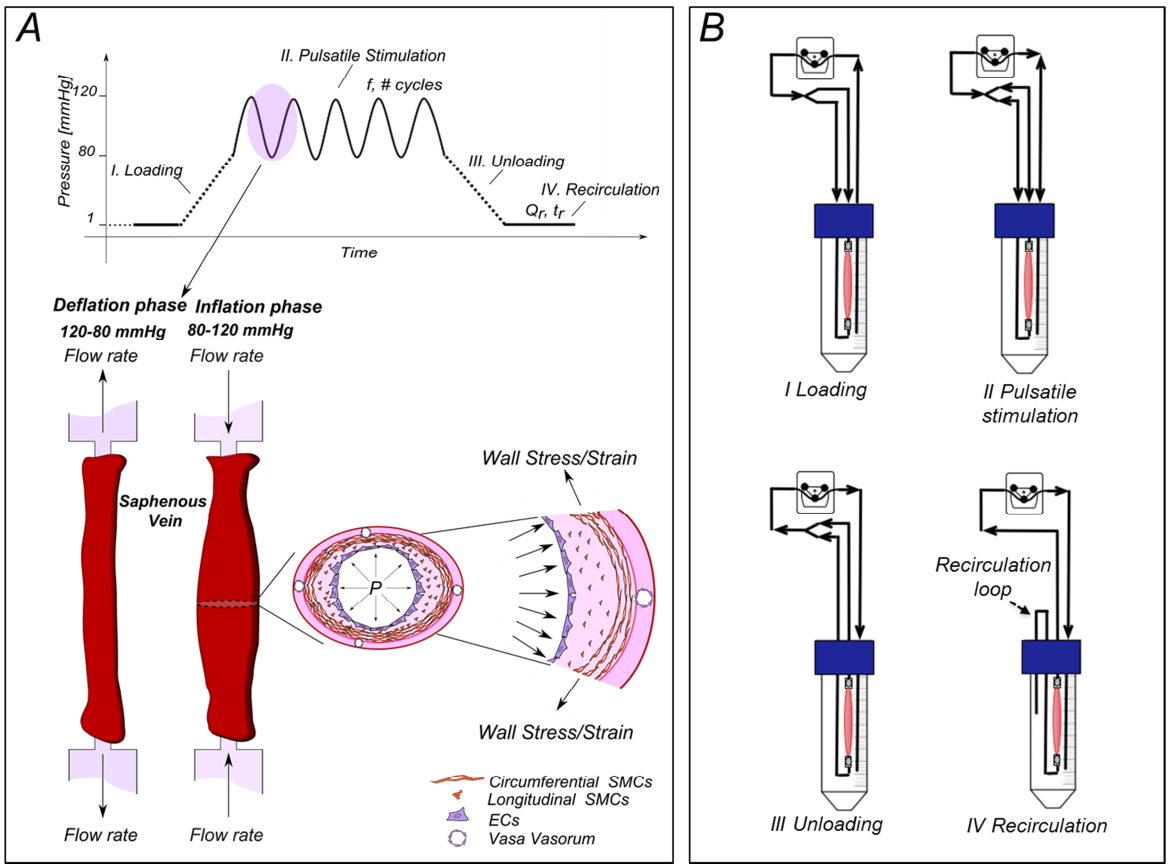

Figure 2.5. *Design of the EVCS. (A) Schematic diagram of the CABG-PS program. The CABG-PS consists of: I) a loading phase up to the lower limit of a pre-defined pressure range, II) a pulsatile stimulation in a pre-defined pressure range, III) a unloading phase, and IV) a recirculation phase. During the inflation phase the SV wall, thus the SMCs, experienced a circumferential wall stress. (B) Simplified layout of the flow paths within the EVCS during the CABG-PS cycle. During pulsatile stimulation the medium is forced into and out of the sample through both ends.*

2.2 Overview of the EVCS

An overview of the EVCS during the assembling phase under laminar flow hood is shown in Figure 2.6. The time necessary to fix the vein to the housing (Figure 2.6 A, B, C and D) was less than 15 minutes; during this period the SV was constantly kept hydrated by pipetting culture medium on the SV surface. Finally, the housing was inserted within the reservoir, and connected to the hydraulic circuit (Figure 2.6 E). Once assembled, the EVCS was placed in the incubator and the culture under mechanical conditioning started imposing either a VP condition or a CABG-PS.

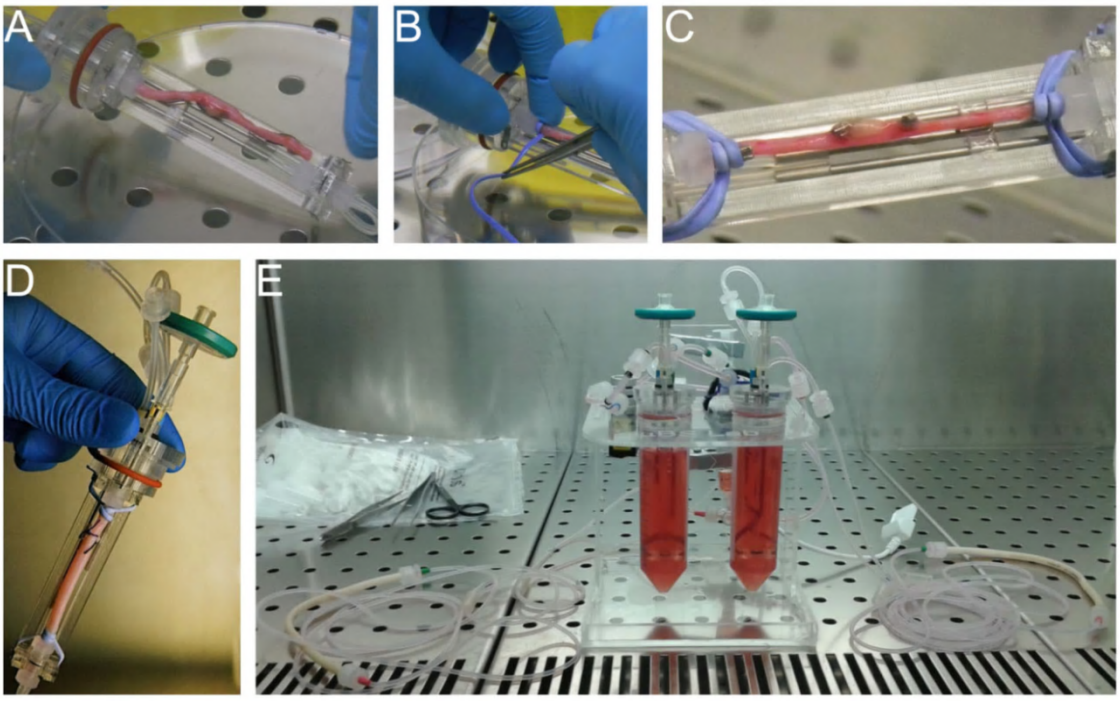

Figure 2.6. *Prototype of the EVCS during the assembling phase. (A) The SV sample is mounted in the housing, and (B) secured via vessel loops. (C) After vessel fixing, (D) the HEPA filter is mounted onto its port, and then the vessel housing is inserted within the reservoir and connected through a silicone O-ring coupling resulting in a compact culture chamber. (E) The culture chamber is then connected to the hydraulic circuit and the entire system is filled with culture medium.*

2.3 Functional experiments for testing the performance of the EVCS

2.3.1 Pressure-volume measurements of SV segments

Pressure-volume relationship of human SV segments was obtained in order to dimension the fluid volume that the pump has to process for obtaining the desired pressure increments within the vessel. To this aim, a custom-made system was developed to measure the pressure-volume relationship during SV filling. A Schematic diagram of the custom-made system is reported in Figure 2.7. For each SV specimen ($n=6$, length of the sample > 35 mm), the inner diameter (Di) was measured using a caliper (for the preparation of the human samples refers to *Chapter 4, paragraph 4.1.1*). Then, each SV segment was mounted in the custom-made system and pre-tensioned by imposing a 10% axial strain, corresponding to a length named $l_{10\%}$. Table 2.1 reports the geometrical characteristics (D_i and $l_{10\%}$) of the SV and the volume at zero pressure (V_0), calculated as the volume of a straight cylinder of diameter equal to D_i and length equal to $l_{10\%}$. SV segments were pre-conditioned by imposing five cycles of loading (0 to 120 mmHg) and

unloading (120 to 0 mmHg), as described in the literature (Costantino *et al.*, 2004a; Costantino *et al.*, 2004b). Thereafter, the vessel lumen was exposed to incremental pressure (0 to 120 mmHg, step 10 mmHg) and the associated inner volume increment was measured (*ΔV*, Figure 2.7) using an interposed graduated pipette. For each sample, this procedure was repeated three times. The volume increment was normalized to V_0.

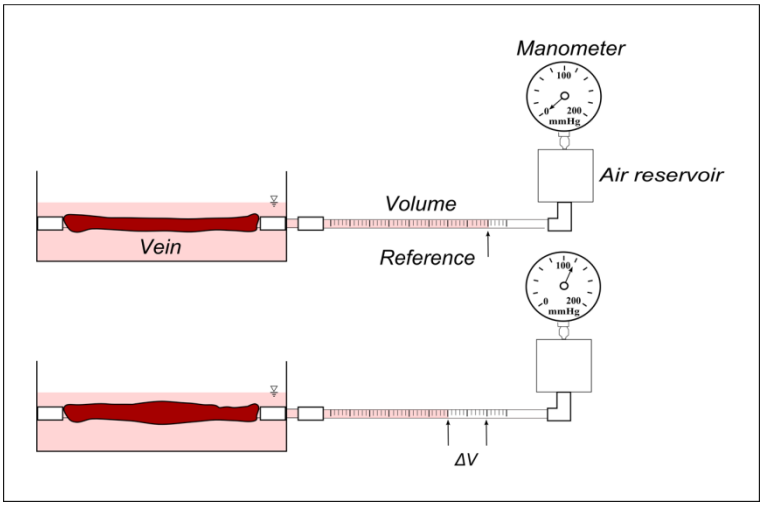

***Figure 2.7**. Schematic of the custom made set-up developed for the compliance measurements. Pressure is measured with a manometer and inner volume increments (ΔV) are measured using a graduated pipette.*

Sample	D_i [mm]	$l_{10\%}$[mm]	V_0 [ml]
SV01	3.2	59	0.47
SV02	3.1	35	0.26
SV03	3.8	60	0.68
SV04	3.4	35	0.27
SV05	3.2	35	0.28
SV06	3.8	60	0.68
Mean	3.4	46.5	0.44

***Table 2.1**. Geometric values of the SV samples (n=6) used for the pressure-volume measurements. D_i represent the inner diameter; $l_{10\%}$ is the length of the sample hosted within the custom-made device, and V_0 was calculated as the volume of a straight cylinder of diameter D_i and length $l_{10\%}$.*

2.3.2 Functional assessment of the EVCS

Preliminary tests were performed using a SV sample (for the preparation of the human samples refers to *Chapter 4, paragraph 3.1.1*), mounted within the EVCS, in order to validate the robustness and the reliability over time of the system. The EVCS was placed in the incubator and the performances were evaluated by changing the pulse frequency and the pressure stimulation range. The tested pulse frequency was 0.5 Hz, 0.75 Hz, 1 Hz and 1.2 Hz, while the pressure range was 60 – 90 mmHg (Hypotension), 80 – 120 mmHg (Normal) and 100 – 140 mmHg (Hypertension).

For the following tests the EVCS components were sterilized by EtO or autoclaving, where appropriate. The EVCS sterility maintenance was verified with two tests using a sterile silicone vessel substitute and a SV sample. In both conditions, the system was assembled under laminar flow hood and filled with 42 ml Roosvelt Park Memorial Institute medium 1640 (RPMI, Lonza Group LTD, Switzerland) without antibiotics, and placed in the incubator (37°C and 5% CO_2) for 7 days with a partial medium replacement at day 3, reproducing standard culture conditions. As a control, a Petri dish containing the same medium was also incubated. At every time step (day 0, day 3, and day 7) the culture medium was added to the Thioglycollate broth (BD, Maryland, USA) for microbiological analyses.

2.4 Results of the functional experiments for testing the EVCS performance

2.4.1 Pressure-volume measurements of SV segments

Figure 2.8A reports the pressure-volume relationship obtained by progressively inflating fluid volume in human SV segments. The results showed an initial rapid volume rise with the first pressure increment step from 0 to 10 mmHg (a physiologic pressure range for veins), followed by a decreasing slope of the pressure-volume relationship, indicating that a considerable stiffening of the SV tissue progressively occurred when shifting towards the arterial pressure range (Figure 2.8 A).

Figure 2.8 B reports the luminal volume increment within the vein after imposing a pressure in the range of 0 – 10 mmHg, 10 – 80 mmHg and 80 – 120 mmHg. According to these results, the mean inflation fluid volume necessary to generate a pressure increment from 80 mmHg to 120 mmHg, was 0.06±0.025ml (Figure 2.8 B). This value was used as

rough estimate for selecting the dimensions of the relevant hydraulic components, such as the volume of the compliance chamber and the inner diameter of the pump tubing.

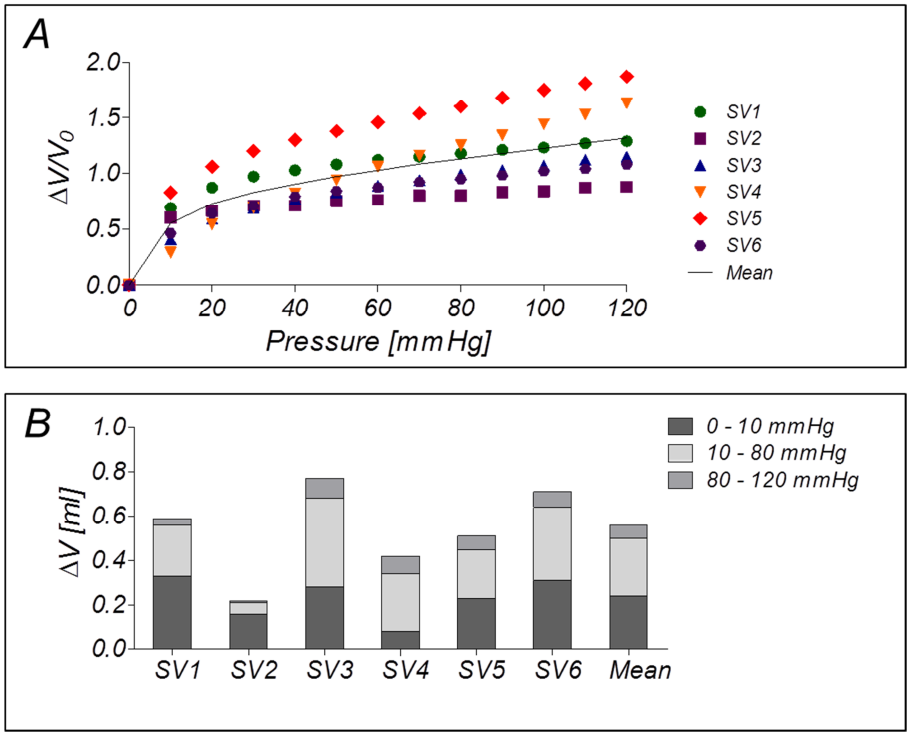

Figure 2.8. *Pressure-volume measurements of SV segments (A) Pressure versus volume relationship for 6 human SVs. An initial rapid volume rise at physiological venous pressure range (0 - 10 mmHg) is followed by a decreasing slope at physiological arterial pressure (80 - 120 mmHg). (B) Representative histogram of the inflation volume necessary to generate pressure ranges (0 – 10 mmHg, 10 – 80 mmHg, and 80 – 120 mmHg) in the vein lumen.*

2.4.2 Functional assessment of the EVCS

Figure 2.9 A reports representative screen printouts of the M/C software of the EVCS, showing an example of pressure tracing during the CABG-PS cycle. The outcomes of the functional tests indicated a good reliability of the M/C system. Figure 2.9 B shows the system's response to different pressure conditions reproducing hypertension (100 – 140 mmHg), normal (80 – 120 mmHg) and hypotension (60 – 90 mmHg) conditions; while the system's response to different values of frequency (0.5, 0.75, 1 and 1.2 Hz) is shown in figure 2.9 C. In both configurations, the stimulation pressure tracings are fairly regular, repeatable and compliant to the user's settings. Finally, microbiological tests showed no contamination in the culture medium after 7 days of culture in either tested configurations (silicone vessel or SV sample). Absence of any apparent contamination was also observed in the subsequent CABG-PS and VP culture tests.

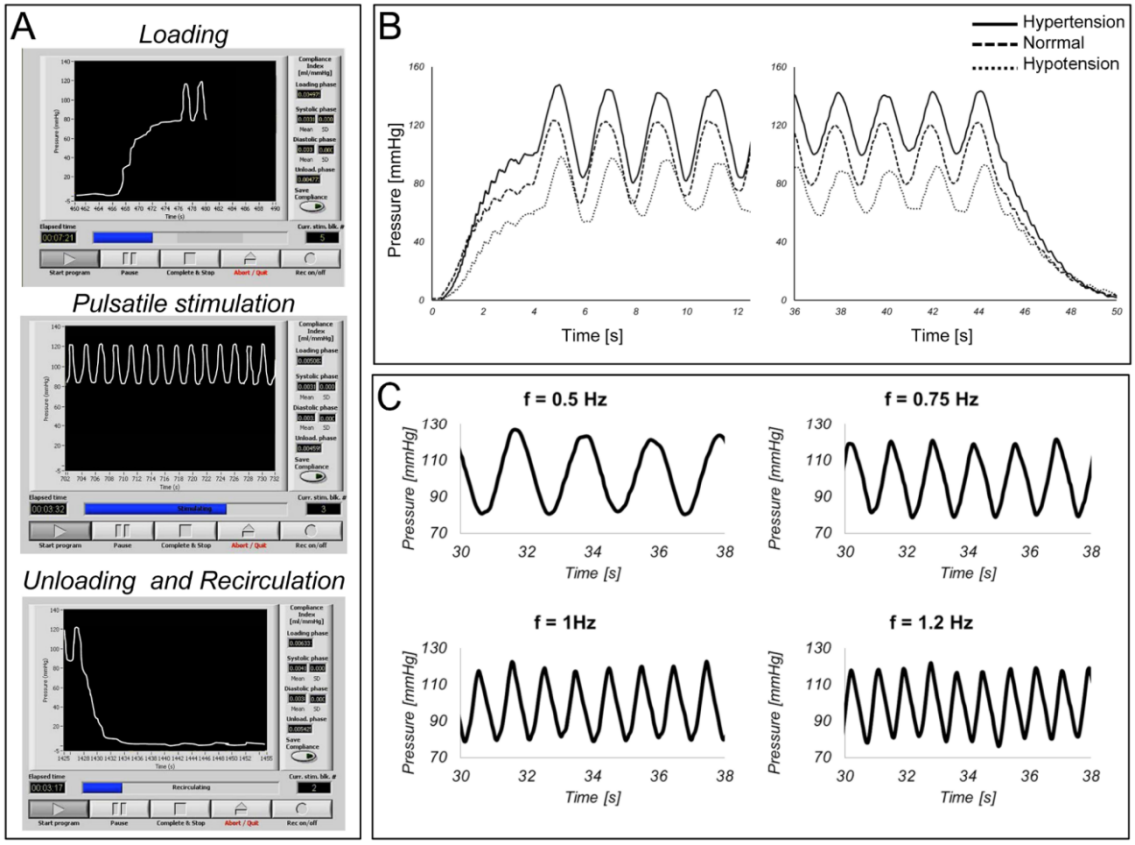

Figure 2.9. *(A) Printout of the resulting pressure tracing during the four steps of CABG-PS cycle. (B) Pressure tracings of CABG-PS cycle of a SV segment obtained changing the pressure within the ranges: 60 – 90 mmHg (Hypotension), 80 – 120 mmHg (Normal), and 100 – 140 mmHg (Hypertension) at a pre-defined pulse frequency of 0.5 Hz. (C) Fragments of CAGB-PS cycle of a SV segment obtained changing the pulse frequency (0.5 Hz, 0.75 Hz, 1 Hz and 1.2 Hz) and applying a Normal pressure range to the vessel.*

2.5 Conclusions

The design of a novel and versatile platform to perform dynamic stimulation of SV segments mimicking the physiological pressure patterns of the coronary circulation is described. This is indicated as one of the major insults received by the SV segments following their CABG implantation (Anwar *et al.,* 2012; Berceli *et al.,* 1990; John 2009; Muto *et al.,* 2010; Owens 2010). Hence, the rationale of its inclusion as a controlled factor for conditioning SV segments in our culture device is to enable *ex vivo* campaigns for elucidating the role of a major biomechanical factor in SV arterialization. The EVCS was verified to reliably apply the desired pressure patterns to SV segments in a controlled and sterile environment.

Regarding the EVCS design, the specifications of an easy assembly and handling were satisfied thanks to the technical solutions adopted. First, the entire system is very compact through the adoption of an integrated medium reservoir, which makes the device easy to be used into a standard cell culture incubator, minimizing the need for dedicated culture instrumentation. In addition, compactness allowed abating the overall priming volume to 42 ml, substantially lower than the 5000 ml reported by Voisard and colleagues (Voisard *et al.,* 2010) and the 300 ml stated by Clerin (Clerin *et al.,* 2002), and comparable with the overall priming volume of 20 ml declared by Dummler and colleagues (Dummler *et al.,* 2011). Finally, working in vertical conditions facilitates the air de-bubbling through the HEPA-port during the assembling and filling of the EVCS and during the culture experiments. This configuration avoids the air bubbles accumulation within the vessel during the mechanical conditioning culture.

Compared to other EVCS reported in literature (Piola *et al.,* 2012), with particular reference to the systems by Dummler and colleagues (Dummler *et al.,* 2011) and Voisard and colleagues (Voisard *et al.,* 2010), our EVCS is designed to ensure the perfusion of the hosted SV segments, or to impose controlled physiologic CABG-PS conditions, resulting in a cyclic wall circumferential strain. To this purpose, the EVCS is equipped with dedicated control hardware and software, which, from the user's standpoint, implies interaction with a programmable and user-friendly graphical interface. In this way the device is suitable to automatically manage the generation of the pressure pulse or the medium recirculation for fluid refreshing and tissue oxygenation.

The strategy we adopted for the pressure stimulation consists of inflating and deflating the SV by forcing small volumes of medium into and out of the vessel through both ends. Thus, a recirculation phase is mandatory in order to re-establish the correct amount of nutrients within the luminal region of the vein. In addition, pulse generation is based on the commands of a robust programmable M/C system, which operates via a pressure-based auto-tuning feedback loop. A main feature of the M/C system is the possibility to freely set different stimulation parameters such as pressure range, pulse frequency, and number of cycles in order to modulate properly the stimulation pattern. In this manner, a versatile system is envisaged with the capability to perform simultaneous stimulation of SV segments in different conditions to perform more stringent paired biological observations on SVs segments or for mechanical conditioning of tissue-engineered blood vessels.

However the EVCS suffers from some limitations. The system does not allow for the application of a coronary-mimicking flow through the vessel, hence the shear stress stimulus deriving from the arterial transposition of the vein is not replicated. Specifically, being the net flow approximately zero during the stimulation period, the resulting shear stress experienced by the ECs in the EVCS is negligible with respect to arterial shear stress. On the one hand, this allowed us to selectively study the early remodeling effects caused by wall strain alone as a biomechanical stimulus. On the other hand this did not represent a fully biomimetic condition, because in real CABG pulsatile strain is always associated to pulsatile wall shear. The system, however, is prone to a fully biomimetic upgrade; this will require minimal changes to the culture chamber design (such as, changes in conduit diameters), whereas appropriate refinements will be needed for the hydraulic circuit layout and for the M/C system. In addition, the system is not suitable for replicating the artery/vein compliance mismatch, hampering the possibility of study its contribution on the early remodeling events associated with IH.

Pressure-volume relationship of human SVs, obtained experimentally, was used in order to determine the volume of medium to be processed within the vessel to obtain the desired intraluminal pressure oscillation within CABG-PS range. In addition, the results indicated that the pressure-volume curves are non-linear and revealed a considerable hardening of the SV tissue occurring at arterial pressures. These data fully comply with data reported in literature (Stooker *et al.*, 2003). It is worth to notice that, as attested in our

functionality tests as well as in the subsequent 7-day device use experience, pulse generation stability was not affected at all by the strong nonlinearity of the treated samples. From a strict engineering viewpoint, this is an index of the system's robustness as an automated tool for biomechanical SV sample stimulation.

For these enhanced design characteristics this platform is therefore a novel laboratory-oriented tool that, will be useful to carry out *in vitro* culture campaigns under strictly controlled hemodynamic conditions and dissect the contribution of different biomechanical factors involved in the early IH priming in vein CABGs.

3

An arterialization study of human SVs in the EVCS

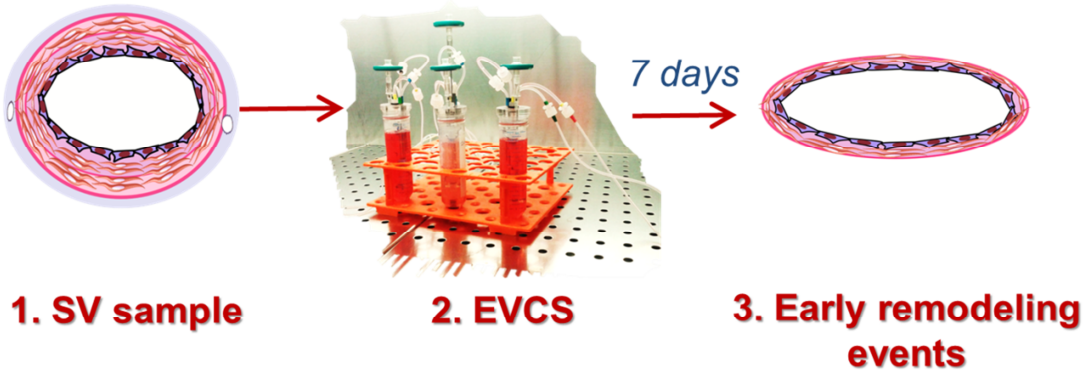

This chapter is partially based on*:* "M. Piola, F. Prandi, N. Bono, M. Soncini, E. Penza, M. Agrifoglio, G. Polvani, M. Pesce, and G. B. Fiore. *A compact and automated ex-vivo vessel culture system for the pulsatile pressure conditioning of human saphenous veins*. Journal of Tissue Engineering and Regenerative Medicine, [*Epub ahead of print*] doi:10.1002/term.1798".

Introduction

The impact of arterial pressure (thus, wall strain and wall stress) on early human SV remodelling was finally investigated within the EVCS. Using this system, segments of human SV (collected as remaining vessel after CABG surgery interventions at the Cardiac Surgery Department of the Centro Cardiologico Monzino) were exposed to CABG-pressure stimulation or venous perfusion for a period of 7 days.

This chapter reports the results of the preliminary biomechanical conditioning campaign on human SV segments, using the EVCS developed in the *Chapter 2*. The conditioning experiments were carried out at the Laboratory of Cardiovascular Tissue Engineering of the Centro Cardiologico Monzino in Milan. Epigenetic analyses were carried out at and in collaboration with the Università Cattolica del Sacro Cuore of Rome and the Goethe University of Frankfurt, while zymography and western blot analyses were mainly performed by biologists of the Laboratory of Cardiovascular Tissue Engineering of the Centro Cardiologico Monzino.

3.1 Design of the conditioning experiment

3.1.1 SV samples preparation

For the arterialization experiments, the use of human SV segments was authorized by the local Ethical Committee with the approval of an informed consent. SV segments were obtained from the Department of Cardiovascular Surgery of the Centro Cardiologico Monzino. Briefly, surplus segments of SV were obtained from 11 patients undergoing CABG surgery (mean age of 66.7±7.4, Table 3.1). SV samples were harvested with a “no touch” technique avoiding venous spasm and dilatation, and ensuring endothelial, medial and adventitial integrity (Dashwood and Tsui 2013); the SV was exposed by a continuous incision, all the visible collateral branches were ligated, and finally the vein is harvested with a pedicle of surrounding tissue, which protects the vein from spasm therefore obviating the need for distension. The distal end of each SV segment was cannulated in the operating room, thus allowing the identification of the valves direction, side branches were ligated, and SVs were immediately stored at 4°C in Dulbecco Modified Eagle’s Medium (DMEM) supplemented with 10% Fetal Bovine Serum (FBS), 1% L-Glutamine, and 1% Penicillin/Streptomycin. All the SV segments were maintained at 4°C up to 48h before

their use. In all the experiments described in the following paragraphs, the distal end of each sample was mounted onto the inlet connector of the EVCS culture chamber after gently removing the existing cannula.

Patients ID	Sex	Diabetes	Nicotin	Hypertension	Dislipidemia	Hyper-colesterolemia	Culture conditions
SV69 (65 years)	M	--	--	X	X	--	CABG-PS
SV73 (54 years)	M	X	--	X	X	--	CABG-PS
SV79 (62 years)	M	--	X	X	--	--	CABG-PS
SV82 (70 years)	M	--	--	X	--	X	VP
SV83 (72 years)	M	--	--	X	X	--	VP
SV84 (65 years)	M	--	--	X	--	--	VP
SV85 (62 years)	M	X	--	X	X	--	VP
SV88 (69 years)	M	--	--	--	X	--	CABG-PS
SV91 (73 years)	F	--	--	--	--	X	VP
SV92 (60 years)	M	--	--	X	X	--	CABG-PS VP
SV94 (81 years)	M	--	X	X	--	--	CABG-PS

Table 3.1. *Data of the patients enrolled for the conditioning experiments. Surplus SV grafts from 11 patients undergoing coronary bypass grafting were cultured in venous (VP) or arterial hemodynamic(CABG-PS) conditions.*

3.1.2 Mechanical conditioning of human SV within the EVCS

Generally, SV samples were divided into two segments (only in one case, the length was sufficient for cutting the vein into three segments). One portion was immediately stored and used as control (native segment); the second portion (length > 5.5 cm) was cultured in the EVCS. SV samples were cultured under CABG-PS conditions (luminal pressure: 80 - 120 mmHg; pulse frequency (*f*): 0.5 Hz with a stimulation interval (*Ts*) of 10

minutes; recirculation flow rate (Q_R): 1 ml/min, with a luminal pressure between 1-2 mmHg, and recirculation interval (T_R) of 2 min, or VP conditions (steady flow with luminal pressure: 5 mmHg; flow rate: 3 ml/min). After the sterilization of the EVCS, SV segments were mounted as previously described (*paragraph 2.2* and Figure 3.1A –E); then the EVCS was filled with 42 ml of DMEM with 10% Fetal Bovine Serum (FBS), 1% L-Glutamine, 1% streptomycin-penicillin. Then, the EVCS was kept in the incubator at 37° C and 5% CO_2 for a culture period of 7 days. The culture medium was partially changed at day 3. At the end of the mechanical conditioning period, SV samples were disassembled, vein ends were discharged (thus avoiding any edge effects induced by the mounting onto rigid connectors), and the central portion of the SV was processed for the following analyses.

Figure 3.1. *The compact and automated ex-vivo vessel culture system able to artificially produce the effects of the pulsatile arterial pressure-related cyclic wall distention. The EVCS during system assembling under laminar flow hood: the SV segments are cannulated on both ends with barbed luer fittings, and bounded on the connectors using a vessel loop (A-D). Then, the SV housing is inserted within the 50-ml falcon tube acting as reservoir (E). Once assembled, the culture chamber is connected to the stimulation circuit (F).*

3.2 Methods for morphological and IF assessment of the mechanically conditioned human SV segments

3.2.1 Tissue viability evaluation

To assess tissue viability, methylthiazol tetrazolium (MTT, Sigma Aldrich) staining was used (Miyakawa *et al.,* 2008). Rings of cultured and native (positive control) SV samples were used. MTT powder was dissolved in PBS, obtaining a final concentration of 0.5 mg/ml. SV rings were incubated at 37°C for 1 hour in PBS/MTT solution. As a negative control, a SV ring was fixed with 4% formaldehyde overnight and then incubated with MTT staining. Pictures were taken using a stereo microscope (STEMI 2000-C, Carl Zeiss®, Germany).

3.2.2 Histological, immunofluorescence and immunohistological analysis

To assess vessel wall integrity after VP and CABG-PS conditioning, hematoxylin/eosin (H&E) and Masson's trichrome staining of transversally cut sections were performed. Furthermore, immunofluorescence (IF) analysis for smooth muscle cells (SMC) marker αSMA and for endothelial cell (EC) marker vWF and CD31 were carried out in order to evaluate the impact of pulsatile pressure on the organization and arrangement of these cellular components.

Cultured (*n=6* VP, and *n=6* CABG-PS treated samples) and control (*n=11*) SV samples were fixed with 4% formaldehyde overnight, paraffin embedded, and cut in 5-µm-thick sections using a microtome. Sections were stained with H&E and Masson's trichrome staining (Bio-Optica Milano SpA, Italy), according to manufacturer's protocol. Six slices of each SV sample were observed for qualitative inspection, and digital images were acquired using a light microscope (AxioVision Bio Software, Carl Zeiss®, Germany) at a magnification of 10x.

For IF analysis, 3 samples for each group (VP, CABG-PS and related controls) were observed (6 slices for each sample). Briefly, 4-µm-thick sections were obtained from formalin-fixed/paraffin-embedded SV specimens. Sections were dewaxed and hydrated, and antigen retrieval was performed with 10mM Tris-HCL/1mM EDTA for 10 minutes in microwave. Therefore, sections were blocked with 3% bovine serum albumin (room temperature, 1 hour), and incubated (4°C, overnight) with mouse anti human-αSMA

(1:500; cat. M-0851, Dako) for labeling SMCs, goat anti human-CD31 (1:200; cat. sc-1506 Santa Cruz Biotechnology, Inc.) and rabbit anti-human vWF (1:200; cat. A-0082, Dako) for labeling endothelial cells (ECs). Slides were incubated with Alexa Fluor 488 anti-mouse, Alexa Fluor 546 anti-goat, and Alexa Fluor 633 anti-rabbit (1:200; Invitrogen, UK) secondary antibodies for 1 hour at room temperature, and nuclei were counterstained with DAPI (Vector Laboratories, CA, USA). Finally, digital images were obtained using a multicolor detection protocol in a LSM-710 confocal scanning microscope (Carl Zeiss®, Germany).

For Ki67 staining, 3 samples for each group (VP, CABG-PS and related controls) were observed (6 slices for each sample). 3,3'-diaminobenzidine (DAB) substrate kit (SK-4100, Vector Laboratories) were used. Briefly slides were placed in 10 mM Sodium Citrate Buffer, 0,05% Tween 20, pH 6.0 and heated at 98°C for 10 minutes for antigen retrieval. Sections were blocked with 3% BSA in 0.1% Triton X-100, moreover for blocking the endogenous peroxidase, sections were incubated in 3% H_2O_2, 0.1% NaN_3 for 10 minutes. Slides were incubated with primary Ki-67 antibody 1:100 (Abcam, Cambridge, UK, ab15580) for 1 hour at room temperature and subsequently incubated with biotinylated secondary antibody for 30 minutes at room temperature. Then the slides were incubated with horseradish peroxidase for 30 minutes; application of diaminobenzidine hydrochloride chromogen for 10 minutes were performed. Slides were counterstained with hematoxylin staining and were mounted on a slide using Canada balsam.

3.2.3 Morphometric and proliferation measurements

Morphometric analyses were performed on Masson's trichrome stained sections in order to measure wall thickness and luminal perimeter. One section for each sample was used. Thickness measurements were manually processed on digital images taken with AxioVision Bio Software (Carl Zeiss®, Germany) at 10X magnification. At least 40 measurements per sample were made. The inner perimeter was calculated using Image-J software (Version 1.47f-sofware for Java, National Institutes of Health, USA).

The cross sectional area of the sample was estimated assuming a circular shape and taking into account the wall thickness and the luminal perimeter. The cross sectional area (A) was calculated as follow:

$$A = w\,(\pi\, w + p_{inner}) \quad (1)$$

where w is the wall thickness and p_{inner} is the inner perimeter.

To measure the vasa vasorum length density (Pesce *et al.*, 2003), H&E stained sections of native (n=12), VP (n=6), and CABG-PS (n=6) samples were analyzed. Digital images were acquired using a light microscope (Carl Zeiss®, Germany) at a magnification of 40x. Using the AxioVision Bio Software (Carl Zeiss®) major and minor axes of each vasa vasorum were measured in a range comprised between 4μm and 44μm (three subsets were identified: 4-14 μm, 14-24 μm, and 24-44 μm). The classification of the vasa vasorum was performed based on the minor axis assumed as representative of the diameter. The length density was calculated for each interval according to:

$$L_d = \frac{\sum_{i=1}^{n} R_i}{A_d} \quad (2)$$

for i vasa vasorum counted in a given adventitial area (A_d), the length density (L_d) corresponds to the sum of the ratios (R_i) between the major and the minor axes of each vasa vasorum (Pesce *et al.*, 2003). In addition, vasa vasorum displaying no luminal region were not considered for morphometric determination of the length density. The adventitial area (A_d) was calculated on digital micrographs (2.5x) after manual contour identification using GIMP (Version 2.6.12) and Image-J software (Version 1.47f-sofware for Java, National Institutes of Health, USA).

The number of proliferating cells in the tunica media was analyzed by Ki67/Hematoxylin immunohistological staining in native (*n=6*), VP (*n=3*), and CABG-PS (*n=3*) samples. Digital images were acquired using a light microscope at a magnification of 20x. For each samples at least 5 randomly chosen fields were acquired. A manual counting protocol of $Ki67^{+}$ cells was performed by using Image-J software. The quantitative analysis of positive cells for Ki67 was accomplished by only one observer and in a blinded fashion. The number of proliferating cells was normalized to the total cell number. In addition, the cell density was evaluated by normalizing the total cell number to the area of the tissue. The area of the tissue was calculated on digital micrographs (20x)

using Image-J software (Version 1.47f-sofware for Java, National Institutes of Health, USA).

3.2.4 Epigenetic profiling for histones modifications analysis

The role of mechanical strain on the epigenetic landscape modifications was examined by immunofluorescence. This method has been already validated in a previous work (Minetti *et al.,* 2006). The changes in histones H3 (methylation of lysine 4) and H4 (acetylation of lysine 9 and 16) post-translational modifications were mainly monitored in CABG-PS group. This technique allowed the identification of single cell types presented in the tissues by co-staining with cell type-specific antibodies for AcK9 (acetylation of lysine 9), AcK16 (acetylation of lysine 16) and MetK4 (methylation of lysine 4). Cell nuclei were counterstained with TO-PRO®-3 (Invitrogen, UK). In addition, by using confocal microscopy analysis, it was possible to obtain information on the modification level by observing the relative increase in the mean fluorescence intensity (2.5D quantification) of the cell nuclei in tissues treated with mechanical stimuli.

3.2.5 Protein assays

Zymographic analyses were performed on SVs sections to investigate the proteolytic activity of matrix remodeling enzymes MMP-2 and MMP-9. These enzymes are involved in the remodeling of the cardiovascular tissues, and in particular of the blood vessels (Berard *et al.,* 2013; Berceli *et al.,* 2006; Dummler *et al.,* 2011).

Frozen tissues were homogenized in zymogram buffer (50 mM TrisHCL, 150 mM NaCl, 1 μm $ZnCl_2$, 0.01% Triton X-100, 2 mM EDTA pH 7.4). Samples were centrifuged at 4°C, the supernatant containing proteins was removed and 50 μg of extracted protein were mixed with zymogram loading buffer (62.5 mM Tris/HCl, pH 6.8, 10% glycerol, 2% SDS, 0.01% bromophenol blue) and separated in 10% SDS-PAGE gels containing 1 mg/ml type A gelatine from porcine skin (SIGMA-Aldrich, Taufkirchen, Germany). To renature proteins, gels were washed two times in 2.5% Triton X-100 for 15 min at room temperature and subsequently incubated in developing buffer (200 mM NaCl, 50 mM Tris, 20 mM CaCl2 pH 7.4) overnight at 37°C. Gels were stained with 0.5% Coomassie Blue

R250 in 45% methanol/10% acetic acid/ 45% water for 15 min and destained until clear bands of lytic activity appeared.

In addition, Western Blotting analysis was performed. Frozen samples were lysed in SDS lysis buffer (2% SDS, 50 mM Tris, 10% Glicerol pH 6.8) and prepared for sodium-dodecyl sulfate–polyacrylamide gel electrophoresis (SDS–PAGE). Lysates were sonicated and boiled, the protein concentration was determined by DC Protein Assay kit (BioRad). 50 µg of extracted protein were loaded in a SDS gel, 10% Acrilamid, after running proteins were transferred to a PVDF membrane and incubated in a primary antibody solution directed to α-SMA actin (1:5000; M-0851 Dako), tissue metallo-proteinases inhibitor-1 (TIMP-1) (1:1000; cat. 8946, Cell Signaling Technology), and GAPDH (1:5000; cat. sc-25778 Santa Cruz Biotechnology). Incubation was followed by washes in a 0.1% PBS-Tween buffer for 1 hour; following membranes were incubated and agitated in anti-mouse (cat. 61-6520, Invitrogen, UK) or anti-rabbit (cat. 65-6120, Invitrogen, UK) horseradish peroxidase for 1 hour. Membranes were washed in 0.1% PBS-Tween and then subjected to ECLR chemiluminescence detection (Amersham Life Sciences).

3.2.6 Statistical analysis

Statistical comparison was performed using Graph-Pad 5 (Prism) statistical software. All data were initially analysed with the Kolmogorov-Smirnov normality test and then compared using an paired t-test, unpaired t-test and a Mann-Whitney rank sum test, where appropriate. Differences were considered to be significant at values of $p < 0.05$.

3.3 Results of the human SVs pressure stimulation

At the end of the mechanical conditioning period, the vessels were un-mounted and immediately processed for different investigations.

3.3.1 MTT and Ki67 staining reveal metabolic and proliferative activity, and a reduction of the cell density after 7 days of culture in the EVCS

The MTT analysis showed that after 7 days under VP (Figure 3.2 A) or CABG-PS (Figure 3.2 B) conditions the vessel viability was maintained similarly to freshly harvested SV rings, used as a positive control (Figure 3.2 C).

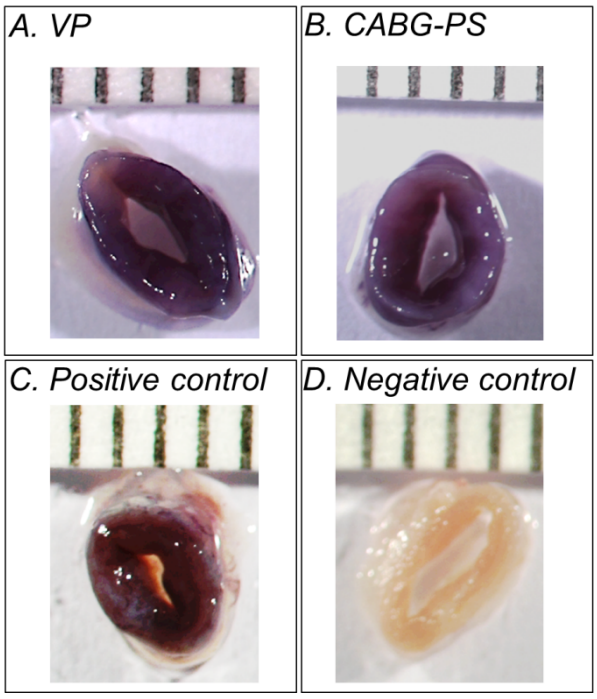

***Figure 3.2**. Images of SV rings stained with MTT after 7-days culture in the EVCS under VP (A), and CABG-PS (B) conditions. Fresh tissue and formaldehyde-fixed tissue were used as positive (C) and negative (D) control, respectively. The images in the figure are representative of the behaviour observed for 3 VP and 3 CABG-PS samples and related controls.*

The results of cell density showed a statistically significant decrease of the cell number on SV samples subjected to CABG-PS (Figure 3.3 D, *left*), while no significant differences between native SVs and SVs subjected to VP were observed (Figure 3.5 D, *right*).

Furthermore, the results of Ki67 staining in the SV wall, subsequent to application of the mechanical strain, highlighted differences in the response of VP *vs*. CABG-stimulated SV segments; in fact, as shown in Figure 3.3 E, the percentage of $Ki67^{+}$ cells in vessels exposed to arterial-like wall strain (CABG-PS group) was higher than in SVs exposed to

venous perfusion (VP-group). Data showed a statistically significant increase of the proliferation rate on SVs subjected to CABG-PS condition with respect to native condition (Figure 3.3 E, *left*), while statistical comparison did not show differences between native SVs and SVs subjected to VP (Figure 3.3 D, *right*).

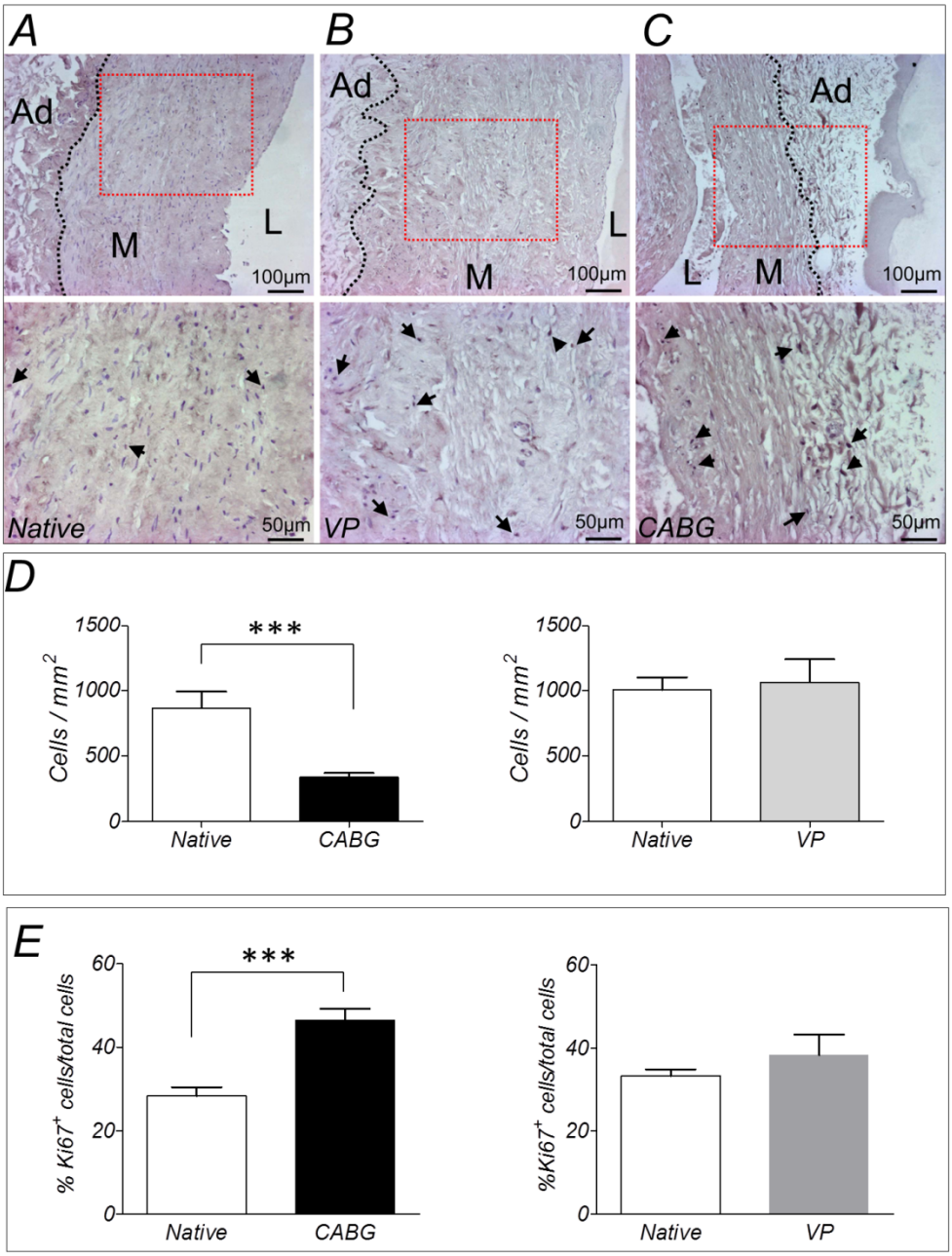

Figure 3.3. *Cell density and proliferation analysis. Representative Ki67/Hematoxilin immunohistological staining of SV samples: native SV (A), SV after VP (B), and SV after CABG-PS (C). Black arrows indicate the Ki67^{+} cells, while Ad, M and L represent the adventia, the median and the lumen of the vessel, respectively. Dotted lines indicate the border between media and adventitia. Quantification of cell density (D) and proliferation (E). Data were compared by an umpaired t-test, and *** indicates p<0.0001 for statistical comparison of Native, CABG-PS and VP veins.*

3.3.2 Morphological and immunofluorescence analyses show structural remodeling of the mechanically-conditioned human SV segments

To assess vessel wall integrity after VP and CABG-PS conditioning, Masson's trichrome staining of transversally cut sections was performed. Results showed a relatively good integrity of the vessel structure with a good preservation of SMCs and the adventitia layers, and without signs of tissue degeneration and swelling (Figure 3.4 A, B and C). Changes in cellular arrangement were instead observed in the VP (Figure 3.4 B) *vs*. CABG-PS (Figure 3.4 C) segments. In fact, in VP-cultured vessel segments (Figure 3.4 B), the arrangement of medial SMC layers appeared similar to that present in non-cultured vessels (Figure 3.4 A); by contrast, the application of CABG-PS caused an almost complete SMCs disarrangement (Figure 3.4 C).

To better evaluate the organization and arrangement of cellular components of the SV following *ex vivo* culture, IF analysis for SMC marker αSMA was performed (Figure 3.4, *right column*). Low magnification imaging of the vessels confirmed a difference in the medial layer of CABG-PS *vs*. VP vessels, again suggesting a loss in circumferential SMCs sheets due to the modified pressure conditions (Figure 3.4 C, *right column*). The observation of the vessel structure by histochemistry and IF showed that vessels cultured under CABG-PS conditions had relatively thinner wall and larger lumen compared to VP or native vessels (Figure 3.4 A-C).

Morphometric analysis were performed on SV sections in order to quantify wall thickness and luminal perimeter alterations. Computer-assisted morphometry indicated, according with literature data (Voisard *et al.,* 2010), a significant reduction of the vessel thickness (327.3±40.5μm *vs.* 575.5±60.8μm) and an increase in the lumen perimeter (12.10±1.14mm vs. 8.77±0.49mm) in CABG *vs*. non-stimulated SV segments (Figure 3.4 D and E, *left column*). Interestingly, veins perfused with a VP did not undergo remodeling, confirming that application of a CABG-PS for 7 days was sufficient to induce structural changes in the SV (Figure 3.4 D and E, *right column*). Finally, cross-sectional area measurements were performed on SV sections stained with Masson's thrichrome staining (Figure 3.4 F). Statistical comparison did not show differences between native SVs and ones subjected to CABG and VP conditioning.

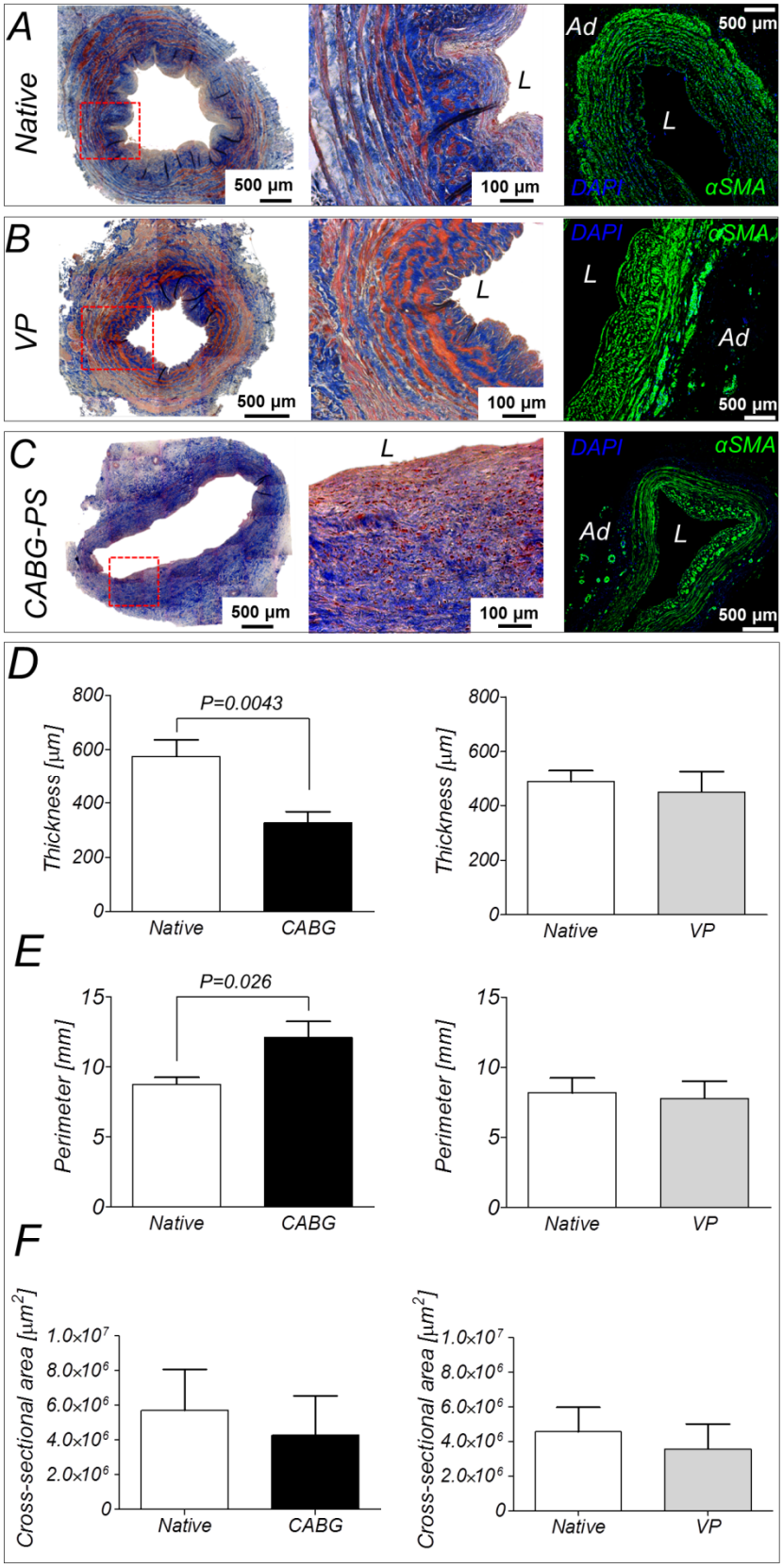

Figure 3.4*. SV tissue sections stained with Masson's trichrome and α-SMA/DAPI after 7-days culture in the EVCS. The images are representative of the behaviour observed for 3 VP and 3 CABG-PS samples and related controls. In each panel, from left to right, low and high power views of Masson's trichrome stained section and low power views of α-SMA stained sections are shown in native tissue (A), VP-cultured (B), and CABG-PS (C) SV samples, respectively. In all images, L indicates the lumen, while Ad the adventitia layer. Thickness (D) and inner perimeter (E) measurements were performed on SV sections stained with Masson's trichrome staining. Thickness and luminal perimeter data were compared by a non-parametric Mann Whitney test; the p value above the bar graph indicates the significance level in these comparisons. The graphs without p value indication indicate absence of statistical significance. (E) Cross-sectional area measurements were finally performed on SV sections stained with Masson's thrichrome staining. Data collected from the samples were compared by a non-parametric Mann Whitney test; the absence of p value above the bar graph indicates the absence of statistical significance.*

Histological analyses did not allow to evaluate whether the SV endothelium is affected by changing in pressure conditions in CABG-PS vessels. To assess this, an IF analysis for endothelial markers vWF and CD31 was performed, followed by low and high power confocal imaging (Figure 3.5). Panels A, B and C show, respectively, low and high power views of the EC layer stained in the same vessels presented in Figure 3.4 A, B and C. While at low magnification the appearance of the endothelial layer is similar in the three conditions, the high power views showed the loss of ECs integrity and the partial detachment of the EC layer in CABG-PS with respect to the native and VP-stimulated veins (compare panels 3.5 C with 3.5 A and 3.5 B). White arrows indicated $vWF^{+}/CD31^{+}$ ECs lining the SV lumen. Lower immunostaining in the CABG-like (Figure 3.5 C) *vs.* VP (Figure 3.5 B)/native (Figure 3.5 A) vessels highlighted an evident endothelial cell rupture as confirmed by partial detachment of the cell from the basal lamina (*, Figure 3.5 C).

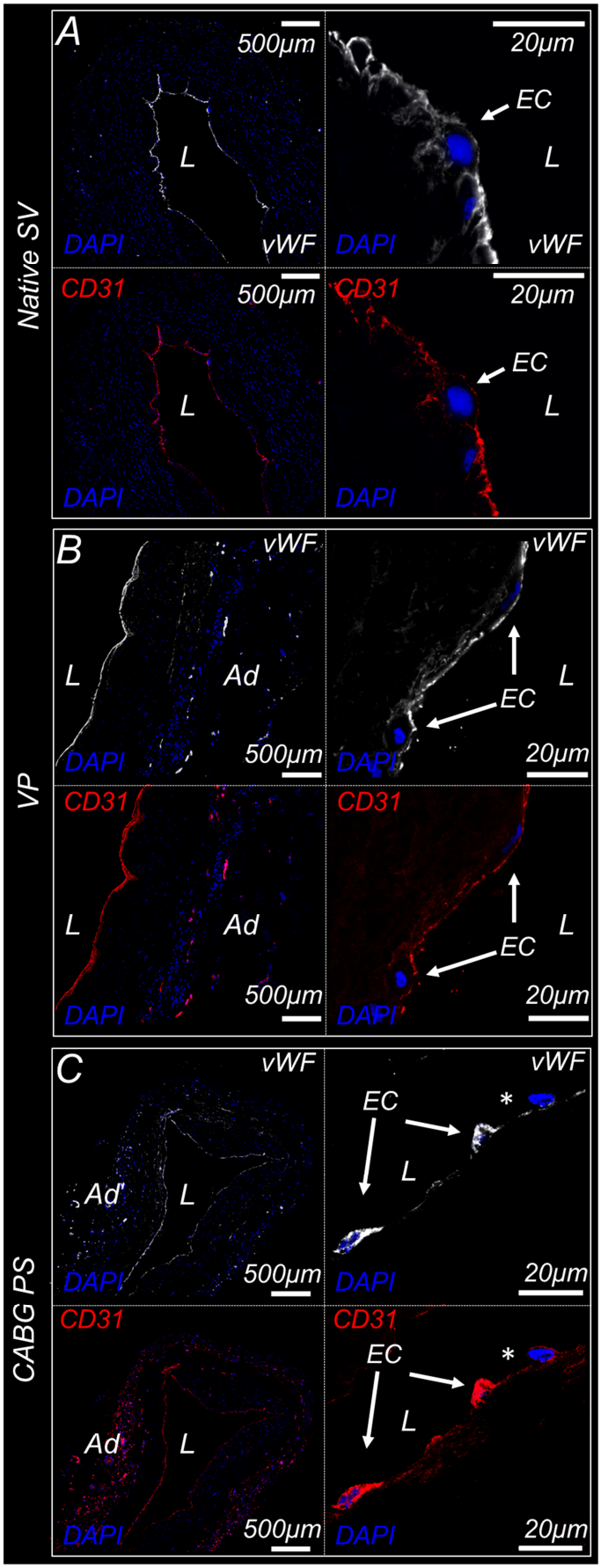

Figure 3.5. *Low and high power views of representative IF images in native (A), VP-cultured (B) and CABG-PS (C) SV samples tissue sections stained with vWF and CD31 specific antibodies. In all panels, L indicates the vessel lumen and Ad the adventitia layer. Arrows in the panel show $vWF^{+}/CD31^{+}$ ECs lining the SV lumen. Note the lower immunostaining in the CABG-like (C) vs. VP (B)/native (A) vessels and evident ECs rupture as indicated by partial detachment of the cell from the basal lamina (*).*

3.3.3 CABG-like pressure stimulation induced morphological remodelling and epigenetic mutations of SV vasa vasorum structures and cells

Exposure of SV segments to arterial-like pressure induced changes and disarrangement in the structure of *vasa vasorum* (Figure 3.6 C). By contrast, veins perfused under VP condition did not undergo *vasa vasorum* remodeling (Figure 3.6 B).

The vasa vasorum length density was also evaluated (Figure 3.6 D). In CABG-PS group (Figure 3.6 D, *left column*), data revealed a statistically significant increase of the length density of the vasa vasorum in the range 24-44 μm, while in the VP group (Figure 3.6 D, *right column*), statistical comparison did not show differences between native SVs and SVs subjected to VP conditions.

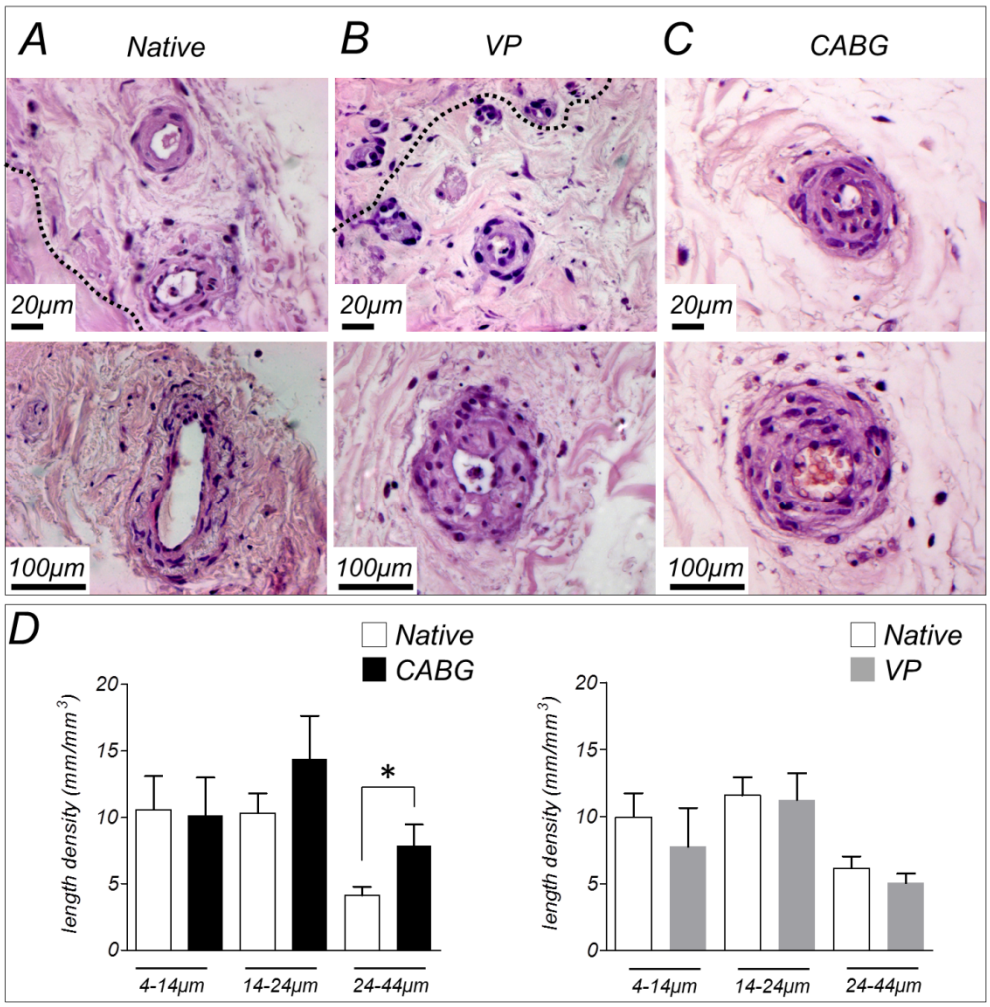

Figure 3.6. *Remodelling of the SV vasa vasorum. Representative H&E stain section of vasa vasorum of native (A), VP (B) and CABG-PS (C) samples. Vasa vasorum length densisty analysis were finally performed on SV sections stained with H&E staining. Dotted lines indicate the border between media and adventitia. Data collected from the samples were compared by a non-parametric Mann Whitney test; the * ($p < 0.05$) above the bar graph indicates the significance level in these comparisons. The graphs without * indicate absence of statistical significance.*

Up-regulation of the AcK9, AcK16 and MetK4 levels were observed in CABG-PS group. In fact, by comparing the 2.5D graphs of the native (Figure 3.7 A) and CABG-PS group (Figure 3.7 B), the pixels intensity was higher (read peaks) in CABG-PS group with respect to native control. Interestingly, these phenomena involved cells of the *vasa vasorum.*

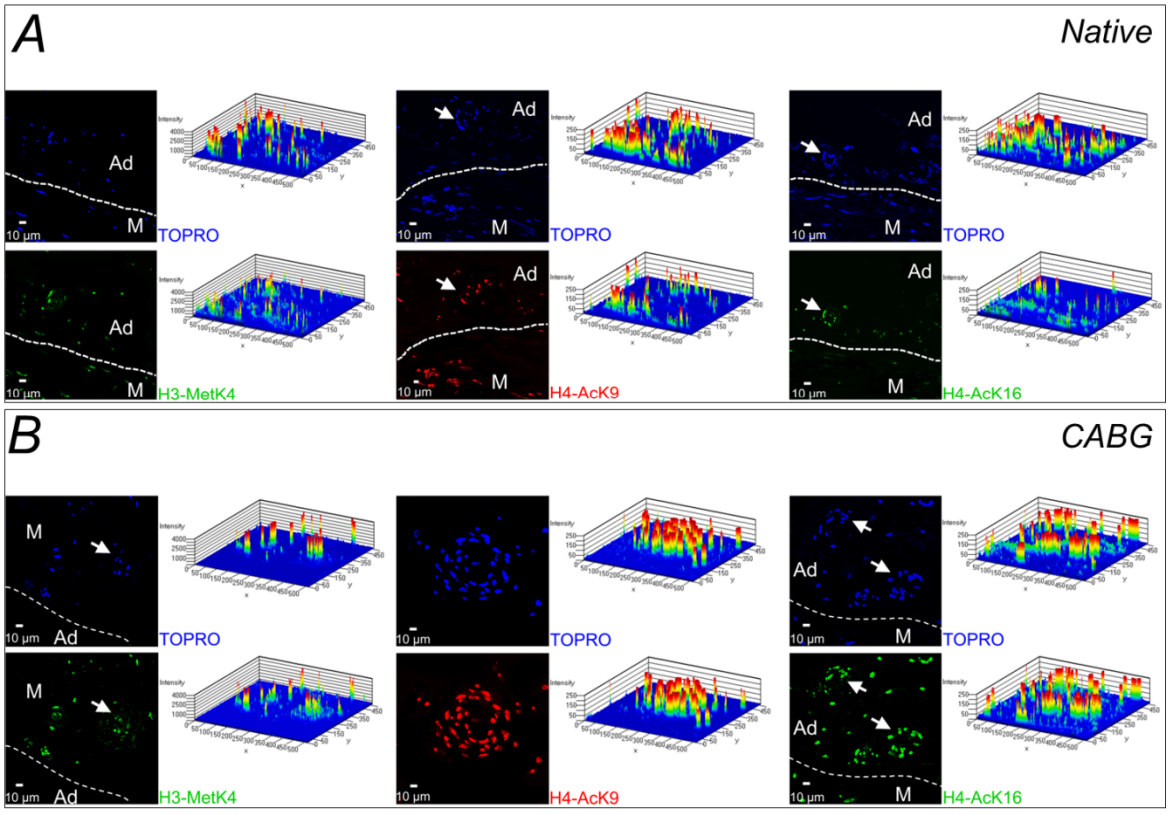

Figure 3.7.*Comparison of epigenetic mutation of the histones H3and H4 between native (A) and CABG-PS group segments (B). Ad and M indicates the advential region and the media layer of the SV, respectively. The white arrows indicate the vasa vasorum. Graphs 2.5D showed the quantification of the pixels intensity which was related with the level of acetylation/methylation.*

3.3.4 Protein analyses confirm the remodelling of mechanically-conditioned human SV segments

To assess whether the morphological rearrangement, observed in CABG-stimulated samples, actively involved vessel-resident cells, a zymography to detect metallo-proteinases activity (Figure 3.8 A and B) and western blot (Figure 3.8 C, D and E) analyses were performed. As shown in Figure 3.8 (A and B), and according to previous reports (Meng *et al.*, 1999), the MMP-2 and MMP-9 were activated in both CABG-PS and VP conditions. On the other hand, testing the TIMP-1 (Figure 3.8 C, D and E) by western blot analysis showed a lower expression in CABG-PS *vs.* VP condition, thus justifying the

lower remodelling observed in VP samples compared to veins exposed to arterial wall strain. In addition, western blot analysis showed a significant reduction of the αSMA content in CABG-PS samples, confirming a remodelling of the SMCs and supporting the loss in circumferential SMCs sheets due to the modified pressure conditions (Figure 3.4 C).

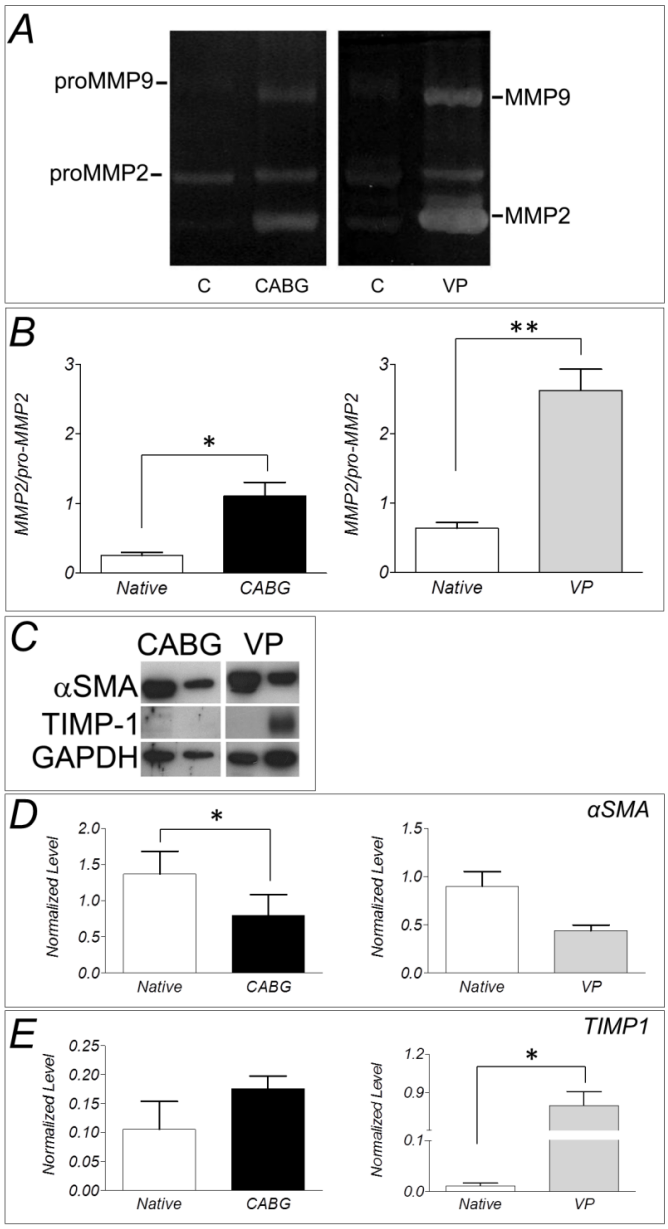

***Figure 3.8**. Results of the zimography analysis (A) Quantification of the MMP-2 upregulation in CABG and VP treated samples (B). C is the control. Results of the western blot analysis (C) for αSMA and TIMP-1. Quantification of αSMA(D) and TIMP-1 (E) expression normalized to GAPDH level. A paired t-test for was used to evaluate statistical significance between Native, CABG-PS and VP veins. The * ($p < 0.05$) and ** ($p < 0.001$) above the bar graph indicate the significance level in these comparisons.*

3.6 Comments to the arterialization study results

A major interest for vascular biologists in developing devices to perform vessel biomechanical conditioning, consists in the possibility to investigate the specific contribution of hemodynamic forces involved in vessel pathologies. In particular, platforms able to apply arterial-like pressure patterns to vein segments may be crucial to solve the timely issue of graft patency reduction following CABG surgery, a very frequent side effect of arterialization in patients receiving venous grafts (Owens 2010; Piola *et al.*, 2012).

Two major biomechanical components are believed to contribute to vein arterialization; these are the flow-related shear stress, which is increased in CABG due to a raise in flow velocity, and the wall stress/strain, which is also increased due to a switch from venous to arterial pressures (John 2009). Flow shear stress and wall strain may have antagonistic functions in vein arterialization process. In fact, arterial shear stress enhances the EC release of vaso-relaxing molecules such as Nitric Oxide which is also known to inhibit neointima formation (Berard *et al.*, 2013; Gusic *et al.*, 2005a). By contrast the wall strain is involved in the remodeling of the venous wall, causing the reduction of the SV thickness, and the mechanical rupture of the endothelial layer and the underlying SMC sheets (John 2009; Owens 2010; Saucy *et al.*, 2010).

In a wider view of addressing the role of the different mechanical components involved in IH, the approach followed in the present doctoral project confirms an important contribution of arterial-like wall strain in SV structural changes. The model system used here has been devised to obtain original information on the effects of arterial-like wall strain on structural (present work) and molecular (ongoing activities) changes, predisposing SV to remodeling events observed in human CABG transplantation. Our data indicated a clear thinning of the SV wall and a marked enlargement of the luminal perimeter, two parameters which have been found significantly changed during arterial positioning of vein segments in patients and animal models ((Owens 2010) and reference therein). Interestingly, the cross-sectional area of the tissue (thus the mass of the vessel wall) did not change after 7 days of arterial-like pressure stimulation. Taking together these results demonstrate a reorganization of the cellular/matrix elements of the vessel during the early stage of the pathological adaptation of the SV to the new hemodynamic environment.

The thinning of the vessel wall is in part related with a significant decrease of cell density as reported in literature (Chen *et al.,* 2013; Miyakawa *et al.,* 2008; Voisard *et al.,* 2010). Decrease of cell density was followed by a significant increase in cellular proliferation rate. These latter findings are in accordance with reports of Miyakawa (Miyakawa *et al.,* 2008) and Voisard (Voisard *et al.,* 2010), showing a first signs of reactive cell proliferation after days. In addition, we observed a contribution of the CABG-PS to determine microscopic ruptures in the endothelial layer and a striking disarray in the SMC layers in the medial tissue, two factors known to predispose the vessel to pathologic remodeling (Motwani and Topol 1998). Exposure of SV segments to CABG-PS induced changes in the histones H3/H4 acetylation/methylation levels, especially in adventitial cells and cells of the *vasa vasorum*. This correlates with an increase in *vasa vasorum* length density (range 24-44 μm) and their structural disarrangement. These changes were accompanied by up-regulation of MMP-2 and MMP-9 and differential activation of TIMP-1. Taken together, these results showed that application of pure pulsatile pressure (80-120 mmHg) was sufficient to induce a major structural rearrangement in the SV wall. These results were in agreement with previous investigations (Miyakawa *et al.,* 2008; Saucy *et al.,* 2010; Voisard *et al.,* 2010).

In this work, experiments of 7 days were carried out on purpose. In fact the purpose of the investigation aimed at studying the very early events induced by SV arterial-like pressure stimulation, to come up with a consistent model system to be used in molecular dissection of the initial events predisposing the vessels to develop neointima. Furthermore, literature data indicate that vessel mechanical damage occurring as a consequence of the arterialization is an immediate relevant cause for later restenosis.

At this stage of the project, studies are currently performed to investigate the establishment of cellular and molecular *pro*-pathologic pathways involved in the SV graft disease. In particular, ongoing analysis are aimed to identify microRNAs (miRNAs, short non-coding RNAs that regulate gene expression through post-transcriptional mechanisms) that are dysregulated (down or up regulated) during the early stage of the engraftment. The regulation of miRNA-21, miRNA-138, miRNA-146, miRNA-221, miRNA-126 and miRNA-220c will be analyzed and quantified by qRT-PCR analysis.

In summary, the compact and automated EVCS appears to be a well-suited system able to reproduce the wall strain conditions typical of the coronary circulation. The system maintains an optimal tissue viability, without signs of tissue degeneration and swelling, operates under sterility and performs vessel stimulation in a low-volume culture chamber. For these design characteristics this platform is therefore a novel laboratory-oriented tool that will be useful to carry out *in vitro* culture campaigns under controlled hemodynamic conditions and dissect the contribution of pressure and wall strain/stress involved in the early IH priming in vein CABGs.

4

Current upgrading of the EVCS for a better biomimicking

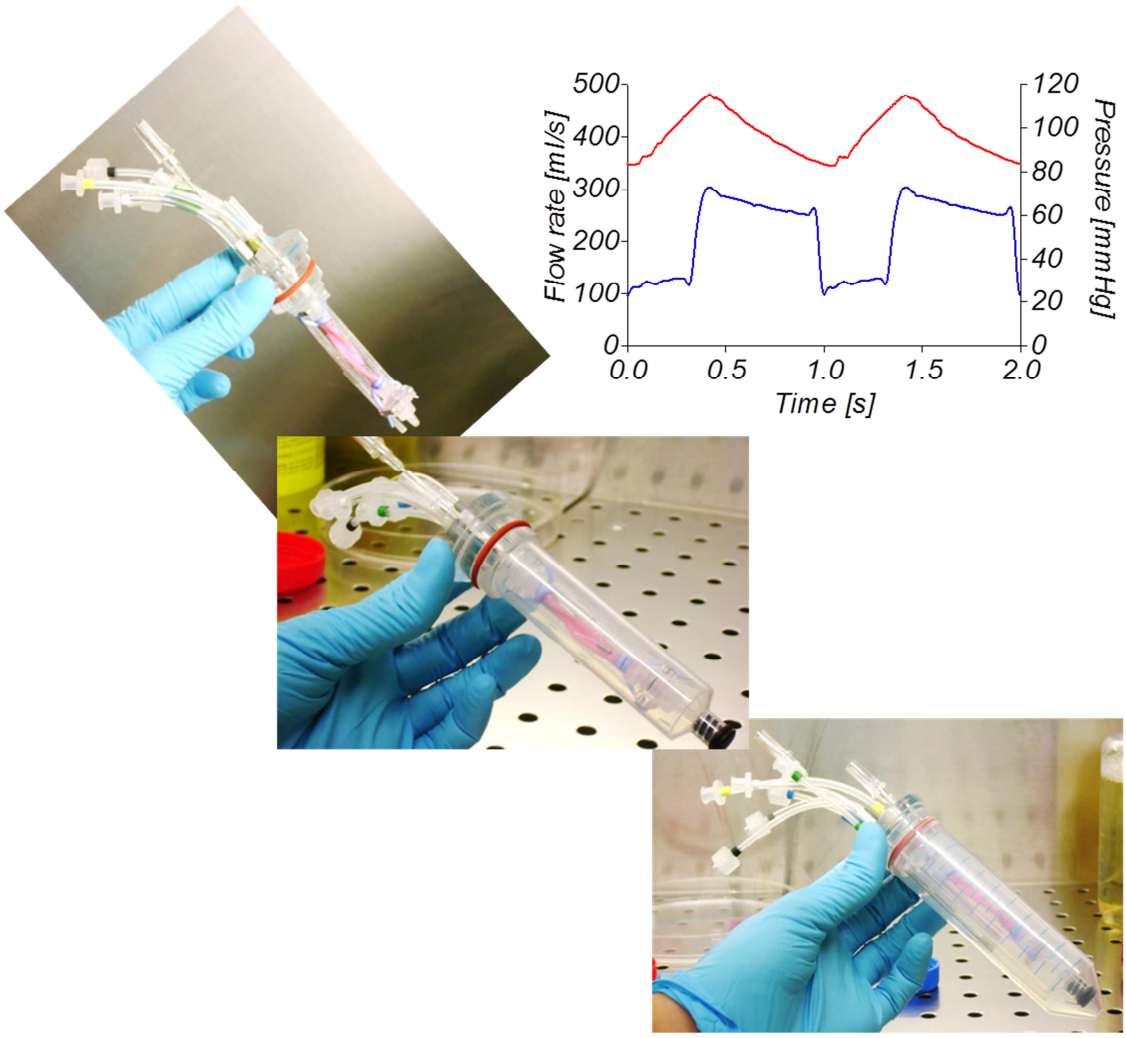

Introduction

In the present chapter, the development of a novel bioreactor platform, characterized by full mechanical/environmental bio-mimesis, starting from the basic bioreactor model previously described (*Chapter 2*) is presented. The work aimed to include biomimetic features into the existing devices in a cascade fashion: first, the separation between inner and outer vessel stimulation circuits was tackled (the double-compartment *ex vivo* vessel culture system, DC-EVCS, *paragraphs 4.1 and 4.2*), then the task of including full biomechanical control of CABG-like pressure and flow was attempted with integration of the coronary artery pulse duplicator circuit (CPD-EVCS, *paragraphs 4.3 and 4.4).*

The first upgrade (DC-EVCS) to the previous bioreactor version included a separated environmental control for the intra-luminal and extra-luminal culture media, giving the possibility to expose the intimal and the adventitial layers to distinct vessel chemical conditions (e.g. *hypoxia* of the adventitial layer, while blood-like oxygen condition of the lumen), thus mimicking the real status of CABG vessels *in vivo*. This configuration will also permit to expose the outer and/or the inner vessel compartments to pharmacologic conditioning *ex vivo*. The regulation of the oxygen tension in the outer medium was attained by means of a purpose-developed de-oxygenation module, whose dimensioning was carried out by combining mathematical modeling and experimental design using dissolved oxygen probing within the conditioned culture medium.

The CPD-EVCS was a further-improved bioreactor version, including the replication of the so-called ‘paradox’ behavior of central coronary circulation hemodynamics, consisting in pressure and flow peaks occurring in counter-phase in the systolic/diastolic intervals. The CPD-EVCS was conceived for providing a controlled and strictly reproducible biomechanical coronary environment.

The approach for the design and manufacture of the upgraded devices entailed a first phase of literature analysis, and interaction with the final user; on these bases, the general and functional requirements of the upgraded version of the bioreactor were identified, and a preliminary design of the system proposed. The design of the dynamic culture system made use of the 3D CAD software Pro/Engineering Wildfire 4.0 (Parametric Technology Corporation, PTC, Needham, MA), while the prototypes were manufactured using a parallel lathe (OPTI D 240x500 G-Vario, Optimum, DE), a numerical control machine (Roland MDX-40, Roland Corporation, Tokyo, JP), and a laser cutting (Versalaser

VSL2.30, SK Laser, Germany), plus additional manual finishing. These activities were carried out at the Laboratory of Experimental Micro and Biofluid Dynamics of the Dipartimento di Elettronica, Informazione e Bioingegneria of the Politecnico di Milano.

4.1 Evolution towards a double-compartment ex vivo vessel culture system

4.1.1 Design specification

The design of the double-compartment *ex vivo* vessel culture system (DC-EVCS) took into account the general specifications of a bioreactor for tissue engineering application (Martin *et al.*, 2004), with particular emphasis on the ease of assembly under laminar flow hood, and the safety of use in a cell culture laboratory (*Chapter 2*). In addition, the following requirements were addressed: *i)* separation between the intra-luminal vessel compartment and the outer extra-adventitial region, *ii)* integration of a fluidically independent second chamber reservoir, *iii)* integration of a de-oxygenator module in order to expose the intimal and the adventitial layers to distinct vessel chemical conditions, and *iv)* minimization of priming volume, in order to limit the cost of soluble culture medium compounds.

4.1.2 Architecture of the double-compartment ex-vivo vessel culture system

The DC-EVCS was manufactured for recapitulating the parenchymal tissue microenvironment and setting different intra-luminal and extra-adventitial environments (Figure 4.1).

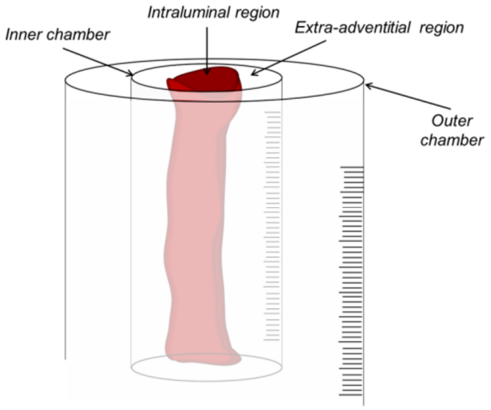

Figure 4.1. *Schematic rappresentation of the double-compartment culture chamber.*

A schematic representation of the system's layout is shown in Figure 4.2. During the culture, SV grafts are hosted in the inner culture chamber (Figure 4.2, *red chamber*), inserted in the outer culture chamber (the falcon reservoir). The entire culture chamber is then accommodated inside a cell culture incubator. Also in this version of the system, the culture chamber is connected to a hydraulic circuit and actuators (pump and solenoid pinch-valve) to apply pressure stimulation to the human vessels or to allow the medium recirculate within the vessel. The hydraulic actuators are managed by a programmable monitoring and control (M/C) system, which operates via a pressure-based feedback loop.

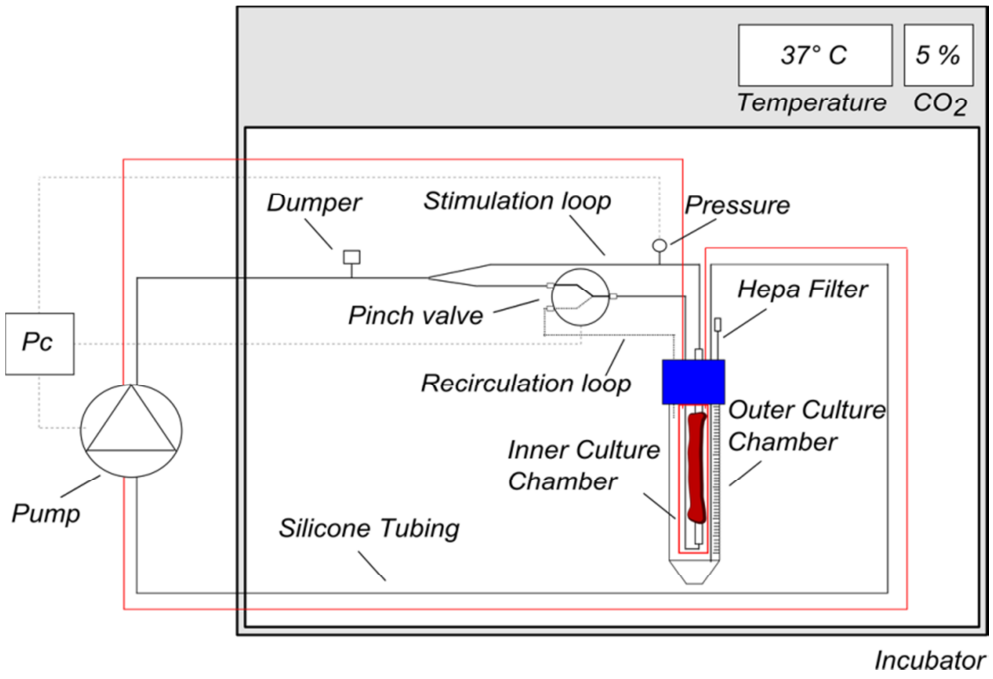

Figure 4.2. *Layout of the DC-EVCS: thick-black lines represent the hydraulic circuit connected to the outer culture chamber; thick-red lines represent the hydraulic circuit connected to the inner culture chamber (red chamber); thin-dot lines represent the monitoring and control (M/C) signals. In particular, the M/C system manages the hydraulic actuators (a pump and a solenoid pinch-valve) via a pressure-based signal registered by the pressure sensor.*

4.1.3 Double-compartment SV culture chamber

The DC-culture chamber (Figure 4.3) includes two commercial reservoirs and a purpose-developed vessel housing, which is integrated with the reservoir cap. All the culture chamber parts, built in house, are designed with 3D-CAD Pro/Engineer Wildfire 4.0 (PTC, Needham, MA), and manufactured by laser cutting (Versalaser VSL2.30, SK Laser, Germany), and/or computer numerical control machining (Modela MDX-40, Japan) from polymethylmethacrylate blocks (Plasting S.r.l., Segrate, Italy). All the utilized

materials are suitable for EtO sterilization. The length of the housing is reduced to host SV segments up to 5 cm in length. The hosted vessel segment is cannulated at both ends using polypropylene (PP) barbed fittings (Cole Parmer, IL, USA), and secured using an extensible vessel loop (Esafarma S.r.l., Italy) as an elastic tourniquet.

This version of the vessel chamber is also characterized by two distinct hydraulic circuits, fed by two different reservoirs (Figure 4.2). The culture medium contained in the inner reservoir (red chamber in Figure 4.2) constitutes the extra-adventitial milieu, while the outer chamber reservoir feed the stimulation circuit of the vessel. In this version, a 50-ml falcon tube (International PBI S.p.A, Italy) is used as outer chamber, while the inner chamber is made by a modified 20-ml syringe (Figure 4.2). The outer reservoir and the housing are coupled trough a silicone O-ring, while the syringe reservoir and the housing through mechanical interference.

Eight ports through the cap ensure the chamber's connection to the outside. Two ports ensure injection/removal of the culture medium to/from the vessel (Figure 4.3, port a and b). Two other ports provide connection for recirculation of the reservoir medium, *i.e*. the medium external to the hosted SV (Figure 4.3, port c and d). Two ports guarantee the connection to the stimulation circuit (Figure 4.3, port f and g). Two additional port provides communication with the incubator environment through a HEPA filter, to guarantee a sterile gas exchange while keeping the pressure inside the culture chamber atmospheric (Figure4.3, port e, and h).

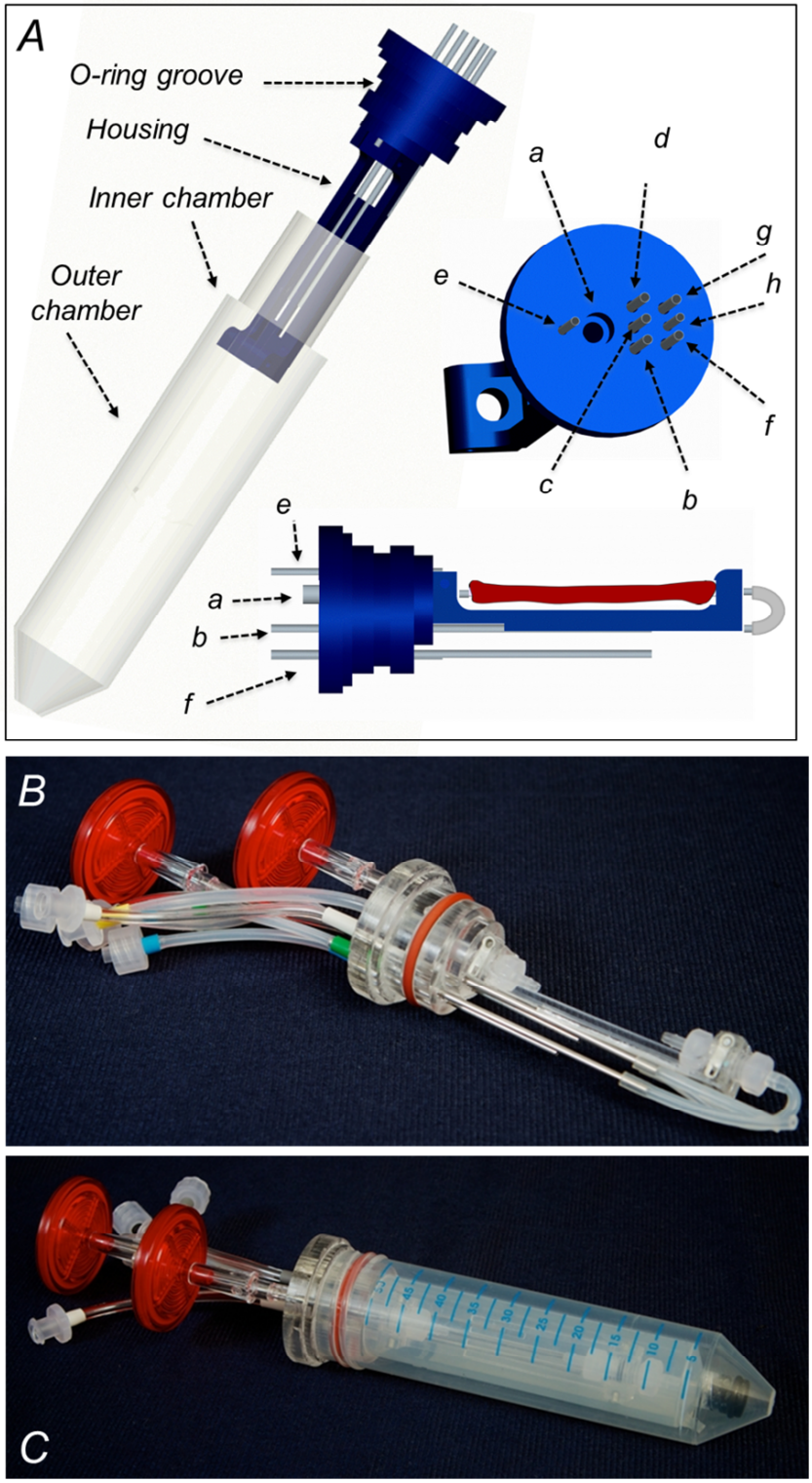

Figure 4.3. *(A) 3D CAD model of the DC-SV culture chamber. The chamber consists of the SV housing coupled with a siringe and then into a 50-ml falcon tube; a and b are the ports for the vessel connection sites; c and d are the ports for connecting the inner reservoir (siringe) to the hydraulic circuit; e is the port for HEPA filter of the inner reservoir; f and g are the ports for connecting the outer reservoir (falcon) to the hydraulic circuit; and h is the port for HEPA filter of outer reservoir. (B) Image of the DC- SV housing, with connectros and ports and (C) of the DC-EVCS coupled with the siringe and the falcon reservoir.*

4.1.4 The hydraulic circuit

Two independent fluidic circuit are connected to the DC-EVCS: *i*) the stimulation circuit (*paragraph 2.1.5*), and *ii*) an additional fluidic circuit connected to the de-oxygenator module. The aim of the de-oxygenation circuit is to lower the extra-adventitial compartment oxygen concentration to 4.9×10^{-5} mmol/ml, corresponding to an oxygen partial pressure of 38 mmHg (5% O_2). The circuit consists of a Watson-Marlow peristaltic pump (323 Du, Watson Marlow Group), with 314D pumping head (Watson Marlow Group), a de-oxygenation component and a low O_2 permeable hydraulic circuit. Figure 4.4 shows a schematic of the de-oxygenation circuit coupled with the DC-EVCS.

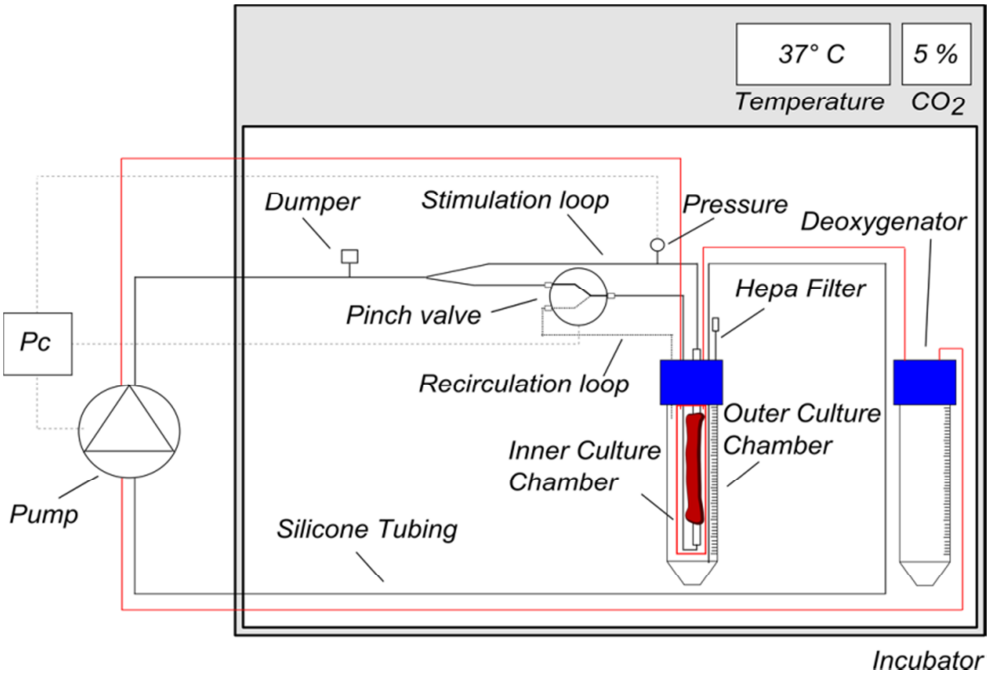

Figure 4.4. *Schematic of the DC-EVCS coupled with the deoxygenator module. The thick-black lines represent the hydraulic circuit connected to the to the outer culture chamber; thick-red lines represent the hydraulic circuit connected to the inner culture chamber and to the deoxygenator module; thin-dot lines represent the monitoring and control (M/C) signals.*

4.1.4.1 Dimensioning of the de-oxygenation circuit

In the present paragraph, a preliminary dimensioning of the de-oxygenation circuit is carried out by using the mathematical model of oxygen transfer described in the paragraph 2.1.4.1 (Orr and Burg 2008) (Figure 4.5). The tubing length (L), the recirculating flow rates in the de-oxygenator module (Q), and the oxygen concentration (C_{GAS}, gas side of the de-oxygenator module) were defined through the mathematical modeling. In the design phase

particular attention was dedicated to the size minimization, the limitation of pressure drops, and the achievement of the desired oxygen concentration in the adventitial medium.

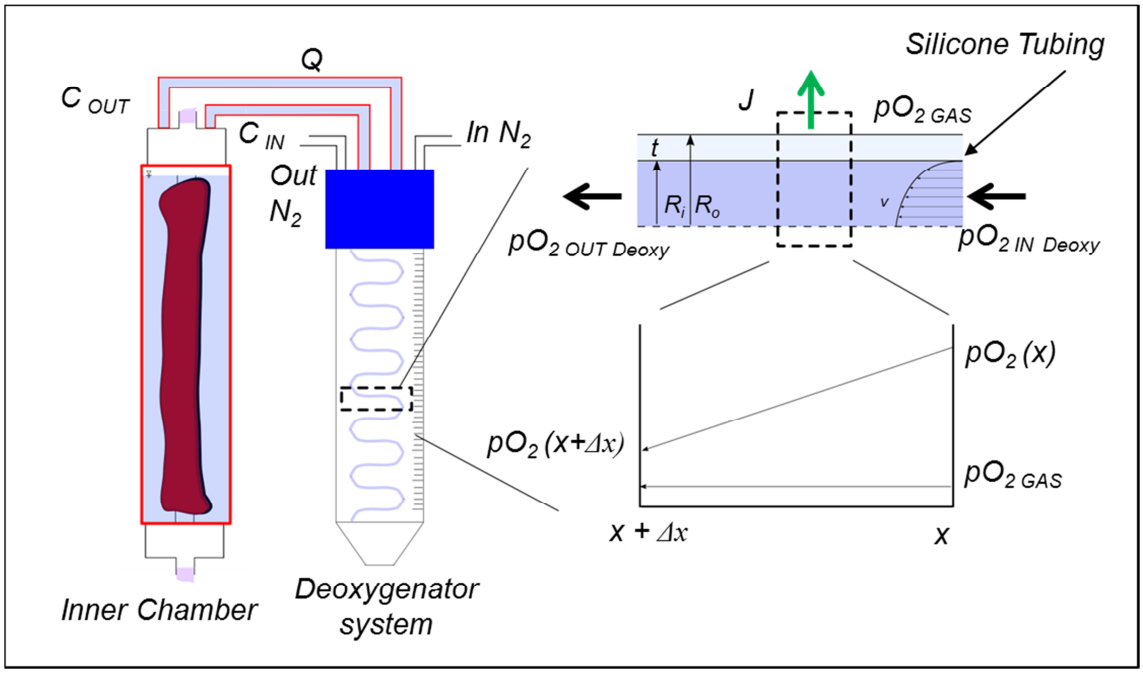

Figure 4.5. *Simplified scheme of the DC-EVCS consiting of the inner chamber and the deoxygenator flow circuit. Physical model of the multiple layers inherent to the silicone tubing membrane system used as deoxygenator. In the figure, C_{IN} and C_{OUT} are the oxygen concentration at the inlet and outlet of the inner culture chamber; In N_2 and Out N_2, are the inlet and outlet port for the nitrogen (N_2) connection line, and Q is the recirculating flow rate. With regard to the tubing, J is the local oxygen transfer per unit length crossing the tubing wall by diffusion (green arrow), t is the tubing thickness, Ro and Ri are the outer and inner radius respectively; v is the fluid velocity through the tubing; $pO_{2\ OUT\ Deoxy}$ and $pO_{2\ IN\ Deoxy}$ represent the oxygen partial pressures at the inlet and at the outlet of a silicone tubing of length L, pO_{2x} and $pO_{2x+\Delta x}$ are the oxygen partial pressures at the inlet and at the outlet of a generic infinitesimal tubing element of length Δx; pO_{2GAS} is the oxygen partial pressure within the deoxygenator chamber.*

Let us consider first the working principle of the de-oxygenator system in a hypothetical single pass condition, *i.e.* with the device fed with a non-recirculated fluid, whose pO_2 is at the equilibrium with air (160 mmHg or 21%).

According with the mathematical model (described in the paragraph 2.1.4.1 (Orr and Burg 2008)), O_2 partial pressure in the fluid at the end of the de-oxygenator silicone tubing ($pO_{2\ OUT\ Deoxy}$) is function of the oxygen level in the medium entering the de-oxygenator silicone tubing ($pO_{2\ IN\ Deoxy} = 160\ mmHg$), the O_2 partial pressure within the de-oxygenator system ($pO_{2\ GAS} = 0\ mmHg$, gas side), and the de-oxygenator silicone tubing length L:

$$pO_{2\ OUT\ Deoxy} = pO_{2\ GAS} - \left(pO_{2\ GAS} - pO_{2\ IN\ Deoxy}\right) e^{-\frac{UWL}{\alpha Q}} \qquad (11)$$

where U is the overall mass transfer coefficient of the silicone tubing, W the log mean of the inner and outer tubing circumference, α is the solubility coefficient of oxygen in the culture medium, and Q is the medium recirculating flow rate. Given a desired reduction in the fluid pO_2 caused by the de-oxygenator system, the necessary de-oxygenator silicone tubing length L is calculated as:

$$L = -\frac{\alpha Q}{UW} ln \frac{pO_{2\,GAS} - pO_{2\,OUT\,Deoxy}}{pO_{2\,GAS} - pO_{2\,IN\,Deoxy}} \tag{12}$$

Figure 4.6 shows the trend of L as a function of different medium recirculating flow rate and for a tube with an inner diameter equal to 0.8 mm, wall thickness of 0.8 mm. In the graphs, L is parameterized for different values of desired $pO_{2\,OUT\,Deoxy}$, imposing a $pO_{2\,GAS}$ equal to 0 mmHg.

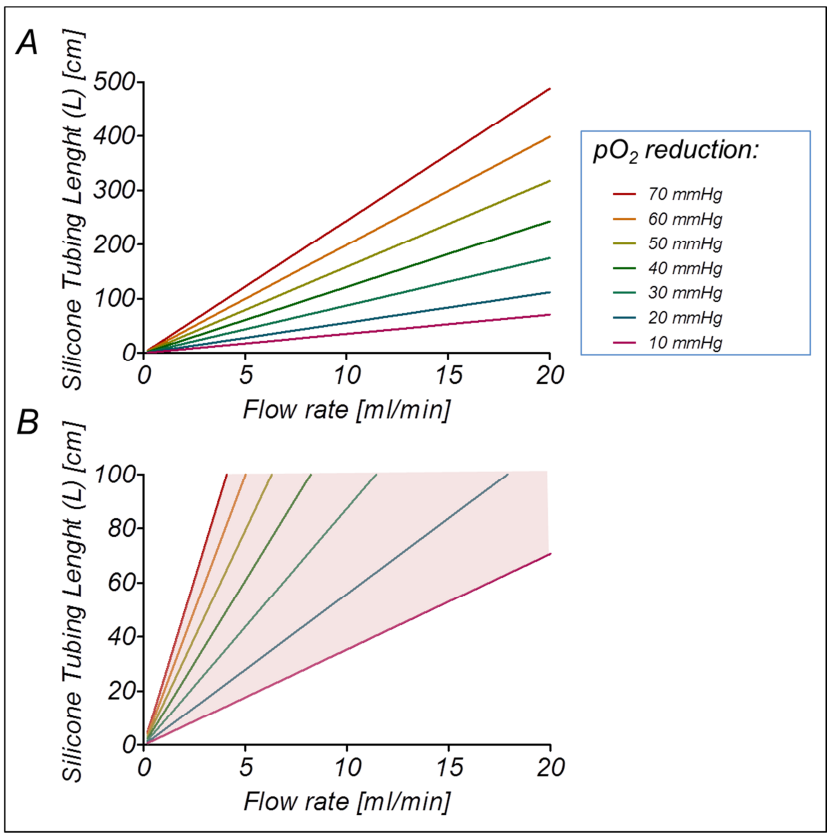

Figure 4.6. *(A) Length of the silicone tubing as a function of the recirculating medium flow rate. The tubing length is parameterized for different values of the desired reduction of fluid oxygen partial pressure at the outlet of the silicone tubing. The oxygen reduction is defined as:* $pO_{2\,IN\,Deoxy}$ - $pO_{2\,OUT\,Deoxy}$*.(B) The pink area higlights the suitable solution region (silicone tubing length < 100 cm) in the lenght/flow rate graph.*

Data emerging from the de-oxygenator dimensioning showed that as the flow rate increases the tubing length increases too. The length of the tubing represents a crucial point. Practical reasons related to encumbrance suggested to keep the de-oxygenator silicone tubing less than 100 cm in length. Thus, in order to minimize the pressure losses and to limit the overall priming volume, three possible lengths of the tubing (*20, 40 and 80 cm*) are chosen.

Let us now switch to the multiple-pass condition, *i.e.* with the fluid being recirculated, through the de-oxygenator system, to and from the reservoir that constitutes the extra-luminal environment of the vessel.

With the tentative length of the tubing (*20, 40, and 80 cm*) previously considered, the transient state of the system, consisting of the de-oxygenator module and the extra-adventitial chamber, may be analyzed (Figure 4.7) with the model. The aim of this analysis consists in evaluating the time necessary for the system to reach the steady state. Hence, for simplicity, any possible extrinsic cause for oxygen transfer towards the extra-adventitial chamber was ignored in the calculations.

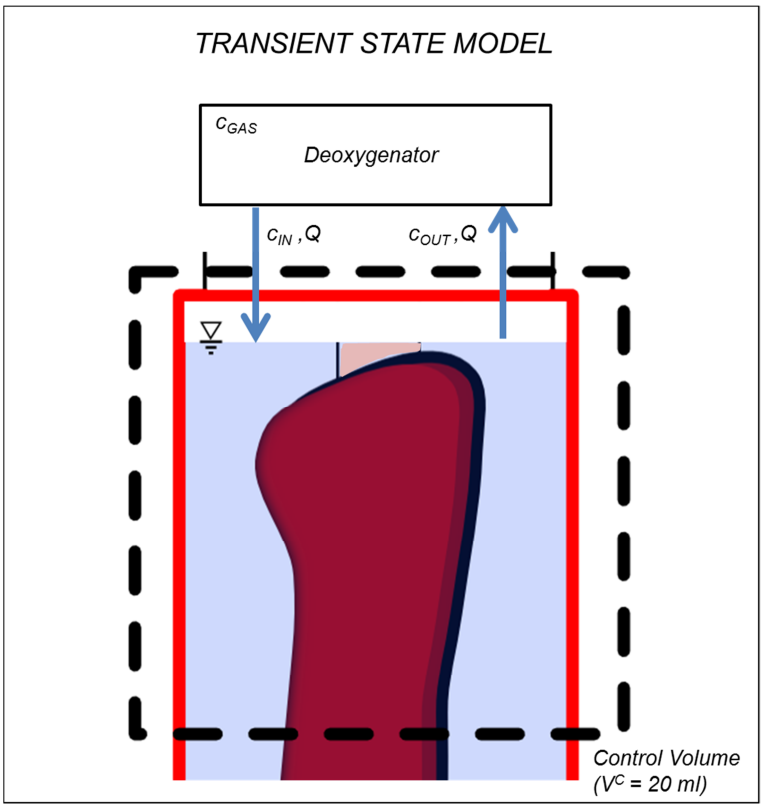

Figure 4.7*. Simplified compartimental model adopted for studying of the behavior of the deoxygenator system during the transient state. V^c is the control volume, c_{IN} e c_{OUT} are the oxygen concentration at the outlet and inlet of the V^c, Q represents the flow rate of recirculation of the fluid inside the compartment, and c_{GAS} is the oxygen concentration within the de-oxygenator module.*

Taking into account the Henry Law, the oxygen concentration (c) is given by:

$$c = \alpha\, p \tag{13}$$

where c is the concentration of the solute, p is the partial pressure of the solute, and α is the oxygen solubility coefficient equal to 1.31 μM/mmHg.
The mass balance across the control volume V^c (Figure 4.7) is:

$$V^c \frac{dc}{dt} = Q\,(c_{OUT} - c_{IN}) \tag{14}$$

where c_{OUT} and c_{IN} are the oxygen concentration at the outlet and inlet of the control volume V^c set equal to 20 ml of medium, which is the priming volume of the extra-adventitial chamber (Figure 4.7). Substituting equation (11), in term of concentrations, in equation (14), and imposing c_{IN} ($t=0$) equal to c_0 the following equation is obtained:

$$c_{OUT}(t) = c_{GAS} + (c_0 - c_{GAS})\, e^{-\left(\frac{Q}{V^C}\left(1-e^{\left(\frac{-UWHL}{Q}\right)}\right)\right)t} \tag{15}$$

where c_{GAS} is the oxygen concentration in the de-oxygenating gas (set equal to 0 mmol/ml) and c_0 is the initial oxygen concentration (set equal to 2.09×10^{-4} mmol/ml, corresponding to 160 mmHg, or 21% O_2).

In addition, the time constant (τ), and the limit time constant (τ_∞) of the system are calculated for each of the de-oxygenator silicone tubing length according with the following relations:

$$\tau = \frac{V^C}{Q}\left(1 - exp\left(\frac{-UWHL}{Q}\right)\right)^{-1} \tag{16}$$

$$\tau_\infty = \lim_{Q\to\infty} \frac{V^C}{Q}\left(1 - exp\left(\frac{-UWHL}{Q}\right)\right)^{-1} = \frac{V^C}{LUWH} \tag{17}$$

Figure 4.8 shows the trend of $c_{OUT}(t)$ for a silicone tube with an inner diameter equal to 0.8 mm, wall thickness of 0.8 mm, and different lengths (*i.e. 20 (A), 40 (B), and 80 (C) cm*). In the graphs, $c_{OUT}(t)$ is parameterized for different values of the recirculating flow rate, imposing a c_{GAS} equal to 0 mmol/ml and c_0 equal to 2.09×10^{-4} mmol/ml. The mathematical model highlighted that the system time constant τ behaves asymptotically at increasing values for Q, with the limit time constant τ_∞ depending upon silicone tubing length (Figure 4.8 D).

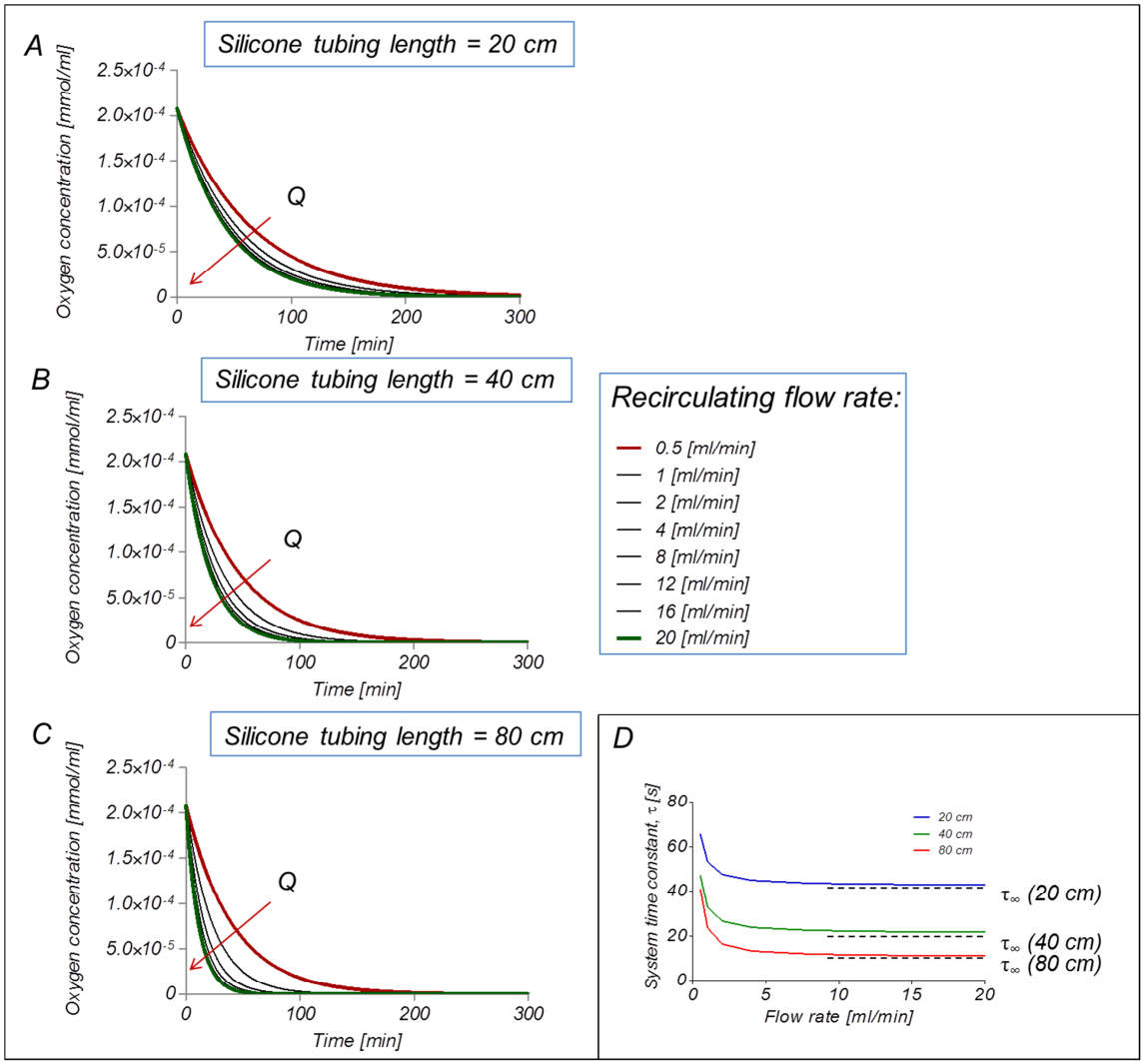

Figure 4.8. *Oxygen concentration (C_{OUT}) trend as a function of time. The oxygen concentration is parametrized for different values of recirculation flow rate (Q), and for different silicone tubing length: 20 cm (A), 40 cm (B) and 80 cm (C).* c_{GAS} *is set equal to 0 mmol/ml and* c_0 *equal to to 2.09* 10^{-4} *mmol/ml. (D) System time constant* τ *as a function of the recirculating flow rate (Q). Dot-lines represent the theoretical limit time constant* τ_∞.

By setting a 10% difference between the design time constant (τ^*) and the theoretical limit time constant ($\tau^* = 1.1\ \tau_\infty$), one can choose a reasonable optimal value of flow rate, Q^*, above which no significant enhancement is met concerning the time for the system to reach the steady state. The graphs in figure 4.9 show that as the length of the tubing increases the time constant decreases (Figure 4.9 A), while the value of the optimal recirculation flow Q^* increases (Figure 4.9 B).

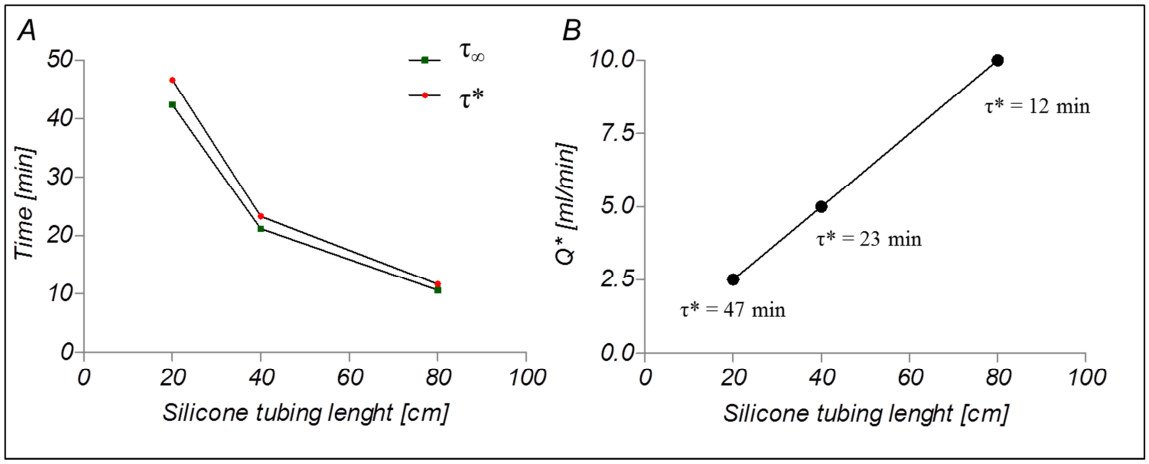

Figure 4.9. *(A) The graph shows the trend of time constant as a function of the silicone tubing lenght. (B) The graph shows the value of Q* as a function of the silicone tubing length L.*

Finally, it is possible to use the modeling approach to estimate the steady state behavior of the system (de-oxygenator and extra-adventitial chamber) in more realistic conditions, *i.e.* accounting for the possible sources of oxygen transfer towards the extra-adventitial environment, which tend to affect the deoxygenating process.

The aim of this analysis consists of evaluating the oxygen concentration in the de-oxygenator chamber necessary to maintain a venous oxygen concentration in the extra-adventitial region (set equal to 4.9 10^{-5} mmol/ml, and corresponding to 38 mmHg, 5% O_2). This modeling took into account the phenomena affecting the equilibrium state (*i.e.* the gaseous exchange between the inner culture chamber and the incubator environments occurring via the free surface of the medium ($VO_{2\,Atm\,Port}$), the oxygen transfer through the SV wall ($VO_{2\,Vessel}$), and the cellular oxygen consumption ($VO_{2\,Cells}$), Figure 4.10)).

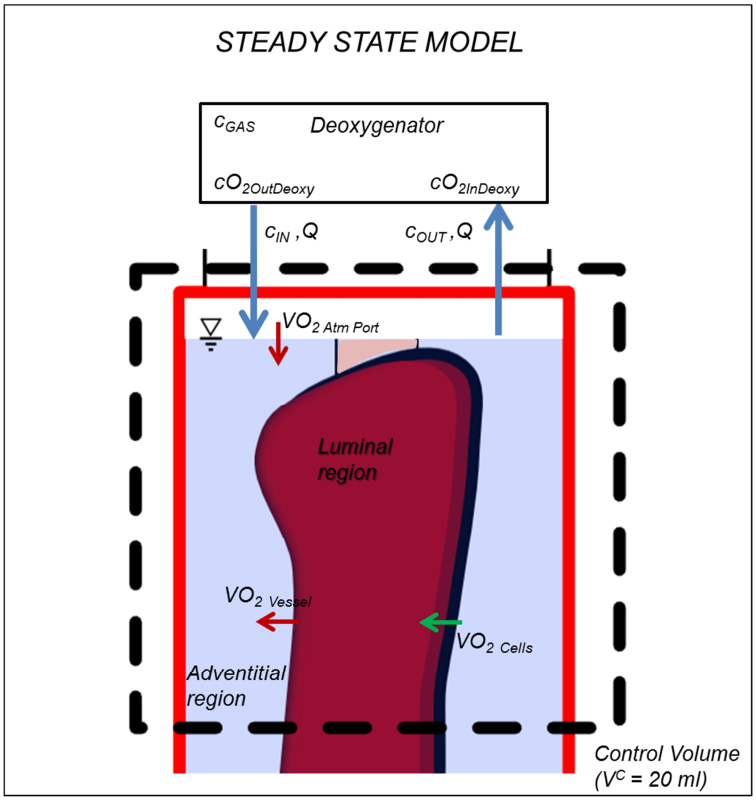

Figure 4.10. *Simplified compartimental model adopted for studying of the behavior of the system during the steady state. V^c is the control volume, c_{IN} (= $cO_{2OutDeoxy}$) e c_{OUT} (= $cO_{2InDeoxy}$) are the oxygen concentration at the outlet and inlet of the control volume, Q represents the flow rate of recirculation of the fluid inside the compartment, and c_{GAS} is the oxygen concentration within the de-oxygenator module. $VO_{2\,Atm\,Port}$ represents the gaseous exchange between the inner culture chamber and the incubator environments occurring via the free surface of the medium, $VO_{2\,Vessel}$ is the oxygen transfer through the SV wall, and $VO_{2\,Cells}$ is the cellular oxygen consumption.*

The mass balance across the control volume V^c in steady state condition is:

$$V^c\frac{dc}{dt} = Q\ (c_{OUT} - c_{IN}) + VO_{2AtmPort} + VO_{2Vessel} - VO_{2Cells} \qquad (18)$$

where $VO_{2\,Atm\,Port}$ represents the gaseous exchange between the inner culture chamber and the incubator environments occurring via the free surface of the medium, $VO_{2\ Vessel}$ is the oxygen transfer through the SV wall, and $VO_{2\ Cells}$ is the cellular oxygen consumption which was set equal to zero (this assumption is in favor of safety) (Figure 4.10). In steady state condition $\frac{dc}{dt} = 0$, the oxygen concentration at the outlet of the de-oxygenator chamber ($cO_{2Out\ Deoxy}$) tends asymptotically to the constant oxygen concentration within the de-oxygenator chamber (C_{GAS}):

$$c_{IN} = c_{GAS} = cO_{2Out\ Deoxy} \tag{19}$$

In these condition the equation (18) was simplified as follow:

$$c_{OUT} = c_{GAS} + \frac{VO_{2\,AtmPort} + VO_{2Vessel}}{Q} \tag{20}$$

The $VO_{2AtmPort}$ and the $VO_{2Vessel}$ were calculated according with the Fick's Law:

$$VO_{2\ Atm\ Port} = \frac{A_{Inner\ Chamber}\, D\ (c_{Air} - c_{Inner\ Chamber})}{h} \tag{21}$$

$$VO_{2\ Vessel} = \frac{A_{SV}\, D_{SV}\, (c_{SV\ Inner\ region} - c_{SV\ Outer\ region})}{t_{SV}} \tag{22}$$

where $A_{Inner\ Chamber}$ is the section of the inner culture chamber, D is the diffusion coefficient of oxygen into culture medium (2.18 10^{-5} cm^2/s), c_{Air} and $c_{Inner\ Chamber}$ are the oxygen concentration in air and in the inner chamber, respectively, h is the thickness of the medium within the inner chamber, A_{SV} is the lateral surface of the SV (mean inner diameter of 3.5 mm, wall thickness of 0.5 mm and length of 5 cm); D_{SV} is the oxygen diffusion coefficient through the SV wall tissue (equal to 2×10^{-6} cm^2/s (Sasaki *et al.,* 2012)), $c_{SVInner\_region}$ and $c_{SV\ Outer\ region}$ are the oxygen concentration in the luminal and extra-adventitial region of the SV, respectively, and t_{SV} is the SV wall thickness.

Finally, the following relations were imposed:

$$c_{SV\ Inner\ region} = c_{Air} \tag{23}$$

$$c_{SV\ Outer\ region} = c_{Inner\ Chamber} \tag{24}$$

In these conditions, combining equations (20) and (11), in terms of concentrations it was possible to estimate the oxygen concentration in the de-oxygenator chamber (c_{GAS}) necessary to maintain a venous level of oxygen concentration in the extra-adventitial region:

$$c_{GAS} = \frac{c_{OUT} - \left(c_{OUT} + \frac{\Delta c}{Q}\left(\frac{A_{SV}\, D_{SV}}{t_{SV}} + \frac{A_{Inner\ Chamber}\, D}{h}\right)\right) e^{\left(\frac{-UWHL}{Q}\right)}}{1 - e^{\left(\frac{-UWHL}{Q}\right)}} \qquad (23)$$

where c_{OUT} is the desired oxygen concentration (4.9×10^{-5} mol/ml, corresponding to a pO_2 of 38 mmHg) in steady state conditions, Δc is the oxygen concentration difference between the inner luminal region (2.08×10^{-4} mmol/ml) and the adventitial region (4.9×10^{-5} mmol/ml) of the SV vessel.

Figure 4.11 shows the trend of c_{GAS} as a function of different recirculation flow rate and for a tube with an inner diameter equal to 0.8 mm, wall thickness of 0.8 mm. In the graph, c_{GAS} is parameterized for different values of *L*.

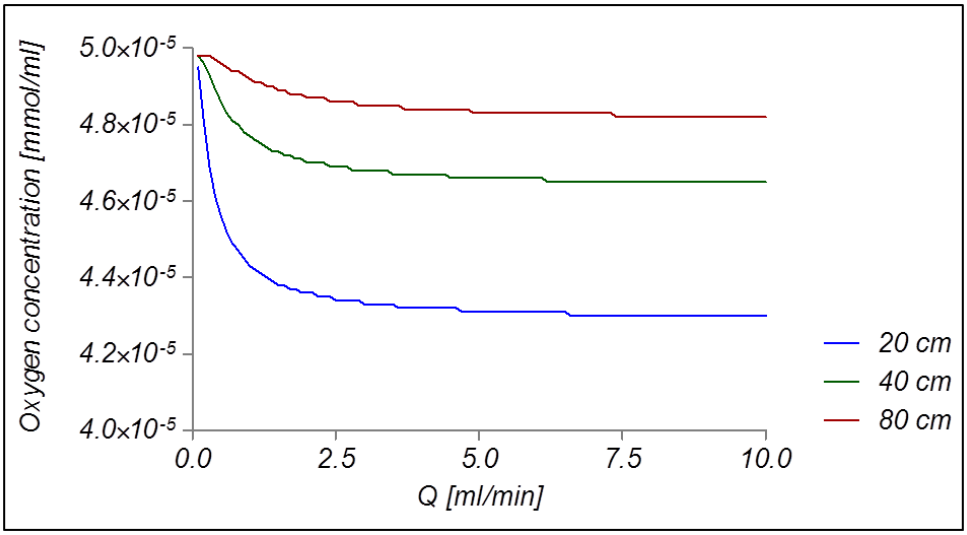

Figure 4.11. *Trend of the oxygen concentration needed within the gas side of the deoxygenator module (C_{GAS}) as a function of recirculating flow rate (Q). These values of concentrations are necessary to maintain a venous level of oxygen concentration in the extra-adventitial region. The oxygen concentration is parametrized for different silicone tubing length (L) of 20 cm, 40 cm, and 80 cm.*

The graph shows that, for increasing flow rate, the O_2 concentration needed to meet the desired steady state has an asymptotic behavior. It is interesting to notice that, regardless of the tubing length chosen, the curves have nearly reached their asymptotes for flow rate ≅ 5 ml/min. This value, in particular, corresponds to the "optimal" flow rate *Q** found for a tubing length of 40 cm when the transient phenomena were studied (Figure 4.9 B)

4.1.4.2 De-oxygenator silicone tubing dimensioning

Based on the analysis carried out in the previous paragraph, it appears that combining a tubing length of 40 cm with a rated recirculation flow rate of 5 ml/min finds a good compromise between the design needs related to the de-oxygenator system behavior during transient and steady state.

The culture medium is recirculated inside the silicone tubing, while outside a controlled gaseous mixture drives the extraction of oxygen from the fluid. During the transient phase, the gas side is composed by pure N_2, in order to maximize the Δc. This configuration allows to reach the desired oxygen concentration in 2 hours (5τ). This is a short time compared to the overall duration (7 days) of the conditioning experiments with biological samples. According to model predictions, during the steady state, the oxygen concentration within the de-oxygenator is elevated to 4.6×10^{-5} mmol/ml (corresponding to 35 mmHg) in order to obtain an oxygen concentration equal to venous conditions (4.9×10^{-5} mmol/ml, corresponding to 38 mmHg) within the extra-adventitial chamber. This is achieved by providing a gas mixture composed of N_2 and air (3.5:1).

4.1.4.3 The de-oxygenator system layout and manufacturing

The de-oxygenator chamber consists of a purpose designed tubing support (PMMA, Plasting S.r.l., Segrate, Italy) hosted into a commercial 50-ml falcon tube. The falcon tube and the silicone support are coupled trough a silicone O-ring. The tubing support allows to fix 40 cm of oxygen permeable silicone tubing (Platinum Cured, Cole Parmer, IL, USA). PP luer connectors (Cole Parmer, Cole Parmer, IL, USA) are used to guarantee leak-free connections, and facilitate circuit assembly under laminar flow hood.

Four ports through the support ensure the de-oxygenator chamber connection to the outside. Two ports provide connection for recirculation of the medium (Figure 4.12, port a and b). Two other ports ensure injection/removal of the deoxygenating mixture (Figure 4.12, port a and b).

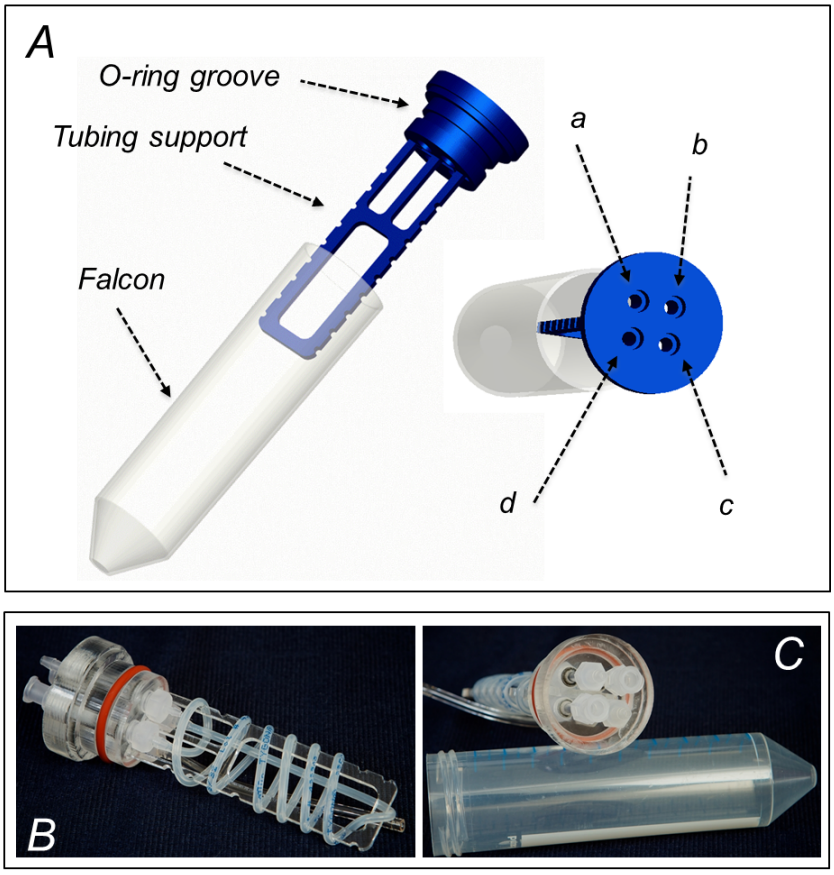

Figure 4.12. *(A) 3D CAD model of the deoxygenator module. The system consists of the tubing support inserted into a 50-ml falcon tube; a and b are the ports for connecting the deoxygenator module to the hydraulic circuit, while f and g are the ports for connecting the deoxygenator module to the gas line. (B and C) Images of the de-oxygenator module: inner module with the silicone tubing rolled on the PMMA tubing support (B) and view of the ports (C).*

4.1.5 Testing of the de-oxygenator performances

Two experimental campaigns were carried out in order to characterize the de-oxygenator module. Deionized water was used. In both the experiments, the oxygen concentration measurements was made by using an Oxygen-Sensitive Spot with Sensor Type PSt3 (PreSens, Precision Sensing GmbH, Germany). The experiments were carry out within a heater in order to control the temperature. The temperature was set at 37°C.

In a first experimental campaign (*open loop configuration*, Figure 4.13), the dimensioning of the de-oxygenator was verified imposing different flow rates (0.5 - 1 - 2 - 5 -10 - 20 ml/min). The gaseous mixture in the de-oxygenator chamber was pure nitrogen (oxygen concentration equal to 0 mmol/ml), and the gas flow rate was set equal to 0.3 l/min. Three experiments were performed for each flow rate. The oxygen concentration at

the outlet of the de-oxygenator silicone tubing was recorded. The specific mass transfer, defined as the difference between the outlet and the inlet oxygen concentration, and the mass transfer, defined as the product of the applied flow rate and the specific mass transfer, were finally estimated. These data were compared with the mathematical model previously described (*paragraph 4.1.4.1*).

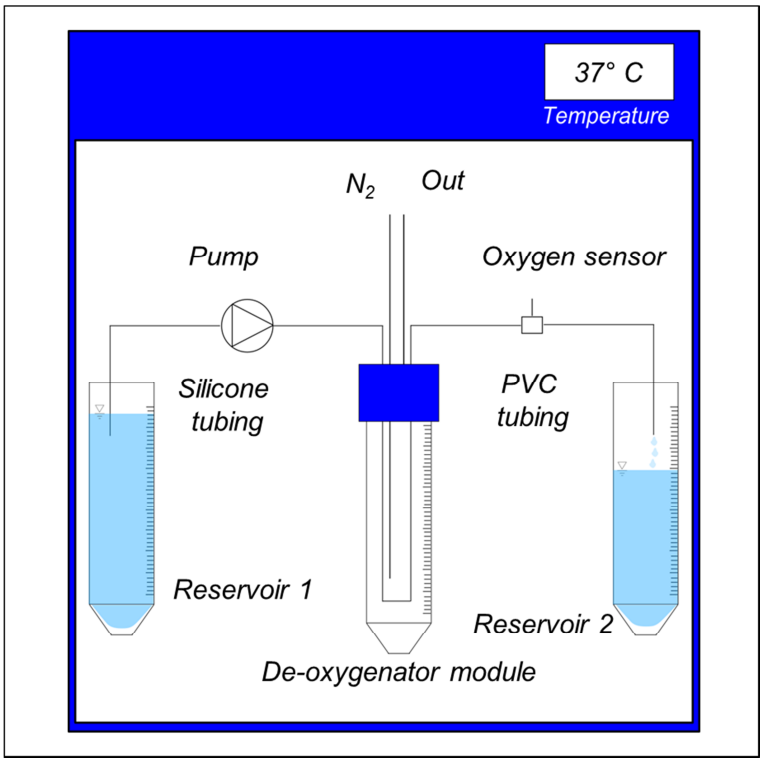

Figure 4.13. *Scheme of the open loop setup for testing without recirculation. The peristaltic pump draws the fluid from the reservoir 1 to the de-oxygenator module and finally to the reservoir 2. Silicone tubing are used for connecting the reservoir1 to the deoxygenator, while PVC tubing (lower permeability to oxygen) are used for connecting the deoxygenator to the reservoir 2. The oxygen flow chamber sensor is placed between the deoxygenator and the second reservoir. Pure nitrogen is used within the deoxygenator for driving the extraction of oxygen from the silicone tubing.*

In a second experimental campaign (*closed loop configuration*, Figure 4.14*)*, the de-oxygenator chamber was connected to the DC-ECVS chamber, thus replicating the real operating conditions. The behavior of the de-oxygenator system in the transient and steady states was studied in the absence of a biological sample mounted within the chamber. A recirculating flow rate of 5 ml/min was applied. Different O_2 saturation levels within the gas side of the de-oxygenator module were imposed: 0%, 25%, 50%, 75% and 100%. Three experiments were performed for each O_2 saturation levels. The oxygen concentration at the outlet of the DC-EVCS was recorded.

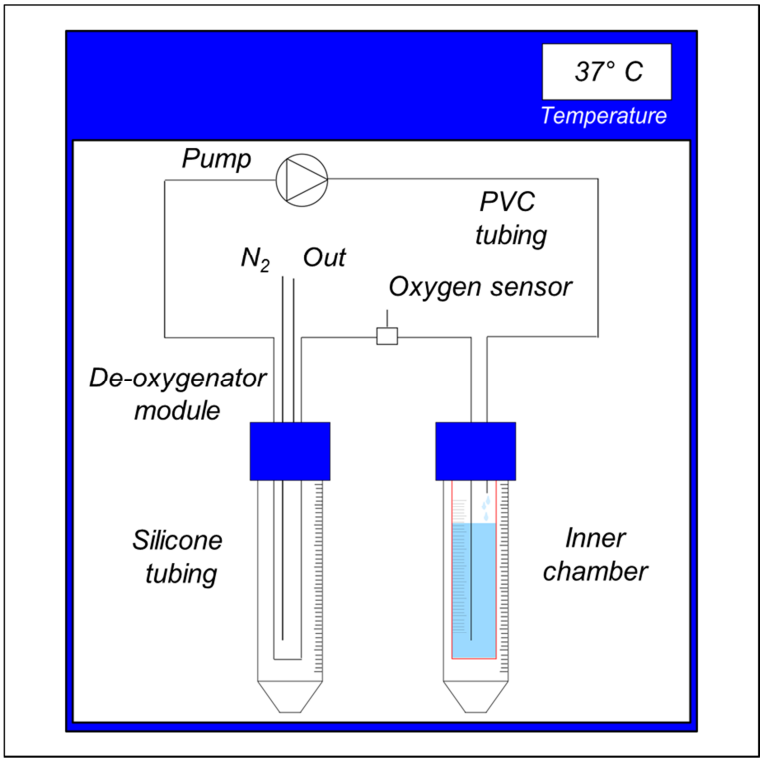

Figure 4.14. *Scheme of the closed loop setup for studying the transient and steady state of the system. PVC tubing (lower permeability to oxygen) are used for connecting the deoxygenator to the inner chamber. The oxygen flow chamber sensor is placed between the inner chamber reservoir (red box) and the deoxygnator module.*

4.1.6 De-oxygenator performances results

The results of the first experimental campaign (*open loop configuration*) are reported in figure 4.15. Theoretical and measured changes in oxygen concentration under various flow rate conditions are compared. Both graphs are in semi-logarithmic scale. As expected, by increasing the recirculating flow rate, the specific mass transfer decreases (Figure 4.15 A), while the mass transfer increases (Figure 4.15 B). In both graphs, the comparison shows that the experimental data undertake the same trend of the mathematical model. However, for flow rate lower than 2 ml/min, the de-oxygenator become less efficient. This is a reasonable behavior considering the possible O_2 infiltration from the outside environment.

The results of the second experimental campaign (*closed loop configuration*) are reported in figure 4.16. As predictable, by decreasing the O_2 saturation within the gaseous mixture in the de-oxygenator module, the resulting O_2 concentration within the extra-adventitial chamber decreases. On the other hand, by imposing a O_2 saturation of 0% (pure N_2), the O_2 concentration within the extra-adventitial chamber decreases down to a stable

value close to 4.9×10-5 mmol/min (corresponding to 38 mmHg or 5% O_2) instead of an expected value of 0 mmol/min.

Taking together these results showed that in working conditions, the performances of the de-oxygenator module are affected by O_2 infiltrations. Nevertheless, the obtained results demonstrated that the designed de-oxygenator module was a suitable tool for testing distinct O_2 concentration in the intra-luminal and extra-adventitial region of the SV vessel

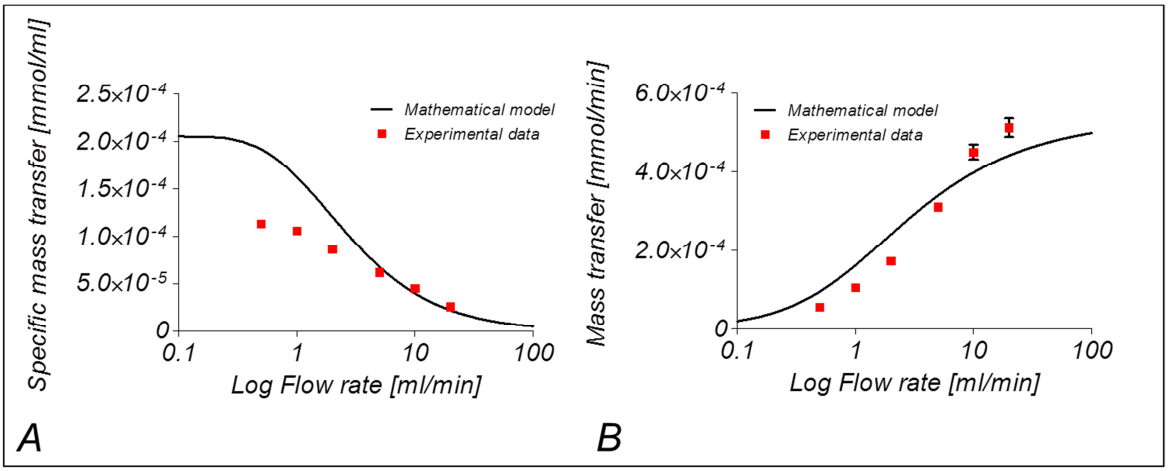

Figure 4.15. *Comparison between mathematical model (black lines) and experimental data (red dots) regarding the specific (A) and global mass transfer (B) behaviour of the deoxygenator module. Data are plotted in a semi-logarithmic scale as function of the recirculating flow rate.*

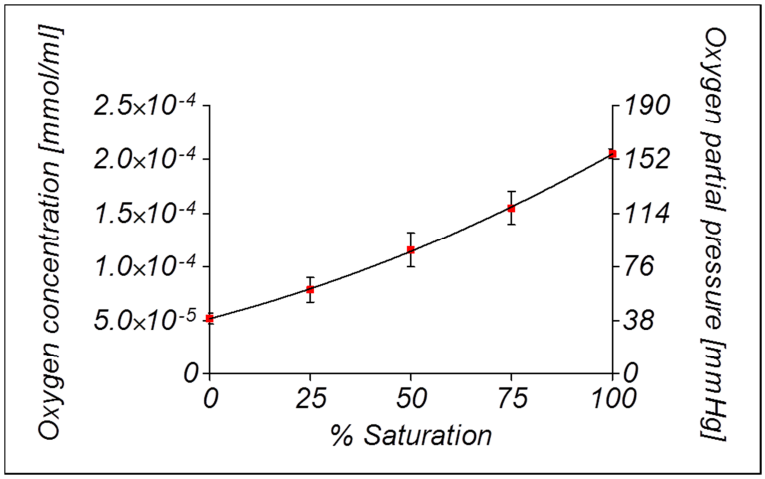

Figure 4.16*. Trend of the oxygen concentraton within the extra-adventitial chamber as a function of the oxgen saturation imposed within the de-oxygenator module.*

4.2 Overview of the DC-EVCS

An overview of the DC-EVCS during the assembling phase under laminar flow hood is shown in Figure 4.17. The time necessary to fix the vein to the housing (Figure 4.17 A and B) was less than 15 minutes; during this period the SV was constantly kept hydrated by pipetting culture medium on the SV surface. Finally, the housing was inserted within the inner chamber and then into the falcon reservoir (Figure4.17 C and D). The chamber is connected to the hydraulic circuit and to the de-oxygenator module (Figure 4.17 E). Once assembled, the DC-EVCS is filled with culture medium (total priming volume of 38 ml) and placed in the incubator. Then the culture under mechanical conditioning started imposing either a VP condition or a CABG-PS.

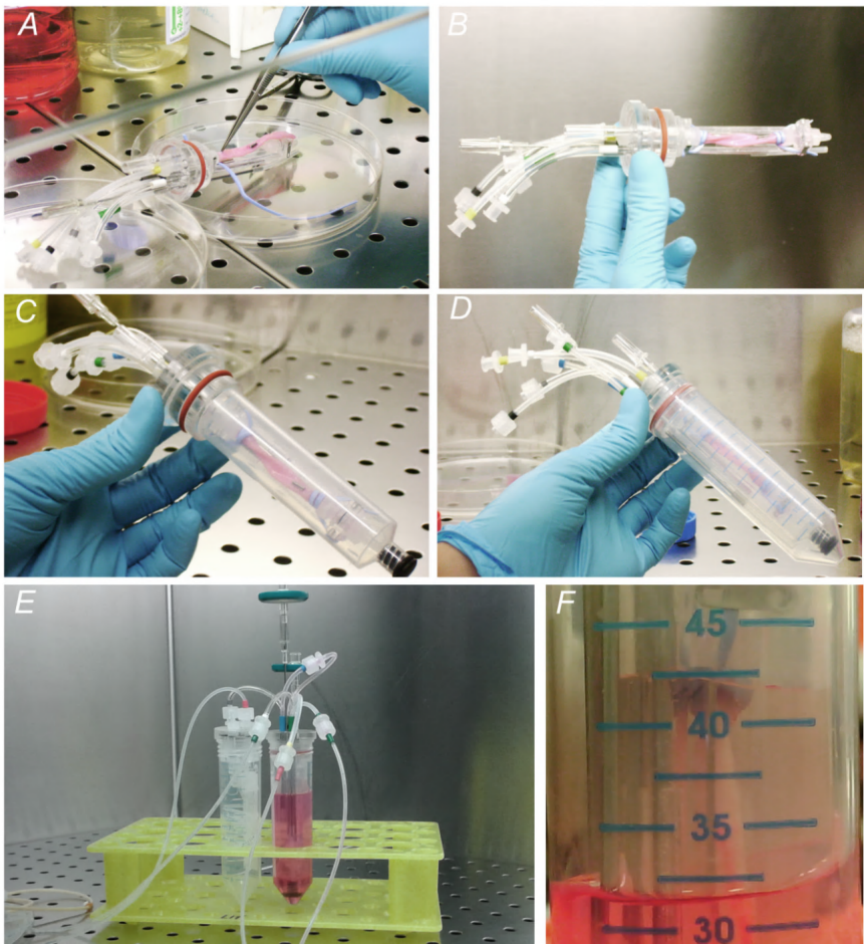

***Figure 4.17**. Prototype of the DC-EVCS during the assembling phase. (A) The SV sample is mounted in the housing, and secured via vessel loops. After vessel fixing (B), the vessel housing is inserted within the modified 20-ml syringe (C). Then the culture chamber is inserted within the outer reservoir (falcon tube) and connected through a silicone o-ring coupling resulting in a compact culture chamber (D). The culture chamber is then connected to the de-oxygenator module and to the hydraulic circuit (E). Finally the entire system is filled with culture medium (F).*

4.2.1 Functional experiments for testing the performances of the DC-EVCS

Surplus segments of human SV ($n = 2$) were obtained from patients undergoing CABG surgery and were used for the functional validation of the DC-EVCS.

After the sterilization of the EVCS, SV segments were mounted as previously described (Figure 4.17 A-E), and then the outer chamber of the EVCS was filled with 18 ml DMEM with 10% Fetal Bovine Serum (FBS), 1% L-Glutamine, 1% streptomycin-penicillin. 18 ml of white RPMI with 10% Fetal Bovine Serum (FBS), 1% L-Glutamine, 1% streptomycin-penicillin was used for filling the extra-adventitial chamber (Figure 5.18 F). Then, the EVCS was kept in the incubator at 37° C and 5% CO_2 for a culture period of 7 days. The culture medium was partially changed at day 3.

One vein was perfused under venous perfusion conditions (steady flow with luminal pressure: 5 mmHg; flow rate: 3 ml/min), while the second vein was subjected to CABG-like stimulation (luminal pressure: 80 - 120 mmHg; pulse frequency (f): 0.5 Hz with a stimulation interval (Ts) of 10 minutes; recirculation flow rate (Q_R): 1 ml/min, with a luminal pressure between 1-2 mmHg, and recirculation interval (T_R) of 2 min). In both preliminary tests the extra-adventitial medium was recirculated imposing a flow rate of 5 ml/min.

During the test under VP conditions the double-compartment system did not show significant changes in the medium levels. Instead during CABG-like stimulation test, an increase of the medium volume in the extra-adventitial compartment was observed after 3 days of culture. Probably, this was due to the interstitial perfusion that took place in the vessel wall. Further experiment are ongoing, allowing to a complete quantification of these phenomena.

4.3 Integration of a novel left coronary artery pulse duplicator

The bioreactor was finally upgraded to better replicate the full biomechanical stimuli involved in CABG arterialization, *i.e.* pulsatile wall stretch and wall shear stresses applied synchronously and with the correct phasing (CPD-EVCS). Integrated with environmental control, this feature makes the device capable of applying complete CABG-like pressure/flow stimulation patterns to the hosted SV segments. Computer-aided design of the novel hydrodynamic circuitry is performed by lumped parameter modeling and numerical simulation are performed by means of Simnon 3.0 (SSPA Maritime Consulting AB, Sweden). Design efforts are dedicated to maintain strict engineering specifications concerning user friendliness, compactness, low-priming volume and low cost, while including the novel hydrodynamic features into the EVCS.

4.3.1 Design specification

The general design specifications were similar to those drawn up for the previous version of the culture system (*paragraph 3.1.1*). Additional design specifications came from the hemodynamic environment of the coronary circulation. Briefly, the mean coronary blood flow is 250 ml/min (4-5% of the cardiac output); 70% (175 ml/min) of the blood flows in the left coronary circulation, while 30% (75 ml/min) in the right compartment. In addition, coronary blood flow during phases of iso-volumetric contraction and ejection (20-35%) is lower than blood flow during diastole (65-80%). In these conditions, the peak flow rate in diastole is 2-3-fold the peak in systolic phase. Finally, coronary pressure and flow are highly pulsatile because of the pulsatile nature of the input driving pressure. In addition to this, the most of the coronary vasculature is imbedded in cardiac muscle tissue and is subjected to the effects of cyclic contraction of the cardiac muscle. Thus, pressure and flow are time-dependent and pressure and flow waveform peaks are in counter-phase (Figure 4.18).

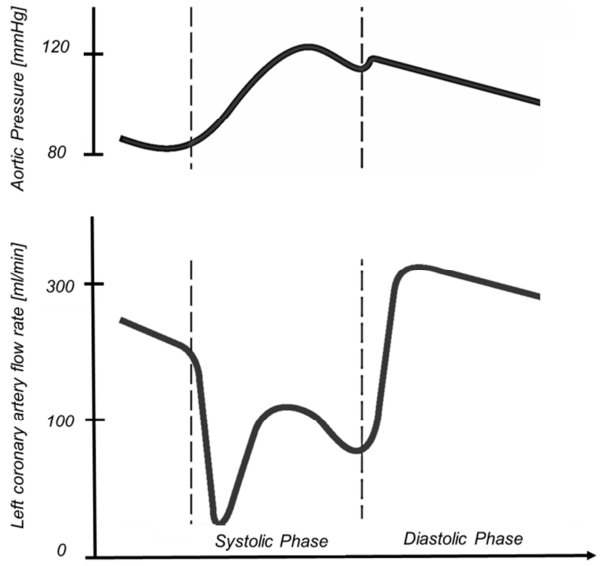

Figure 4.18. *Aortic pressure (upper pannel) and left coronary flow rate (bottom pannel) traces. Pressure and coronary blood flow are in counter-phase: in fact, coronary blood flow during systolic phase is lower than blood flow during diastole.*

4.3.2 Architecture of the coronary artery pulse duplicator

On the basis of the system requirements, a possible solution for the realization of the left coronary artery pulse duplicator was identified. This version of the system was designed in order to apply a fully CABG-like pressure/flow stimulation patterns to the hosted SV segments, *i.e.* a pulsatile pressure oscillating between a diastolic minimum and a systolic maximum (*e.g.* 80-120 mmHg), in counter phase with a pulsatile flow rate. A schematic representation of the coronary pulse duplicator circuitry is shown in figure 4.19.

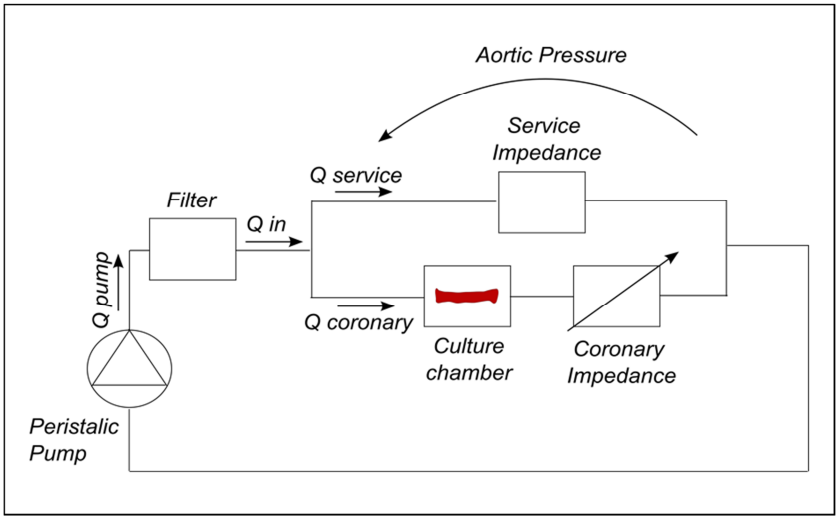

Figure 4.19. *Schematic representation of the EVCS integrated with the coronary pulse duplicator (CPD). The CPD-EVCS consists of 4 main sub-systyems: the filter, the culture chamber, the service impedance, and the time-depedent coronary impedance.*

The coronary pulse duplicator consists of a service and a coronary-like impedance properly dimensioned in order to satisfy the design specifications.

The dimensioning and the implementation of these three impedances is presented in the following three paragraphs. First the dimensioning of the coronary impedance sub-system was presented, followed by the dimensioning of the service impedance and of the filter.

For the dimensioning of the impedances, the lumped-parameter theory was used (Milnor 1989). The model is based on the analogy between electricity and hemodynamics. Assuming that voltage and current in electrical circuit behave like pressure and blood flow in vascular model, it is possible to apply the mathematical expressions for voltage-current relationships. The simplest analogy between electricity and hemodynamics is given by Ohm's law:

$$\boldsymbol{V = z\, I \Leftrightarrow \Delta P = z\, Q} \tag{25}$$

where pressure gradient (***ΔP***) is analogous to voltage (***V***), flow (***Q***) to current (***I***), and electrical impedance to vascular impedance.

4.3.2.1 Dimensioning, design and manufacturing of the coronary impedance subsystem

Dimensioning

The coronary impedance was modeled as two parallel resistances and took into account the left branch of the coronary circulation neglecting the right side. In these conditions, the total coronary resistance increases during the systolic phase, thus reproducing the interactions between the myocardium and the coronary tree (Figure 4.20 A). A *RCR* lumped parameter model of the systemic circulation (Figure 4.20 B) (Sharp and Dharmalingam 1999) is forced by imposing a positive sine waveform with a mean systolic flow rate value equal to 6 l/min (and 0 l/min during diastole) in order to determine the aortic pressure (Figure 4.20 C). The resulting aortic pressure was then used for forcing the coronary impedance in order to determine the coronary flow rate waveform (Figure 4.20 E).

The resulting flow rate waveform was used as target tracing for further analysis. In addition the following relationships (*paragraph 4.3.1*) were used in order to determine the value of the diastolic and systolic resistances. In particular:

$$\bar{Q}_{Left\_Cor} = 0.7\ \bar{Q}Cor \tag{26}$$

$$V_{Syst} = 0.25\ V_{Total} = 0.25\ \bar{Q}_{Left\_Cor}\ T \tag{27}$$

$$V_{Diast} = 0.75\ V_{Total} = 0.75\ \bar{Q}_{Left\_Cor}\ T \tag{28}$$

where $\bar{Q}_{Left\_Cor}$ is the mean flow rate flowing into the left coronary arteries, $\bar{Q}Cor$ is the mean flow rate flowing into the entire coronary artery system (equal to 250 ml/min), V_{Syst} and V_{Diast} are the volume of blood during the systolic and diastolic phase respectively, V_{Total} is the total volume of blood in the left coronary artery during one cardiac cycle, and T is the period of the cardiac cycle.

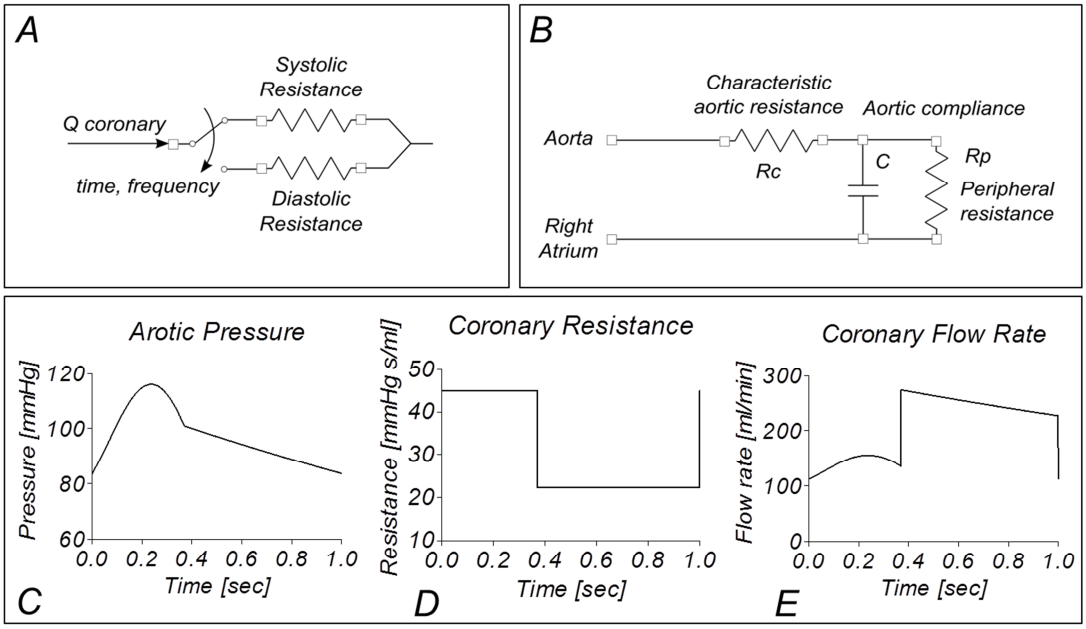

Figure 4.20. *(A) Schematic rappresentation of the coronary-like time-depedent impedance realized with the parallel of two resistances. (B) RCR model of the systemic circulation adapted from Sharp (Sharp and Dharmalingam 1999). The value of the characteristic aoritc compliance is 3 ml/mmHg, while the characteristic aoritc and peripheral resistances are 0.05 mmHg s/ml and 0.9 mmHg s/ml, rispectively. Traces of the aortic pressure (C), and coronary resistance (D) and flow rate (E).*

The values of the diastolic and systolic resistance (Figure 4.20 D) were finally calculated using the hydraulic analogous of the Ohm's law (equation 25). Considering that the systolic interval is approximately equal to 1/3 of the whole cardiac cycle (t_s = 0.33 T, and t_d = 0.67 T), whit simple passages, it is yielded:

$$R_{Syst} = \frac{\bar{P}_{Cor\_Syst}}{\bar{Q}_{Syst}} = \frac{\bar{P}_{Cor\_Syst}}{\frac{V_{Syst}}{t_s}} = 45\ \frac{mmHg\ s}{ml} \tag{29}$$

$$R_{Diast} = \frac{\bar{P}_{Cor\_Diast}}{\bar{Q}_{Diast}} = \frac{\bar{P}_{Cor\_Diast}}{\frac{V_{Diast}}{t_d}} = 22\ \frac{mmHg\ s}{ml} \tag{30}$$

where $\bar{P}_{Cor\_Syst}$ and $\bar{P}_{Cor\_Diast}$ are the mean pressure during systole and diastole, while $\bar{Q}_{Syst}$ and $\bar{Q}_{Diast}$ are the mean flow rate during systole and diastole. As it is expected, the value of the systolic resistance is 2 fold the value of the diastolic one.
Figure 4.20 summarized the step procedure followed for the dimensioning of the coronary-like impedances.

Design

Starting from the values of resistances previously dimensioned, the coronary resistances were realized as tubing bundles. The number, the inner diameter and the length of the tubing were accurately dimensioned in order to: *i*) guarantee a laminar flow within the resistance elements; *ii*) minimize the inlet and outlet minor head losses across the resistance elements; and *iii*) realize a pure resistive element, with negligible inductive and capacitive contributes.

A flow rate of 180 ml/min (which was the peak of the diastolic flow rate divided by 2) was used for the dimensioning of both the coronary resistances.
The laminar flow was guaranteed imposing a Reynolds (*Re*) number less than 2000:

$$Re = \frac{v\,d\,\rho}{\mu} < 2000 \tag{31}$$

where v is the velocity within the single tube, d is the inner diameter of the tubing, ρ and μ are the density and the viscosity of the culture medium, set equal to that of water, 1000 kg/m^3 and 0.001 Pa s, respectively. In addition, assuming that the fluid is viscous and incompressible, and the flow is laminar without fluid acceleration, the head losses across the tubing were estimated by using the Hagen-Poiseuille relation:

$$R = \frac{128\,\mu\,l}{\pi\,d^4} \tag{32}$$

where l is the length of the tubing.

The inlet and outlet minor head losses across the resistance element (ΔPc) are given in equation (33) as:

$$\Delta Pc = \frac{k\,\rho\,v^2}{2} \leq 0.1\,\Delta P \tag{33}$$

where k is the minor head loss coefficient set equal to 0.5. The inlet and outlet minor head losses are required to account for less than 10% of the ΔP.

Finally, while the capacitive effect was neglected by using rigid tubing, the inertance contribution was limited by imposing that the contribution of inertance to the tube impedance be small with respect to that of the tube resistance:

$$\frac{R}{2\,\pi\,f_{max}\,L} \geq 10 \tag{34}$$

where f_{max} is the highest significant frequency of the harmonics constituting the coronary flow rate signal. It was assumed f_{max} equal to 5 Hz. The inertance L was defined as follow (Pennati *et al.*, 2004):

$$L = \frac{4\,\rho\,l}{\pi\,d^2} \tag{35}$$

In addition, the following relations were used:

$$R_{Tot} = \frac{R_{Singol\ Tube}}{n} \tag{36}$$

$$L_{Tot} = \frac{L_{Singol\ Tube}}{n} \tag{37}$$

where R_{Tot} and L_{Tot} are the total hydraulic resistance and inertance, respectively; $R_{Singol\ Tube}$ $L_{Singol\ Tube}$ are the hydraulic resistance and inertance of a single tube, respectively; while *n* is the number of parallel tubes.

Combining the equations from (31) to (37), the number (*n*), the inner diameter (*d*) and the length (*l*) of the tubing were dimensioned. The systolic resistance was realized using 7 tubing in parallel with inner diameter of 0.6 mm and length of 160 mm. In addition, considering that the systolic resistance was 2 fold the diastolic resistance, the latter one was realized placing two systolic resistances in parallel.

Manufacturing

The resistances were manufactured by injection-molding/vacuum-casting and curing within purposely manufactured polymethylmethacrylate (PMMA, Plasting s.r.l., Segrate, Italy) molds. The silicone tubing (inner diameter 0.6 mm, Platinum Cured Silicone, Cole Parmer, Vernon Hills, IL) were positioned within the mold, then the mold was filled with a biocompatible silicone elastomer (1:10, Sylgard 184®, Dow Corning Corporation, Midland, MI), and finally the mold was positioned inside the oven for curing. Three resistance elements were manufactured (Figure 4.21 A). After two hours the resistances were characterized by imposing different hydrostatic pressure (20-140 mmHg, step 20 mmHg), and the resulting flow rate recorded. The characterization was repeated thrice. The slope of the pressure/flow rate curve represents the value of the designed resistance (Figure 4.21 B).

Fluid flow switching between the systolic and diastolic resistance modules was realized by using a solenoid pinch-valve (S306-02, SIRAI® Elettromeccanica, Italy). The pinch valve is connected to a PC equipped with a I/O board (NIDAQCard-6036E, National

Instruments Corp.) and is managed via a customized LabView software (National Instruments Corp., TX, USA), imposing the cardiac frequency and the diastolic time (Figure 4.20 C).

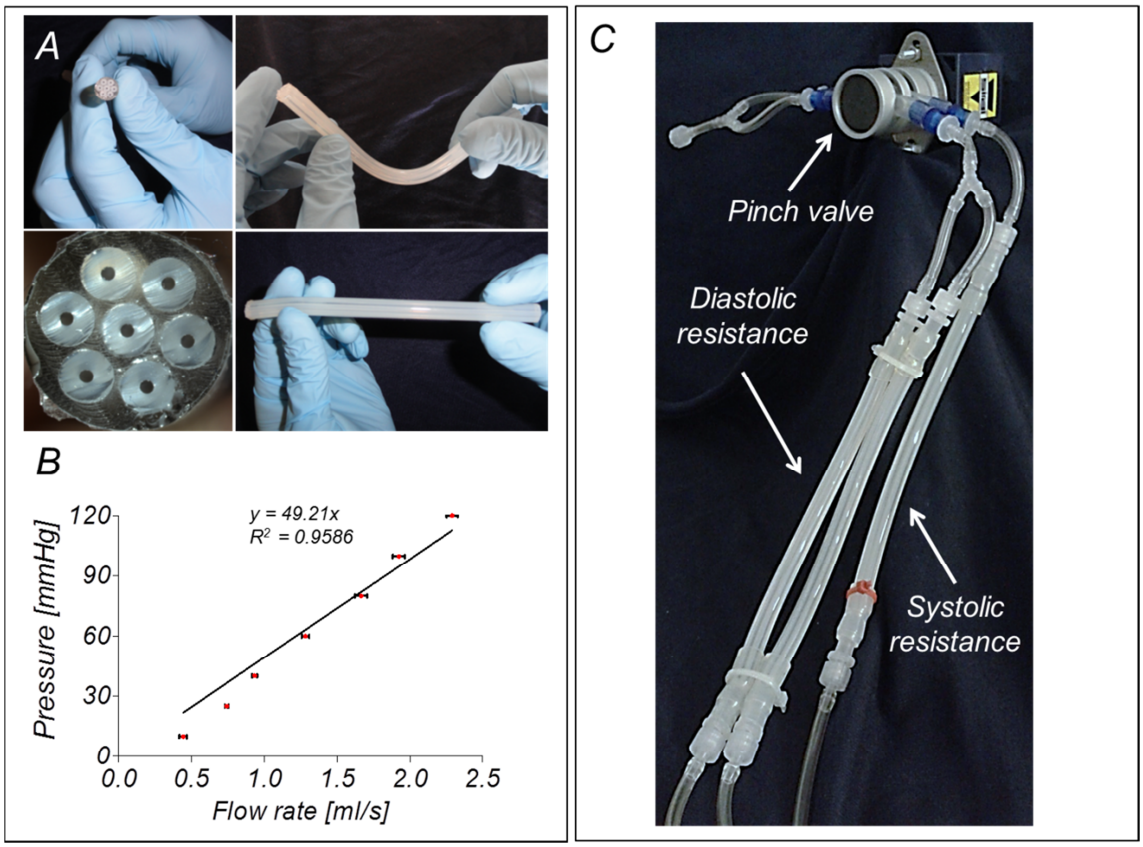

Figure 4.21. *Coronary-like resistance. (A) Prototype of the coronary systolic resistance realized with 7 silicone tubes in parallel. (B) Hydarulic caracterization of the systolic resistance. The slope of the straight line represents the value of the hydarulic resistance expresses in mmHg s/ml. (C) Coronary-like time dependent resistance. The time dependency is realized with a pinch valve managed via PC.*

4.3.2.2 Dimensioning and manufacturing of the service impedance subsystem

Dimensioning

The aim of this sub-system was to generate a coronary-like (or aortic-like) pressure waveform when the whole system is forced with a given inlet flow rate (Figure 4.22).

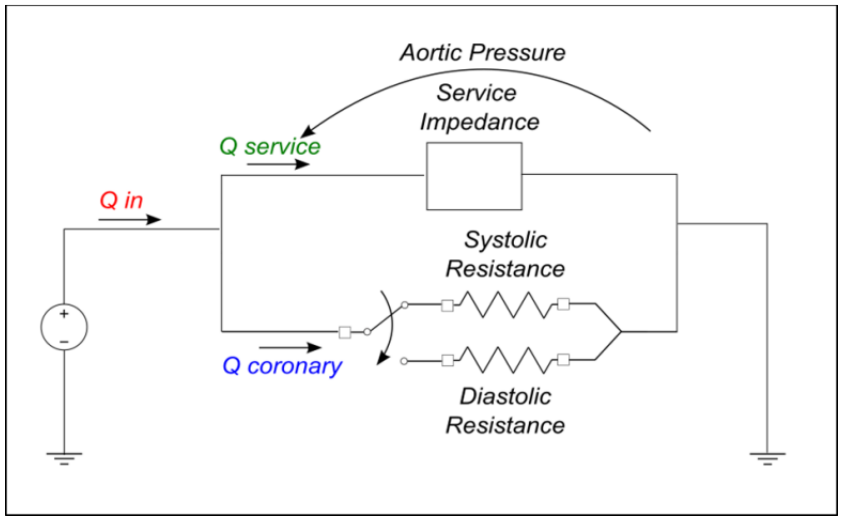

***Figure 4.22**. Schematic of the coronary pulse duplicator. In this step of the dimensionig, different configurations of R, L and C impedances are forced with the aortic pressure (black), and the Qin (blu) and Qservice (green) are analyzed.*

The design specifications were: *i)* minimization of the flow rate flowing through the service branch, *ii)* minimization of the priming volume of the overall circuit, and *iii)* minimization of the number of R, C and L parameters, in order to reduce the number of elements, thus making the system as compact as possible.

Different combinations of the R, C, and L lumped parameters were taken into account, and forced with the desired coronary pressure waveform. The resulting flow rate entering the service impedance ($Q_{service}$), and the flow rate generated by the pump (Q_{in}) were analyzed (Figure 4.22).

In table 4.2 the values of the parameters and the relations used for the numerical simulation are reported, while in figure 4.23 the results of the numerical simulations are shown. Table 4.2 reports value even for those combinations whose theoretical analysis yielded unsatisfactory results, *i.e.* for the *L* and *RL* combinations.

The results of the simulations were analyzed in term of minimization of the number of components, minimization of the mean flow rate entering the service impedance (mean $Q_{service} < 500$ml/min), and evaluation of the pump flow rate waveform (Q_{in}).

Z	**Values**				**Relations**
R		$10\ \frac{mmHg\ s}{ml}$	$22\ \frac{mmHg\ s}{ml}$	$45\ \frac{mmHg\ s}{ml}$	--
C		$0.01\ \frac{ml}{mmHg}$	$0.1\ \frac{ml}{mmHg}$	$1\ \frac{ml}{mmHg}$	--
L		$10\ \frac{mmHg\ s^2}{ml}$	$100\ \frac{mmHg\ s^2}{ml}$	$1000\ \frac{mmHg\ s^2}{ml}$	--
RC series	*R*	$0.5\ \frac{mmHg\ s}{ml}$ and	$3\ \frac{mmHg\ s}{ml}$ and	$8\ \frac{mmHg\ s}{ml}$ and	$(R + R_{Diast})\ C = \tau$
	C	$0.148\ \frac{ml}{mmHg}$	$0.133\ \frac{ml}{mmHg}$	$0.111\ \frac{ml}{mmHg}$	
RC parallel	*R*	$22\ \frac{mmHg\ s}{ml}$	$45\ \frac{mmHg\ s}{ml}$	$100\ \frac{mmHg\ s}{ml}$	(R parallel R_{Diast}) $C = \tau$
	C	$0.3\ \frac{ml}{mmHg}$	$0.223\ \frac{ml}{mmHg}$	$0.184\ \frac{ml}{mmHg}$	
RL series	*R*	$1\ \frac{mmHg\ s}{ml}$	$10\ \frac{mmHg\ s}{ml}$	$100\ \frac{mmHg\ s}{ml}$ and	$\frac{L}{(R + R_{Diast})} = \tau$
	L	$77\ \frac{mmHg\ s^2}{ml}$	$107\ \frac{mmHg\ s^2}{ml}$	$408\ \frac{mmHg\ s^2}{ml}$	
RL parallel	*R*	$45\ \frac{mmHg\ s}{ml}$	$100\ \frac{mmHg\ s}{ml}$	$1000\ \frac{mmHg\ s}{ml}$	$\frac{L}{R \text{ parallel} R_{Diast}} = \tau$
	L	$50\ \frac{mmHg\ s^2}{ml}$	$61\ \frac{mmHg\ s^2}{ml}$	$72\ \frac{mmHg\ s^2}{ml}$	
RCR	R2	$0.05\ \frac{mmHg\ s}{ml}$;	$0.5\ \frac{mmHg\ s}{ml}$;	$10\ \frac{mmHg\ s}{ml}$;	$\frac{Rp}{Rc} = \frac{R1}{R2} \approx 18.7$
	R1	$0.935\ \frac{mmHg\ s}{ml}$	$9.35\ \frac{mmHg\ s}{ml}$	$187\ \frac{mmHg\ s}{ml}$	($R1$parallel($R2 + R_{Diast}$))$C = \tau$
	C	$3.7\ \frac{ml}{mmHg}$	$0.5\ \frac{ml}{mmHg}$	$0.121\ \frac{ml}{mmHg}$	

Table 4.2. *Values of the parameters and the relations used for the numerical simulations.The time constant τ is set equal to 3.33 seconds.*

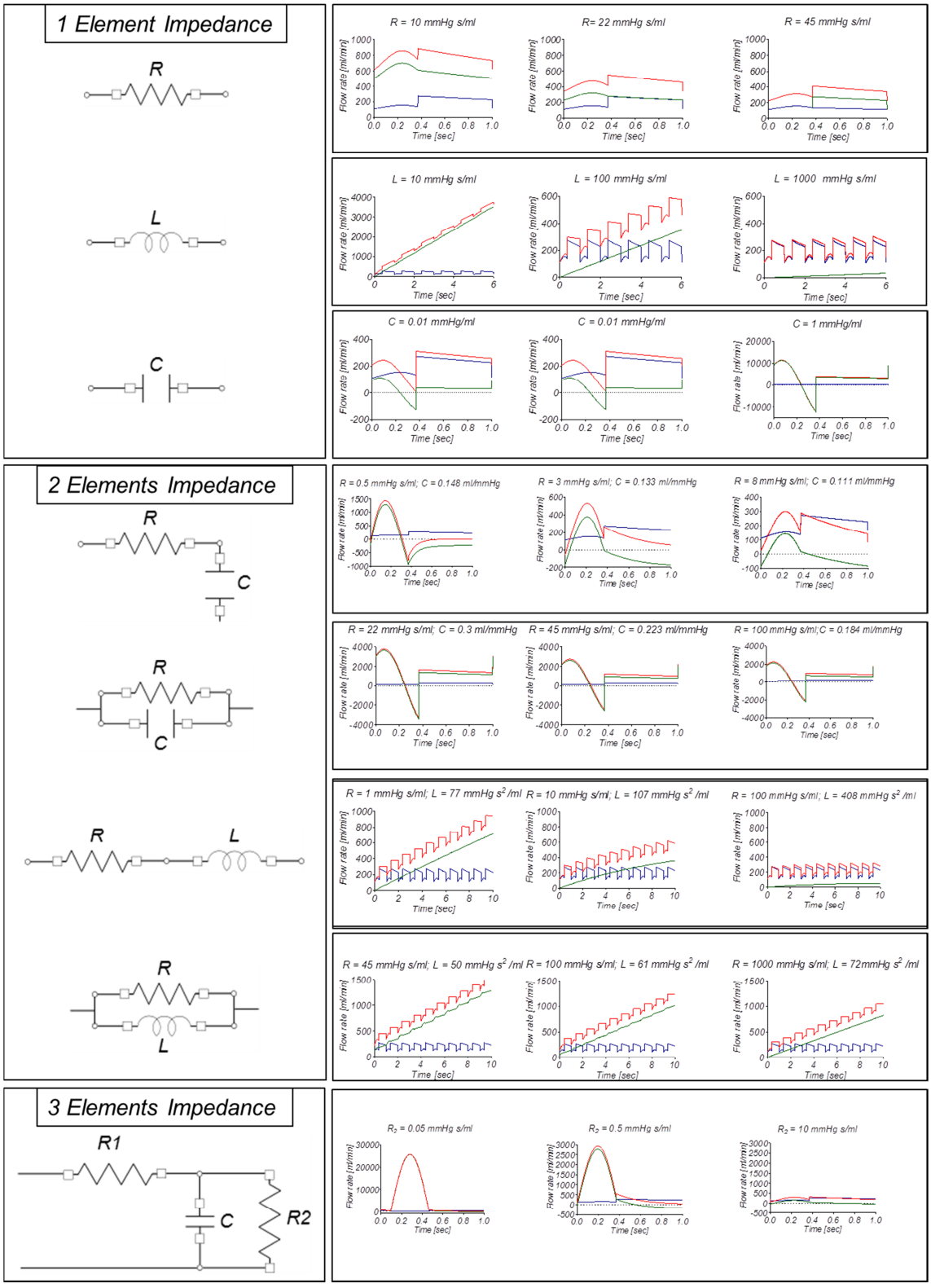

Figure 4.23. *Results of the numerical simulations. Different combinations of the R, C, L lumped parameters are forced with the desired coronary pressure waveform, and the resulting flow rate* $Q_{service}$ (green),*and* Q_{in} (red) *are analyzed. In blu is reported the coronary flow rate.*

Graphs in figure 4.23 show the waveforms of flow rate that should be generated by the pump (red traces) in order to obtain the desired coronary-like pressure and flow rate waveforms. Such solutions could be feasible, but in contrast with the design requirement of using a peristaltic pump (and a damper filter), which represents the standard pumping system used for tissue engineering applications. These waveforms are not suitable for being generated with a peristaltic pump because of the significant variation of the flow peaks between diastolic and systolic phase.

Hence, let us focus on the most promising service impedances which are: *i*) 1 element impedance, *C*, *ii*) 2 elements impedances, *RC series*;, and *iii*) 3 elements impedances, *RCR*.

The selected impedances (Figure 4.24 A and B) were forced by imposing a steady flow rate (210 ml/min for the *C* and *RC series* impedances, and 240 ml/min for the *RCR* impedances, Figure 4.24 C), and the pressure and the coronary flow rate waveform were analyzed and compared with the target coronary pressure and flow rate waveforms. The differences between the results of the simulation and the target waveform were evaluated in term of Root Mean Square Error (RMSE). In addition, the possible solutions were evaluated in terms of ease of realization, user-friendliness, compactness, and low-priming volume. In figure 4.24 D, E and F the results of the numerical simulations are reported.

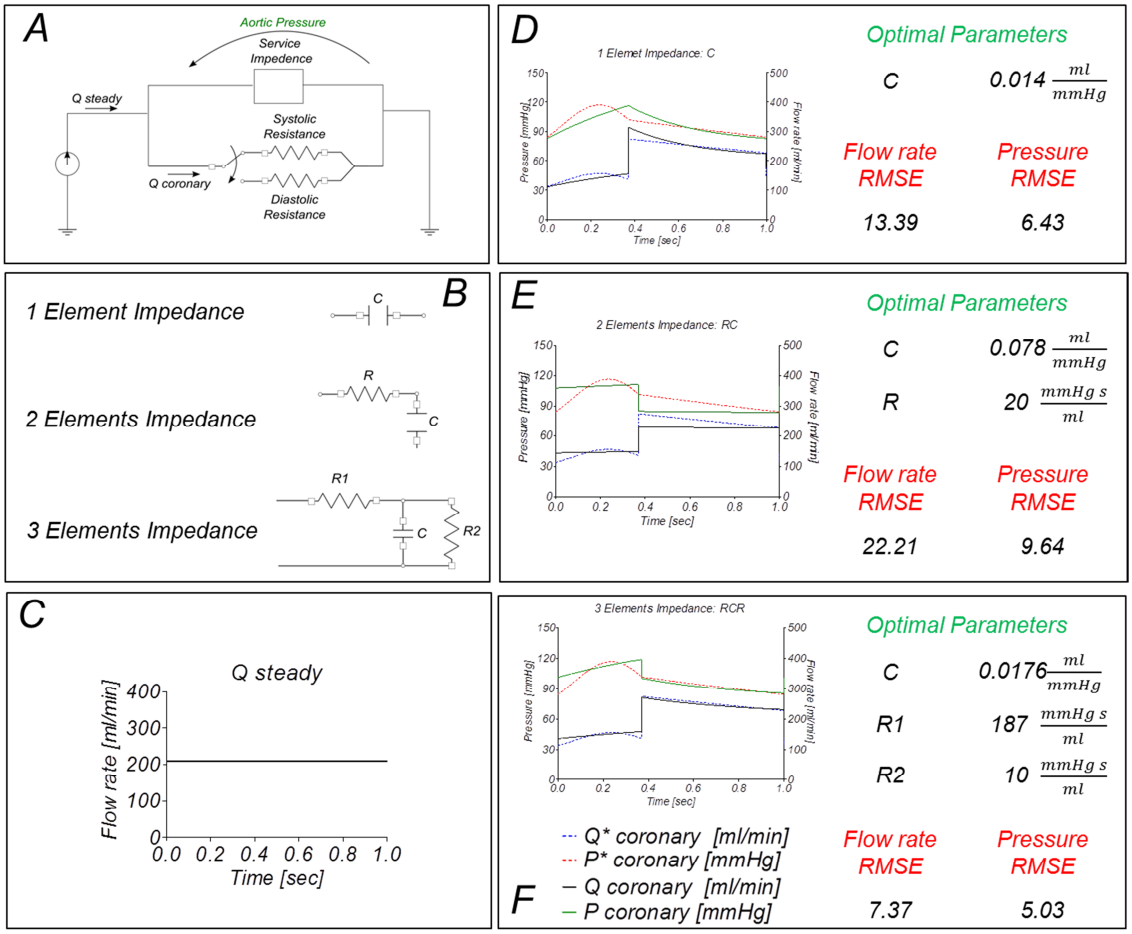

Figure 4.24*(A) Schematic rappresentation of the dimensioning step of the service impedance. A steady Q_{in} was used for studing the response of different service impedances. The impedances (B) were forced by imposing steady flow rate (C). Traces of the coronary pressure and flow rate resulting by imposing a steday flow rate to 1 elemet impedance C(D), 2 elements impedance RC (E), and 3 elements impedance RCR (F). The simulated waveforms (pressure is in green, while flow rate in black) were compared with the target coronary pressure (red-dot lines, P*) and flow rate (blue-dot lines, Q*) waveforms.*

From the comparison of the numerical simulation, the *RC* solution was discarded because of the unacceptable fitting between target and simulated tracings (flow rate RMSE: 22.21; pressure RMSE: 9.64). Between the remaining options (the 3 elements impedance *RCR* and the 1 element impedance *C*), the *C* impedance was selected even if the RMSE comparison suggested the *RCR* as optimal solution (flow rate RMSE: 7.37; pressure RMSE: 5.03). The chosen solution allowed to satisfy the design requirements of minimization of the encumbrance and of the priming volume.

Design and manufacturing

The service impedance C (equal to 0.014 ml/mmHg) was realized by using a properly dimensioned Windkessel model based on compression and expansion of air within a chamber. For the dimensioning of the compliance, absolute pressure was used and air was approximated as a perfect gas. Slow replenishment up to working pressure (P_w) was modeled using isothermal process:

$$P_0 V_0 = P_w V_w \tag{38}$$

where P_o and V_o are the initial pressure and volume of air, while P_w and V_w are the pressure and volume during working condition.

In addition, compression and expansion during the working cycle were considered as adiabatic transformations:

$$P V^k = P_w {V_w}^k \tag{39}$$

where k (=1.4) is the ratio between the specific heat for air in a constant pressure and constant volume process.

Finally, considering C as the variation of volume in response to a variation of pressure,

$$C = \frac{dV}{dP} \tag{40}$$

and combining equation (40) with the relations of isothermal (38) and adiabatic (39) process, the following equation was obtained:

$$C = \frac{dV}{dP} = -\frac{P_w}{P^2} {V_w}^k \frac{1}{k} \left(\frac{P_w}{P} {V_w}^k\right)^{\left(\frac{1-k}{k}\right)} \tag{41}$$

By imposing P equal to P_w and resolving for V_0, it was possible to obtain the initial volume of air of the compliance chamber:

$$V_0 = -k\,C\,\frac{{P_w}^2}{P_0} \tag{42}$$

Considering P_w equal to 860 mmHg, P_0 equal to 760 mmHg and C equal to 0.014 ml/mmHg, the resulting value of V_0 is 19.08 ml. Figure 4.25 A shows the volume/pressure relationship of the service compliance. The related circuit component was then realized with a 60-ml syringe, fixing the plunger at the desired volume value (Figure 4.25 B).

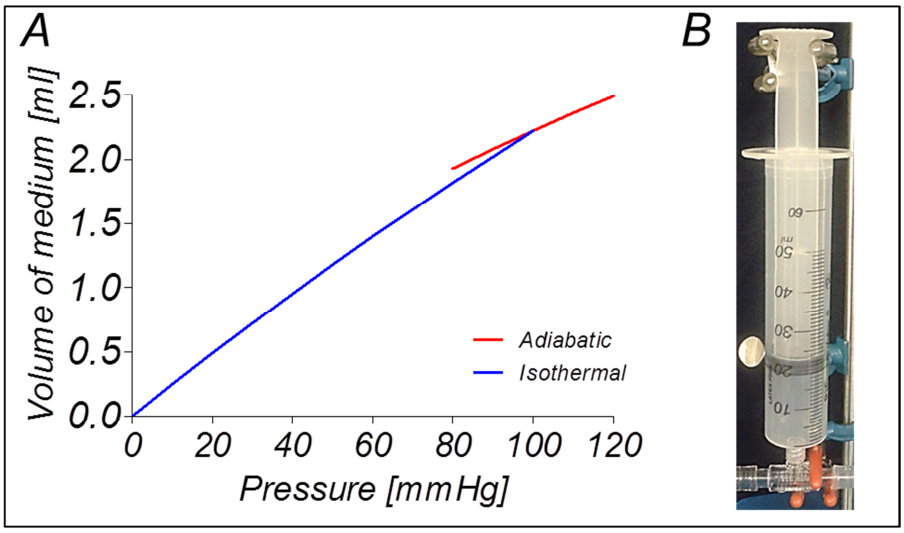

Figure 4.25 *(A) Volume/pressure relationship of the service compliance. (B) The 60-ml syringe used as compliance chamber.*

4.3.2.3 Dimensioning and manufacturing of the damper filter

Dimensioning

A low pass RC-hydraulic filter was dimensioned for damping the peristaltic pump (Watson Marlow 323D with 314D pumping head, 4 rollers, Watson Marlow Group, UK) pulsation, and for generating a *quasi*-steady flow rate (Figure 4.26 A). Different flow rates ($\overline{\mathrm{Q}}_{\mathrm{pump}}$) are taken into account spanning from 100 ml/min to 250 ml/min (step of 10 ml/min). The mean flow rate of the peristaltic pump ($\bar{Q}_{pump}$) is obtained using the following relation:

$$\bar{Q}_{pump} = n\,rpm\,\Delta V \tag{44}$$

where *n* is the number of pump rollers, *rpm* is the number of revolutions per minute and ΔV is the volume of fluid entrapped between two adjacent rollers.
Three different pump tubes with internal diameter of 3.2 mm, 4.8 mm and 6.5 mm, were used for generating the desired flow rate.

The fundamental frequency of the noise (f_{noise}) is then calculated using the following relation:

$$f_{noise} = \frac{n\, rpm}{60} \tag{45}$$

A low-pass RC-hydraulic filter was used to filter this noise by properly attenuating the harmonic components $\geq f_{noise}$, with the aim of obtaining a flow rate signal that well approximates a steady signal. To this purpose the cutoff frequency (f_c) of the filter was set two decades lower than the first harmonic of the noise:

$$f_c = 0.01\, f_{noise} \tag{46}$$

The cutoff frequency of the RC filter is determined by the time constant (τ):

$$f_c = \frac{1}{2\,\pi\,\tau} = \frac{1}{2\,\pi\,R\,C} \tag{47}$$

where τ is the time constant of the RC filter, and R and C are the hydraulic resistance and compliance, respectively. Since the choice for the values of R and C (for a given τ) yielded a degree of freedom, it was possible to include an additional requirement. Specifically, the filter resistance was asked to be high enough to ensure a good decoupling of the filtering stage from the remaining circuit (i.e. from the coronary simulator), still without generating unsafe high pressures in the filter's compliance.
The dimensioning procedure was identical to that one described for the coronary resistances (*paragraph 4.3.2.1*). The value of the R_{Filter} was set higher than the R_{Syst} and R_{Diast} *values*. In particular:

$$R_{Filter} \gg R_{Diast} > R_{Syst} \quad (48)$$

Optimal results were obtained with R_{Filter} equal to 120 mmHg s/ml (whereas R_{Diast} is 22 mmHg s/ml, and R_{Syst} is 45 mmHg s/ml).

The hydraulic compliance (C_{Filter}) was then dimensioned combining equations (45), (46), (47) and (48). The value of the compliance was a function of the flow rate and of the inner diameter of the pump tube (Figure 4.26 B). For instance, considering a mean flow rate of 210 ml/min, and an inner pump tubing diameter of 3.2 mm, the resulting compliance value is 0.008 ml/min (Figure 4.26 C).

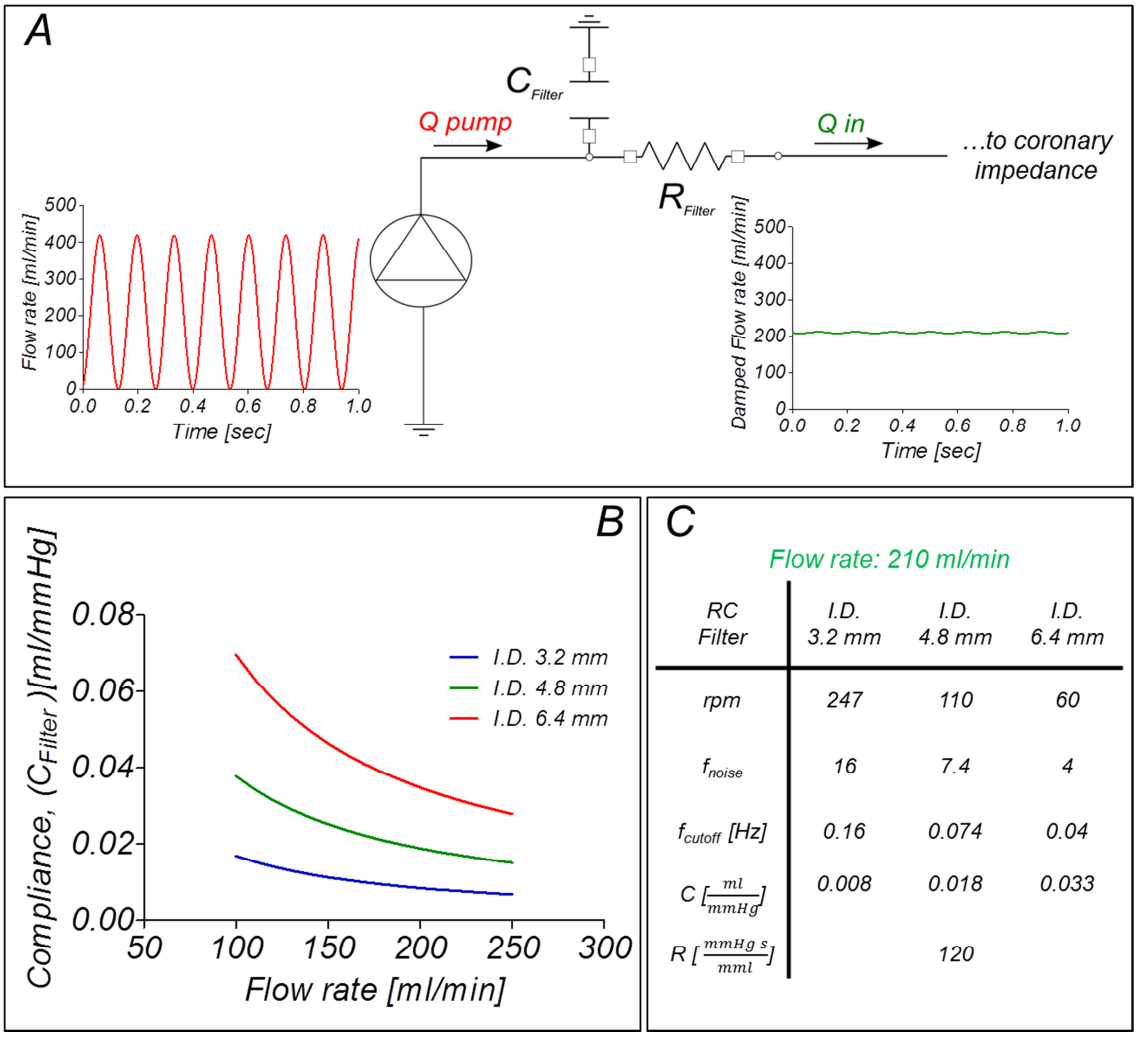

RC Filter	I.D. 3.2 mm	I.D. 4.8 mm	I.D. 6.4 mm
rpm	247	110	60
f_{noise}	16	7.4	4
f_{cutoff} [Hz]	0.16	0.074	0.04
$C\ [\frac{ml}{mmHg}]$	0.008	0.018	0.033
$R\ [\frac{mmHg\ s}{ml}]$		120	

Figure 4.26. *(A) Schematic of the RC filter designed for damping the pump pulsations. (B) Compliance/flow rate relationship parameterized for different pump tubes. C_{Filter} and R_{Filter} are dimensioned in order to obtain a cutoff frequecy of the filter equal to 0.01 of the noise frequency. (C) Results of the dimensioning steps for Q = 210 ml/min and for different inner diameters (I.D.) of the pump tubes.*

Design and manufacturing

The filter resistance was realized with four silicone tubes (inner diameter 0.6 mm, Platinum Cured Silicone, Cole Parmer, Vernon Hills, IL) in parallel embedded within a biocompatible silicone mold (*paragraph 4.3.2.1*). The filter compliance was realized with a Windkessel model (*paragraph 4.3.2.2*). In this case, the P_e was set equal to 1180 mmHg, P_0 equal to 760 mmHg and C equal to 0.008 ml/mmHg. The resulting value of V_0 was 20.5 ml. Figure 4.27 A shows the volume/pressure relationship of the filter compliance. A membrane pressure duomo was used for the filter compliance. Figure 4.27 B exhibits the realized RC filter.

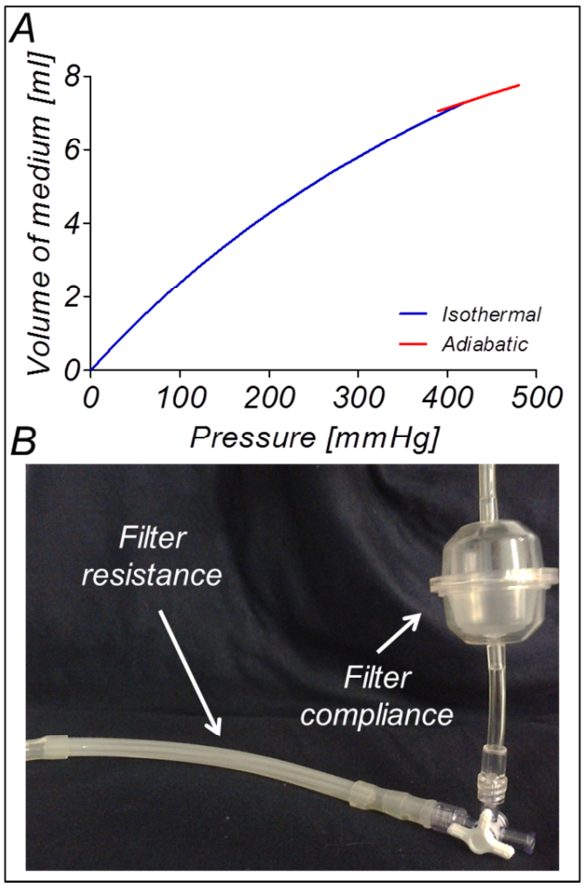

***Figure 4.27**. (A) Volume/pressure relationship of the filter compliance. (B) A membrane pressure duomo and 4 tubes in parallel are used for manufacturing the RC filter.*

4.4 Overview of the coronary pulse duplicator integrated with the EVCS

In figure 4.28 (A and B) the prototype of the overall coronary pulse duplicator is reported. The adopted solution allows to obtain a compact system with low priming volume. In fact the priming volume of the overall system is less than 90 ml. The hydraulic circuit consists of silicone tubing with inner diameter of 3.2 mm and thickness of 0.8 mm

(Platinum Cured, Cole Parmer, IL, USA), and PP-based pump tubing (PharMed BPT®, Carlo Erba Reagenti, Milano, Italy). PP luer connectors (Cole Parmer, Cole Parmer, IL, USA) are used to guarantee leak-free connections, and facilitate circuit assembly (Figure 4.8 B).

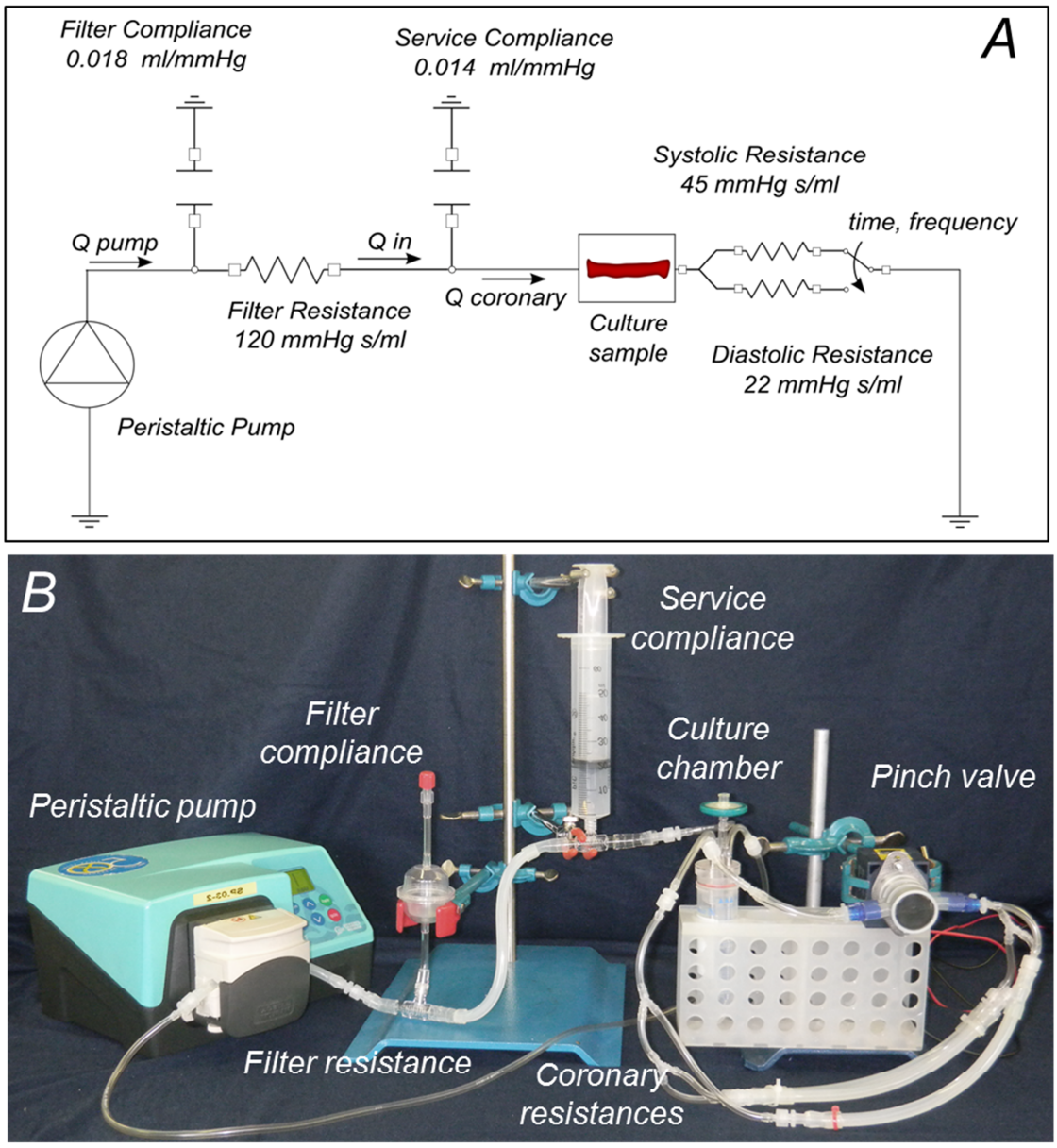

***Figure 4.28**. Scheme (A) and photograph (B) of the coronary pulse duplicator system integrated with the EVCS culture chamber.*

In addition, an upgraded version of the chamber was designed and manufactured for a better integration with the coronary pulse duplicator. In particular, the inner diameter of

the inlet and outlet (ports a, c, d and e) connections was increased up to 3.7 mm in order to minimize the head losses. Figure 4.29 shows the CAD model of the optimized culture chamber.

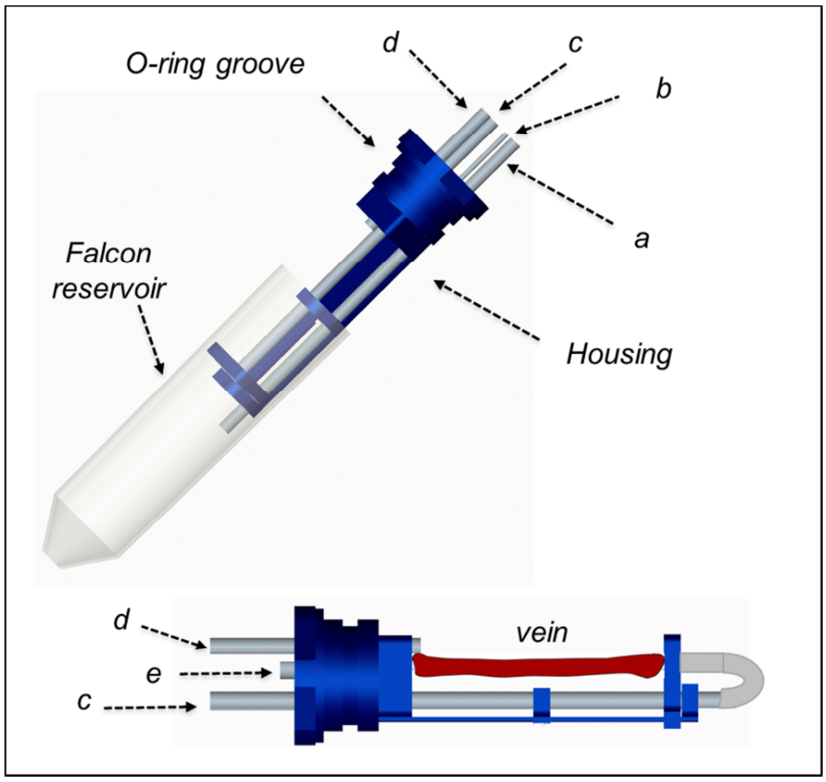

***Figure 4.29**. A) 3D CAD model of the SV culture chamber. The chamber consists of the SV housing inserted into a 50-ml falcon tube; a and e are the ports for the vessel connection sites; c and d are the ports for connecting the chamber to the hydraulic circuit; b is the port for HEPA filter.*

4.4.1 Functional experiments for testing the performance of the pulse duplicator

Preliminary experiments were performed in order to analyze the flow and pressure traces. A silicone tube was used as SV substitute. A transit-time ultrasound flow meter (Transonic System Inc., NJ, USA) equipped with a ¼" probe was used for acquiring the flow rate signal, while a pressure transducer Press-S-000 (PendoTECH, NJ, USA) was adopted for measuring the coronary pressure signal. Both sensors were connected to a PC equipped with a I/O board (NIDAQCard-6036E, National Instruments Corp.), and flow rate and pressure were acquired (60 s, sample frequency of 200 Hz) via a customized LabView software (National Instruments Corp., TX, USA). Two experiments were conducted. In a first set of experiments, the coronary pulse duplicator was tested without

the culture chamber and without the SV silicone substitute (Q_{pump} = 210 ml/min, cardiac frequency of 1 Hz, and diastolic time equal to 0.63 s*)*; while in a second set of experiments, the culture chamber was introduced (Q_{pump} = 152 ml/min, cardiac frequency 1 Hz, and diastolic time equal to 0.63 s*).*

The flow signal was measured on the inlet of the coronary impedance or of the culture chamber, while the pressure signal was acquired near the service impedance. The acquired flow rate signal was post-processed for noise filtering using a Butterworth pass band filter with cutoff frequency of 10 Hz plus an averaging operation on 30 cycles, while for the pressure signal a 30-cycle averaging was sufficient.

Figure 4.30 summarizes the results of the functional experiments. Figure 4.30 A shows the results of the experiments carried out without the culture chamber and the graft substitute. The graphs show that the measured flow rate and pressure are comparable to those expected obtained by numerical simulations. Briefly, the mean coronary blood flow is 210 ml/min, and the flow is lower during systolic phases and higher during diastole. The peak flow rate during diastole is 2-3-fold the peak during the systolic phase. Finally, as expected, coronary pressure and flow rate waveforms are in counter-phase.

Once integrated the culture chamber and the SV graft substitute, it was necessary to reduce the mean flow rate generated by the peristaltic pump down to 150 ml/min and to correct the value of the service compliance (0.008 ml/mmHg). These adjustments were necessary to counterbalance an increase of the total hydraulic resistance (figure 4.30 B). The new working conditions caused a reduction of the mean value of the coronary flow rate, while maintaining the correct ratio between the diastolic and systolic peaks. Moreover, the slope of the systolic/diastolic ramp was less steep than the one without the culture chamber. This was due to the inductive contribution of the inlet and outlet accesses of the culture system. Regarding the pressure tracing, no relevant differences were detected between the measured and expected waveforms.

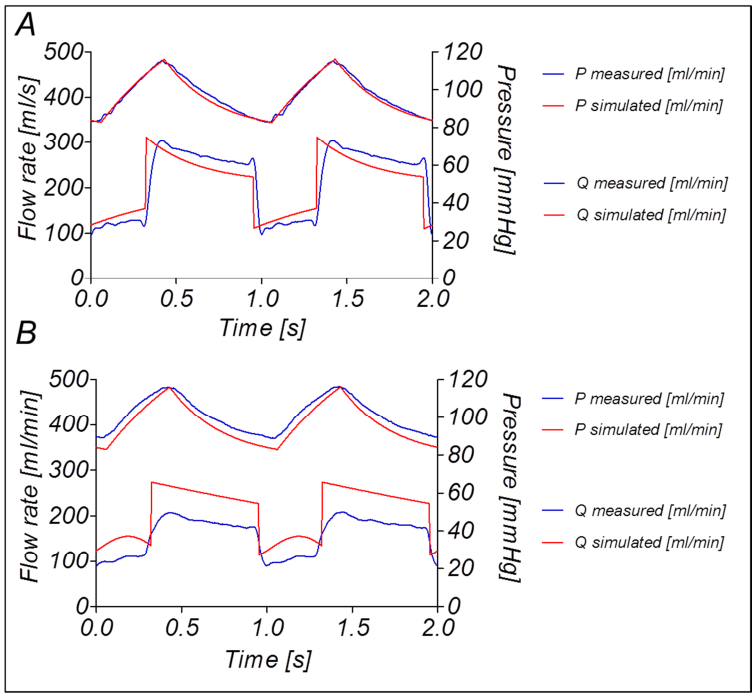

Figure 4.30. *Flow rate and pressure tracings. (A) Results of the experiments without the culture chamber and the graft substitute, and (B) with the culture chamber and with a silicone tube used as SV graft subistitute integrated into the coronary pulse duplicator.*

4.5 Conclusions

In this chapter, the development of a novel bioreactor platform, characterized by full mechanical/environmental bio-mimesis, was presented. Novel biomimetic features were included into the existing culture platform.

First of all, a new device (the DC-EVCS), allowing the separation between inner and outer vessel stimulation circuits, was designed and preliminary tested with human SV samples. The upgraded bioreactor was manufactured using *in-house* technologies, and proved to be a functional, versatile, and easy to use culture system.

Through the integration with the de-oxygenator module, different intra-luminal and extra-adventitial hematochemical conditions could be reproduced. The immediate next step consists of using the DC-EVCS, provided with the de-oxygenator module, for investigating the role of hypoxia in vein graft disease. A specific experimental campaign aimed at evaluating the combined effects induced by the mechanical stimulus (only pressure) and by different level of oxygen partial pressure will be carried out on human SVs samples. During these experiments the effects of different environmental effects will be explored, where luminal and adventitial conditions in terms of oxygen partial pressure will be reproduced for the arterial-like (extra-luminal pO_2 set at 5% and intra-luminal pO_2 at 21%) and venous-like conditions (both set at 5%). To assess the biological effects of trans-wall oxygen gradients, the tissues will be processed for histology. After conventional sections staining, the tissues will be analyzed by immunohistochemistry and immunofluorescence. In particular, the expression of oxygen-regulated factors (e.g. HIF-1alpha, VEGF, SDF-1) will be investigated in the vessel wall. Specific attention will be paid in the assessment of the so called adventitial neo-vascularization, a phenomenon reported to occur in consequence of the sudden adventitia hypoxia, due to the loss of blood supply in the vasa vasorum (McGeachie *et al.,* 1981) and shown to contribute to vessel restenosis (Khurana *et al.*, 2004; Tanaka *et al.,* 2011). Further on-going experiments are investigating cell homing, by seeding CellTracker Orange (CellTracker™Orange CMRA, Invitrogen, UK) labeled monocytes within the luminal region of the vessel.

The DC-EVCS will be also used to perform pharmacological conditioning treatments of the SV grafts before implantation into the patients. This strategy has been already attempted in existing gene therapy trials (Robertson *et al.,* 2012). The human SV segments

will be conditioned in the presence of drugs interfering with the molecular progression of VGD, such as specific siRNAs, antago-Mirs, or pharmacological agents impacting on the global epigenetic makeup.

From a technical point of view, the DC-EVCS is prone to improvements and refinements, as regards the addition of sensors to monitor the culture conditions, *e.g.* pH or glucose content within the culture medium. A significant improvement of the de-oxygenation system could be the integration in the M/C system of pO_2 and gas flow meter sensors, for monitoring and controlling the gas side of the de-oxygenator module via a feedback signal to the software. In this way, it will be possible to counterbalance the potential causes for oxygen transfer, and obtain the desired oxygen concentration at the outlet of the de-oxygenator module.

As a parallel line of development, the task of including full biomechanical control of CABG-like pressure and flow was attempted with the integration of the coronary artery pulse duplicator circuit (the CPD-EVCS). The aim of reproducing a fully biomimetic hydrodynamic mechanical stimuli involved in CABG arterialization, *i.e.* pulsatile wall stretch and wall shear stresses applied synchronously and with the correct phasing, was achieved. The CPD-EVCS was manufactured using *in house* technologies, and bench tests proved the system to be water-tight in operating conditions.

A further improvement consists in the integration of the oxygenator in order to maintain the correct level of oxygen ensuring SV viability. A possible solution is shown in figure 4.31.

The immediate next step consists of an extensively functional validation campaign of the device using human SV samples. Sterilizability and sterility maintenance over time will be followed by preliminary SV conditioning campaign. The midterm next step will be a pulsatile stimulation of SV grafts, in order to study the combined effect of pressure and shear stress on the remodeling of the SV after CAGB surgery. An extensive experimental campaign will be carried out on human SV samples (at least 12 samples per group), where the SVs will be stimulated in a fully realistic coronary–like environment within the CPD-EVCS. Additional SV samples will be stimulated in venous-like conditions (low flow rate perfusion) for comparison and SV fresh samples will be used as control. The oxygen partial pressure conditions will be set properly. Histological, immunohistochemical and

confocal analyses to assess changes occurring at molecular and cellular level will be performed. In this respect it will be interesting to compare the results of the morphological/structural analysis of the vessels conditioned in the bioreactor platforms and assess quantitatively the results of cell proliferation, extracellular matrix remodeling enzymes (MMPs), molecular targets such as mRNAs and miRNAs recently engaged in the vein pro-pathologic programming and specific rearrangement of the vessel epigenetic makeup (McDonald *et al.*, 2013).

The final goal is to produce a complete biomimetic conditioning platform integrating the developed systems in order to accurately reproduce an *ex vivo* model of CABG condition for studying the pathogenesis of the vein graft disease.

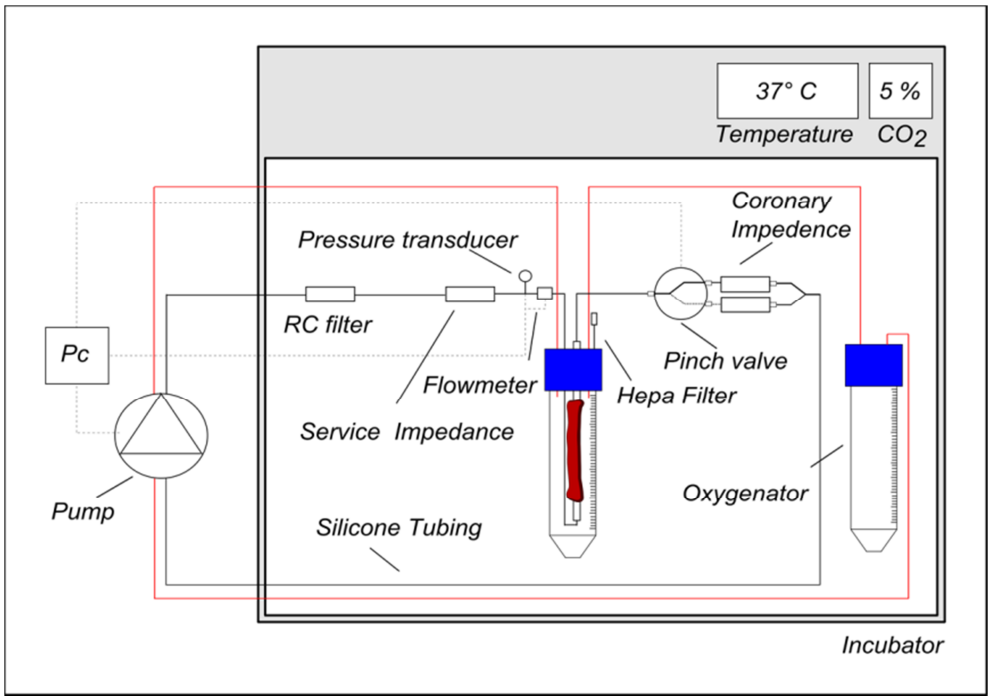

***Figure 4.31**. Schematic of the EVCS coupled with the coronary pulse duplicato and the oxygenator module. The thick-black lines represent the hydraulic circuit, the thick-red lines represent the hydraulic circuit connected the chamaber to the oxygenator module; thin-dot lines represent the monitoring and control (M/C) signals.*

Conclusive remarks

In the present research project, the use of a bioengineering approach to induce arterialization in cultured human vessels provided a valuable tool for studying the cellular and molecular pathways activated by exposure of the human saphenous vein (SV) to arterial-like conditions. The adopted strategy allowed to investigate *ex vivo* the effects of altered mechanical load experienced by the human SV after coronary artery by-pass grafting (CABG). In particular, CABG-like pressure conditioning was performed as first step of this investigation.

The design of a novel *ex vivo* vein culture system capable to replicate the altered biomechanical stimuli pattern experienced by SV after CABG surgery was addressed, using computer-aided engineering and bioengineering modelling tools. The design work was organised in three consecutive steps: it started from the development of a first step-version integrating all the requirements related to laboratory use (ease of use, GMP and GLP-compatibility, and low priming volume) with strain-only mechanical stimulus (the EVCS, *Chapter 2*), followed by the integration of biochemical stimuli (the DC-EVCS, *Chapter 4*), to end up with a fully coronary-mimicking flow culture platform (the CPD-EVCS integrated with a coronary pulse duplicator system, *Chapter 4*).

The EVCS was able to replicate the pulsatile pressure pattern experienced by SV after grafting (*i.e.*, luminal pressure: 80-120 mmHg). A number of dedicated architectural solutions allowed several simplifications to be implemented in the fluidic layout, control system and related equipment. The obtained EVCS is a user-friendly and cost-effective device with respect to most of the state-of-the-art solutions, which are based on the adaptation of cumbersome mechanical work-bench simulators. Functional tests were performed using human SV samples, in order to validate the robustness and the reliability over time of the control system, and to verify the sterility maintenance. The outcomes of these tests indicated that a good reliability of the control system was achieved, and that the maintenance of a sterile environment provided by the EVCS made it suitable for long term stimulation experiments.

Thence, novel biomimetic features were introduced into the existing device. A double-compartment culture chamber equipped with a deoxygenating circuit was dimensioned and manufactured for testing different luminal and extra-adventitial oxygen concentrations. The upgraded bioreactor was manufactured using *in-house* technologies, and proved to be a functional, versatile, and easy to use culture system. Particular attention was paid to design a compact de-oxygenator loop. Functional tests were performed for characterizing the de-oxygenator loop. The obtained results demonstrated that the de-oxygenator module is a usable alternative to unwieldy and expensive O_2-controlled cell culture incubators.

The application of a fully coronary-mimicking flow through the vessel, hence the pulsatile shear stress stimulus deriving from the arterial transposition, was finally replicated by designing a simple coronary-artery pulse duplicator, conceived for tissue engineering applications. In addition, compactness allowed abating the overall priming volume to 90 ml, substantially lower than the 5000 ml reported by Voisard and colleagues (Voisard *et al.,* 2010). Preliminary functional tests revealed a good fitting of simulated and measured tracings (pressure and flow rate), and the capability of the designed coronary pulse duplicator of mimicking the complexity of the coronary hemodynamic environment with a discrete fidelity in comparison with the state-of-the arte pulse duplicator (Iwasaki *et al.,* 2008; Narita *et al.,* 2004; Punchard *et al.,* 2007). An extensive functional validation campaign of the device using human SV samples and comprising sterilizability and sterility maintenance over time represents the immediate next step of this project line. The final goal will be a pulsatile stimulation of SV grafts, in order to study the combined effect of pressure and shear stress on the remodeling of the SV after CAGB surgery.

An arterialization campaign was also extensively conducted using the strain-only version of the EVCS. Human surplus SV segments were subjected to venous perfusion (3 ml/min steady flow), or CABG-like pressure (80-120 mmHg) conditioning for a period of 7 days, and native SV segments served as control. After 7-day CABG-like pressure stimulation, the main findings were: *i)* distension and reorganization of the vessel wall components; *ii*) partial endothelial denudation, *iii*) smooth muscle cells rearrangement; *iv*) disarrangement of the *vasa vasorum*; *v)* decrease of SVs wall thickness, enlargement of the

SVs luminal perimeter, resulting in preservation of the mass of the vessel wall; *vi)* decrease of the cell density; *vii)* increased proliferation rate; *vii)* increased up-regulation of MMP-2 and basal level of TIMP-1 expression and *ix*) mechano-epigenetic mechanism involved in *pro*-pathologic commitment of SV-resident cells, particularly in cells located in the adventitia with SMCs progenitor characteristics.

From a technical point of view, these results suggested that the EVCS is a suitable system for elucidating the mechanisms involved in the SV graft disease, within a controlled and reproducible biomechanical environment. In fact, by providing a comprehensive level of monitoring and control over the biomechanical environmental, the *ex vivo* model provided the technological means to perform controlled arterialization studies aimed to understand which specific biological, chemical or physical parameters were involved in the SV remodeling.

Concerning the mechano-biology, our findings demonstrated that the CABG-like pressure had an important role in the early events associated with the remodeling of the SV wall. In this work, experiments of 7 days were carried out on purpose. In fact the purpose of the investigation aimed at studying the very early events induced by SV arterial-like pressure stimulation, to come up with a consistent model system to be used in molecular dissection of the initial events predisposing the vessels to develop neointima. Furthermore, literature data indicate that vessel mechanical damage occurring as a consequence of the arterialization is an immediate relevant cause for later restenosis.

At this stage of the project, studies are currently performed to investigate the establishment of cellular and molecular *pro*-pathologic pathways involved in the SV graft disease.

The evolution of the *ex vivo* model of vein arterialization from a simple pressure-driven vessel straining system to a platform, which allows for vessel pharmacologic treatment under dynamic conditioning with/without application of arterial-like flow, will finally make possible to test targeting strategies against the selected effectors. The discovery of molecular targets (such as, *miRNAs*, and epigenetic traits) regulated by biomechanical/biochemical stimuli in the SV will produce an unique opportunity for devising novel translational protocols to reduce the consequences of intima hyperplasia. In this scenario, the customization of the conditioning platform to proceed with a tight control

of arterialization process will be instrumental to achieve dynamic conditioning of the vein segments in the presence of drugs, which may interfere with the molecular progression of the pathology. Possible strategies will include, for example, the use of *antagoMIR* biotechnologies to interfere with up-regulation of transcripts and *miRNAs* engaged in adverse vein remodelling.

In conclusion, the present doctoral project laid the basis for a potential clinical translation of graft preconditioning and pharmacologic treatments aimed at reducing the clinical impact of vein graft disease in patients undergoing CABG implantation. In this scenario, the developed *ex vivo* vessel culture system will be the advanced, safe, strictly controlled and reliable bioengineering tool that will permit autologous graft treatments preceding CABG surgery.

Bibliography

Ahmed SR, Johansson BL, Karlsson MG, Souza DSR, Dashwood MR, Loesch A. 2004, Human saphenous vein and coronary bypass surgery: ultrastructural aspects of conventional and "no-touch" vein graft preparations, *Histology and histopathology,* **19**: 421-33.

Amiel GE, Komura M, Shapira O, Yoo JJ, Yazdani S, Berry J, Kaushal S, Bischoff J, Atala A, Soker S. 2006, Engineering of blood vessels from acellular collagen matrices coated with human endothelial cells, *Tissue Engineering,* **12**: 2355-65.

Anwar MA, Shalhoub J, Lim CS, Gohel MS, Davies AH. 2012, The effect of pressure-induced mechanical stretch on vascular wall differential gene expression, *J Vasc Res,* **49**: 463-78.

Arrigoni C, Chitto A, Mantero S, Remuzzi A. 2008, Rotating versus perfusion bioreactor for the culture of engineered vascular constructs based on hyaluronic acid, *Biotechnology and Bioengineering,* **100**: 988-997.

Auger FA, L'Heureux N, Germain L; 1997. Production of contractile smooth muscle; **US5618718**.

Bader A; 2012. Method for producing a bio-artificial transplant; **US20120009677A1**.

Bader A, Macchiarini P. 2010, Moving towards in situ tracheal regeneration: the bionic tissue engineered transplantation approach, *Journal of cellular and molecular medicine,* **14**: 1877-89.

Badylak S, Kokini K, Tullius B, Simmons-Byrd A, Morff R. 2002, Morphologic study of small intestinal submucosa as a body wall repair device, *Journal of Surgical Research,* **103**: 190-202.

Badylak SF, Freytes DO, Gilbert TW. 2009, Extracellular matrix as a biological scaffold material: Structure and function, *Acta Biomaterialia,* **5**: 1-13.

Banes AJ, Wang J, Qi J, Kheradpir K; 2009. Bioreactor for development of blood vessels; **US20090123993A1**.

Barron V, Lyons E, Stenson-Cox C, McHugh PE, Pandit A. 2003, Bioreactors for cardiovascular cell and tissue growth: A review, *Annals of Biomedical Engineering,* **31**: 1017-1030.

Bell E; 1985. Fabrication of living blood vessels and glandular tissues; **US4546500**.

Berard X, Deglise S, Alonso F, Saucy F, Meda P, Bordenave L, Corpataux JM, Haefliger JA. 2013, Role of hemodynamic forces in the ex vivo arterialization of human saphenous veins, *J Vasc Surg,* **57**: 1371-82.

Berceli SA, Jiang Z, Klingman NV, Schultz GS, Keith Ozaki C. 2006, Early Differential MMP-2 and -9 Dynamics During Flow-Induced Arterial and Vein Graft Adaptations, *Journal of Surgical Research*, **134**: 327-334.

Berceli SA, Showalter DP, Sheppeck RA, Mandarino WA, Borovetz HS. 1990, Biomechanics of the venous wall under simulated arterial conditions, *Journal of Biomechanics*, **23**: 985-9.

Berceli SA, Tran-Son-Tay R, Garbey M, Jiang Z. 2009, Hemodynamically driven vein graft remodeling: a systems biology approach, *Vascular*, **17 Suppl 1**: S2-9.

Berger SL. 2007, The complex language of chromatin regulation during transcription, *Nature*, **447**: 407-12.

Bilodeau K, Couet F, Boccafoschi F, Mantovani D. 2005, Design of a perfusion bioreactor specific to the regeneration of vascular tissues under mechanical stresses, *Artif Organs*, **29**: 906-12.

Bischoff J, Kaushal S, Mayer J, Perry TE; 2004. Tissue-engineering vascular structures; **US20040044403**.

Boccafoschi F, Bosetti M, Mosca C, Mantovani D, Cannas M. 2012, The role of shear stress on mechanically stimulated engineered vascular substitutes: influence on mechanical and biological properties, *Journal of Tissue Engineering and Regenerative Medicine*, **6**: 60-67.

Bouten CV, Dankers PY, Driessen-Mol A, Pedron S, Brizard AM, Baaijens FP. 2011, Substrates for cardiovascular tissue engineering, *Adv Drug Deliv Rev*, **63**: 221-41.

Brendel K, Duhamel RC; 1989. Body implants of extracellular matrix and means and methods of making and using such implants; **US4801299**.

Brown MA, Zhang L, Levering VW, Wu J-H, Satterwhite LL, Brian L, Freedman NJ, Truskey GA. 2010, Human umbilical cord blood-derived endothelial cells reendothelialize vein grafts and prevent thrombosis, *Arteriosclerosis, Thrombosis, and Vascular Biology*, **30**: 2150-5.

Campagnolo P, Cesselli D, Al Haj Zen A, Beltrami AP, Krankel N, Katare R, Angelini G, Emanueli C, Madeddu P. 2010, Human adult vena saphena contains perivascular progenitor cells endowed with clonogenic and proangiogenic potential, *Circulation*, **121**: 1735-45.

Campbell GR, Campbell JH. 2007, Development of tissue engineered vascular grafts, *Curr Pharm Biotechnol*, **8**: 43-50.

Carrel A, Lindbergh CA. 1935, The Culture of Whole Organs, *Science*, **81**: 621-3.

Chen Y, Wong MM, Campagnolo P, Simpson R, Winkler B, Margariti A, Hu Y, Xu Q. 2013, Adventitial stem cells in vein grafts display multilineage potential that contributes to neointimal formation, *Arterioscler Thromb Vasc Biol*, **33**: 1844-51.

Cho SW, Lim SH, Kim IK, Hong YS, Kim SS, Yoo KJ, Park HY, Jang Y, Chang BC, Choi CY and others. 2005, Small-diameter blood vessels engineered with bone marrow-derived cells, *Ann Surg*, **241**: 506-15.

Clerin V, Gusic R, Gooch K; 2010. Ex Vivo Remodeling of Excised Blood Vessels for Vascular Grafts; **US20100331964A1**.

Clerin V, Gusic RJ, O'Brien J, Kirshbom PM, Myung RJ, Gaynor JW, Gooch KJ. 2002, Mechanical environment, donor age, and presence of endothelium interact to modulate porcine artery viability ex vivo, *Ann Biomed Eng*, **30**: 1117-27.

Clerin V, Nichol JW, Petko M, Myung RJ, Gaynor JW, Gooch KJ. 2003, Tissue engineering of arteries by directed remodeling of intact arterial segments, *Tissue Eng*, **9**: 461-72.

Costantino ML, Bagnoli P, Dini G, Fiore GB, Soncini M, Corno C, Acocella F, Colombi R. 2004a, A numerical and experimental study of compliance and collapsibility of preterm lamb tracheae, *Journal of Biomechanics*, **37**: 1837-47.

Costantino ML, Bagnoli P, Dini G, Fiore GB, Soncini M, Corno C, Acocella F, Colombi R. 2004b, Pressure drop vs flow relationship in isolated preterm lamb tracheae, *Journal of applied biomaterials & biomechanics : JABB*, **2**: 177-82.

Crapo PM, Gilbert TW, Badylak SF. 2011, An overview of tissue and whole organ decellularization processes, *Biomaterials*, **32**: 3233-3243.

Dahan N, Zarbiv G, Sarig U, Karram T, Hoffman A, Machluf M. 2012, Porcine Small Diameter Arterial Extracellular Matrix Supports Endothelium Formation and Media Remodeling Forming a Promising Vascular Engineered Biograft, *Tissue Engineering Part A*, **18**: 411-422.

Dancu M; 2011. Method of conditioning a hybrid synthetic tubular structure to yield a functional human hybrid coronary bypass graft; **US7968329B2**.

Dashwood MR, Loesch A. 2009, The saphenous vein as a bypass conduit: the potential role of vascular nerves in graft performance, *Curr Vasc Pharmacol*, **7**: 47-57.

Dashwood MR, Savage K, Dooley A, Shi-Wen X, Abraham DJ, Souza DSR. 2005, Effect of vein graft harvesting on endothelial nitric oxide synthase and nitric oxide production, *The Annals of Thoracic Surgery*, **80**: 939-44.

Dashwood MR, Tsui JC. 2013, 'No-touch' saphenous vein harvesting improves graft performance in patients undergoing coronary artery bypass surgery: A journey from bedside to bench, *Vascul Pharmacol*, **58**: 240-50.

de Waard V, Arkenbout EK, Vos M, Mocking AI, Niessen HW, Stooker W, de Mol BA, Quax PH, Bakker EN, VanBavel E and others. 2006, TR3 nuclear orphan receptor prevents cyclic stretch-induced proliferation of venous smooth muscle cells, *Am J Pathol*, **168**: 2027-35.

Dermenoudis S, Missirlis YF. 2010, Bioreactors in Tissue Engineering, *Advanced Engineering Materials*, **12**: B592-B608.

Dummler S, Eichhorn S, Tesche C, Schreiber U, Voss B, Deutsch M-A, Hauner H, Lahm H, Lange R, Krane M. 2011, Pulsatile ex vivo perfusion of human saphenous vein grafts under controlled pressure conditions increases MMP-2 expression, *BioMedical Engineering OnLine*, **10**: 62.

Dunkelman N, Peterson AE, Landeen LK, Zeltinger J; 1998. Apparatus and method for sterilizing, seeding, culturing, storing, shipping and testing tissue, synthetic or native, vascular grafts; **US005792603A**.

Dunkern TR, Paulitschke M, Meyer R, Buttemeyer R, Hetzer R, Burmester G, Sittinger M. 1999, A novel perfusion system for the endothelialisation of PTFE grafts under defined flow, *European Journal of Vascular and Endovascular Surgery*, **18**: 105-110.

Elizondo DR, Campbell TD, Totten RP; 1999. Methods and apparatus for processing and shipping cardiovascular products, within sterile and aseptic environment; **US005916800A**.

Ergun S, Tilki D, Klein D. 2011, Vascular wall as a reservoir for different types of stem and progenitor cells, *Antioxidants & redox signaling*, **15**: 981-95.

Fan Y, Zou C, Li J, Huang X, Gong X; 2009. Perfusion type vascular tissue bioreactor with rotary and stretching functions; **US2009181448A1**.

Fomovsky GM, Thomopoulos S, Holmes JW. 2010, Contribution of extracellular matrix to the mechanical properties of the heart, *Journal of Molecular and Cellular Cardiology*, **48**: 490-496.

Frerich B; 2011. Perfusable Bioreactor for the Production and/or Cultivation of a Human or Animal Blood Vessel and/or a Human or Animal Tissue; **US20110014597A1**.

Galili U. 2005, The alpha-gal epitope and the anti-Gal antibody in xenotransplantation and in cancer immunotherapy, *Immunology and Cell Biology*, **83**: 674-686.

Gilbert TW, Sellaro TL, Badylak SF. 2006, Decellularization of tissues and organs, *Biomaterials*, **27**: 3675-3683.

Goldman S, Zadina K, Moritz T, Ovitt T, Sethi G, Copeland JG, Thottapurathu L, Krasnicka B, Ellis N, Anderson RJ and others. 2004, Long-term patency of saphenous vein and left internal mammary artery grafts after coronary artery bypass surgery: results from a Department of Veterans Affairs Cooperative Study, *J Am Coll Cardiol*, **44**: 2149-56.

Gong Z, Niklason LE. 2006, Blood vessels engineered from human cells, *Trends in cardiovascular medicine*, **16**: 153-6.

Griese DP, Ehsan A, Melo LG, Kong D, Zhang L, Mann MJ, Pratt RE, Mulligan RC, Dzau VJ. 2003, Isolation and transplantation of autologous circulating endothelial cells into denuded vessels and prosthetic grafts: implications for cell-based vascular therapy, *Circulation*, **108**: 2710-5.

Gusic RJ, Myung R, Petko M, Gaynor JW, Gooch KJ. 2005a, Shear stress and pressure modulate saphenous vein remodeling ex vivo, *Journal of Biomechanics,* **38**: 1760-1769.

Gusic RJ, Petko M, Myung R, Gaynor JW, Gooch KJ. 2005b, Mechanical properties of native and ex vivo remodeled porcine saphenous veins, *Journal of Biomechanics,* **38**: 1770-1779.

Hoenicka M, Wiedemann L, Puehler T, Hirt S, Birnbaum DE, Schmid C. 2010, Effects of Shear Forces and Pressure on Blood Vessel Function and Metabolism in a Perfusion Bioreactor, *Annals of Biomedical Engineering,* **38**: 3706-3723.

Hoerstrup SP. 2006, Functional Growth in Tissue-Engineered Living, Vascular Grafts: Follow-Up at 100 Weeks in a Large Animal Model, *Circulation,* **114**: I-159-I-166.

Hoerstrup SP, Zund G, Sodian R, Schnell AM, Grunenfelder J, Turina MI. 2001, Tissue engineering of small caliber vascular grafts, *Eur J Cardiothorac Surg,* **20**: 164-9.

Hoglund VJ, Dong XR, Majesky MW. 2010, Neointima formation: a local affair, *Arterioscler Thromb Vasc Biol,* **30**: 1877-9.

Hu Y, Mayr M, Metzler B, Erdel M, Davison F, Xu Q. 2002, Both donor and recipient origins of smooth muscle cells in vein graft atherosclerotic lesions, *Circulation Research,* **91**: e13-20.

Hu Y, Xu Q. 2002, New mouse model of vein bypass graft atherosclerosis, *Heart Lung Circ,* **11**: 182-8.

Hu Y, Zhang Z, Torsney E, Afzal AR, Davison F, Metzler B, Xu Q. 2004, Abundant progenitor cells in the adventitia contribute to atherosclerosis of vein grafts in ApoE-deficient mice, *The Journal of clinical investigation,* **113**: 1258-65.

Hwang M, Berceli SA, Garbey M, Kim NH, Tran-Son-Tay R. 2011, The dynamics of vein graft remodeling induced by hemodynamic forces: a mathematical model, *Biomechanics and Modeling in Mechanobiology*.

Iwasaki K, Kojima K, Kodama S, Paz AC, Chambers M, Umezu M, Vacanti CA. 2008, Bioengineered three-layered robust and elastic artery using hemodynamically-equivalent pulsatile bioreactor, *Circulation,* **118**: S52-S57.

Jiang Z, Wu L, Miller BL, Goldman DR, Fernandez CM, Abouhamze ZS, Ozaki CK, Berceli SA. 2004, A novel vein graft model: adaptation to differential flow environments, *Am J Physiol Heart Circ Physiol,* **286**: H240-5.

John LCH. 2009, Biomechanics of coronary artery and bypass graft disease: potential new approaches, *The Annals of Thoracic Surgery,* **87**: 331-8.

Jungebluth P, Bader A, Baiguera S, Moller S, Jaus M, Lim ML, Fried K, Kjartansdottir KR, Go T, Nave H and others. 2012, The concept of in vivo airway tissue engineering, *Biomaterials,* **33**: 4319-26.

Kaushal S, Amiel GE, Guleserian KJ, Shapira OM, Perry T, Sutherland FW, Rabkin E, Moran AM, Schoen FJ, Atala A and others. 2001, Functional small-diameter neovessels created using endothelial progenitor cells expanded ex vivo, *Nature medicine*, **7**: 1035-40.

Khurana R, Zhuang Z, Bhardwaj S, Murakami M, De Muinck E, Yla-Herttuala S, Ferrara N, Martin JF, Zachary I, Simons M. 2004, Angiogenesis-dependent and independent phases of intimal hyperplasia, *Circulation*, **110**: 2436-43.

Konig G, McAllister TN, Dusserre N, Garrido SA, Iyican C, Marini A, Fiorillo A, Avila H, Wystrychowski W, Zagalski K and others. 2009, Mechanical properties of completely autologous human tissue engineered blood vessels compared to human saphenous vein and mammary artery, *Biomaterials*, **30**: 1542-1550.

Kouzarides T. 2007, Chromatin modifications and their function, *Cell*, **128**: 693-705.

L'Heureux N, Dusserre N, Konig G, Victor B, Keire P, Wight TN, Chronos NA, Kyles AE, Gregory CR, Hoyt G and others. 2006, Human tissue-engineered blood vessels for adult arterial revascularization, *Nat Med*, **12**: 361-5.

L'Heureux N, Germain L, Labbe R, Auger FA. 1993, In vitro construction of a human blood vessel from cultured vascular cells: a morphologic study, *J Vasc Surg*, **17**: 499-509.

L'Heureux N, Paquet S, Labbe R, Germain L, Auger FA. 1998, A completely biological tissue-engineered human blood vessel, *Faseb Journal*, **12**: 47-56.

Lantz GC, Badylak SF, Hiles MC, Coffey AC, Geddes LA, Kokini K, Sandusky GE, Morff RJ. 1993, Small intestinal submucosa as a vascular graft: a review, *J Invest Surg*, **6**: 297-310.

Lemson MS, Tordoir JH, Daemen MJ, Kitslaar PJ. 2000, Intimal hyperplasia in vascular grafts, *Eur J Vasc Endovasc Surg*, **19**: 336-50.

Majesky MW, Dong XR, Hoglund V, Mahoney WM, Jr., Daum G. 2011, The adventitia: a dynamic interface containing resident progenitor cells, *Arteriosclerosis, Thrombosis, and Vascular Biology*, **31**: 1530-9.

Martin I, Wendt D, Heberer M. 2004, The role of bioreactors in tissue engineering, *Trends Biotechnol*, **22**: 80-86.

McAllister TN, l'Heureux N; 2002. Tissue engineered blood vessels and apparatus for their manufacture; **US20020188349A1**.

McCulloch AD, Harris AB, Sarraf CE, Eastwood M. 2004, New multi-cue bioreactor for tissue engineering of tubular cardiovascular samples under physiological conditions, *Tissue Eng*, **10**: 565-73.

McDonald RA, Hata A, MacLean MR, Morrell NW, Baker AH. 2012, MicroRNA and vascular remodelling in acute vascular injury and pulmonary vascular remodelling, *Cardiovascular Research*, **93**: 594-604.

McDonald RA, White KM, Wu J, Cooley BC, Robertson KE, Halliday CA, McClure JD, Francis S, Lu R, Kennedy S and others. 2013, miRNA-21 is dysregulated in response to vein grafting in multiple models and genetic ablation in mice attenuates neointima formation, *Eur Heart J,* **34**: 1636-43.

McFetridge PS; 2005. Decellularized grafts from umbilical cord vessels and process fro preparing and using same; **US20050203636A1**.

McGeachie J, Campbell P, Prendergast F. 1981, Vein to artery grafts. A quantitative study of revascularization by vasa vasorum and its relationship to intimal hyperplasia, *Ann Surg,* **194**: 100-7.

Meng X, Mavromatis K, Galis ZS. 1999, Mechanical Stretching of Human Saphenous Vein Grafts Induces Expression and Activation of Matrix-Degrading Enzymes Associated with Vascular Tissue Injury and Repair, *Experimental and Molecular Pathology*, **66**: 227-237.

Milnor WR. 1989. Hemodynamics. Baltimore: Williams & Wilkins.

Minetti GC, Colussi C, Adami R, Serra C, Mozzetta C, Parente V, Fortuni S, Straino S, Sampaolesi M, Di Padova M and others. 2006, Functional and morphological recovery of dystrophic muscles in mice treated with deacetylase inhibitors, *Nat Med,* **12**: 1147-50.

Mitra AK, Gangahar DM, Agrawal DK. 2006, Cellular, molecular and immunological mechanisms in the pathophysiology of vein graft intimal hyperplasia, *Immunology and Cell Biology*, **84**: 115-24.

Miyakawa AA, Dallan LAO, Lacchini S, Borin TF, Krieger JE. 2008, Human Saphenous Vein Organ Culture under Controlled Hemodynamic Conditions, *Clinics*, **63**: 683-688.

Montoya CV, McFetridge PS. 2009, Preparation of Ex Vivo-Based Biomaterials Using Convective Flow Decellularization, *Tissue Engineering Part C-Methods,* **15**: 191-200.

Morrow D, Scheller A, Birney YA, Sweeney C, Guha S, Cummins PM, Murphy R, Walls D, Redmond EM, Cahill PA. 2005, Notch-mediated CBF-1/RBP-J{kappa}-dependent regulation of human vascular smooth muscle cell phenotype in vitro, *American journal of physiology Cell physiology*, **289**: C1188-96.

Motwani JG, Topol EJ. 1998, Aortocoronary saphenous vein graft disease: pathogenesis, predisposition, and prevention, *Circulation,* **97**: 916-31.

Muto A, Model L, Ziegler K, Eghbalieh SDD, Dardik A. 2010, Mechanisms of Vein Graft Adaptation to the Arterial Circulation, *Circulation Journal,* **74**: 1501-1512.

Naito Y, Shinoka T, Duncan D, Hibino N, Solomon D, Cleary M, Rathore A, Fein C, Church S, Breuer C. 2011, Vascular tissue engineering: Towards the next generation vascular grafts, *Advanced Drug Delivery Reviews,* **63**: 312-323.

Narita Y, Hata K, Kagami H, Usui A, Ueda M, Ueda Y. 2004, Novel pulse duplicating bioreactor system for tissue-engineered vascular construct, *Tissue Eng,* **10**: 1224-33.

Nerem RM. 2000, Tissue engineering a blood vessel substitute: the role of biomechanics, *Yonsei Med J,* **41**: 735-9.

Niklason LE, Gao J, Abbott WM, Hirschi KK, Houser S, Marini R, Langer R. 1999, Functional arteries grown in vitro, *Science,* **284**: 489-493.

Niklason LE, Gao J, Langer RS; 2003. Tissue-engineered tubular construct having circumferentially oriented smooth muscle cells; **US6537567B1**.

Orr DE, Burg KJL. 2008, Design of a modular bioreactor to incorporate both perfusion flow and hydrostatic compression for tissue engineering applications, *Ann Biomed Eng,* **36**: 1228-1241.

Orton EC; 1993. Treated tissue for implantation and methods of treatment and use **US5192312**.

Ott HC, Clippinger B, Conrad C, Schuetz C, Pomerantseva I, Ikonomou L, Kotton D, Vacanti JP. 2010, Regeneration and orthotopic transplantation of a bioartificial lung, *Nature Medicine,* **16**: 927-U131.

Ott HC, Matthiesen TS, Goh SK, Black LD, Kren SM, Netoff TI, Taylor DA. 2008, Perfusion-decellularized matrix: using nature's platform to engineer a bioartificial heart, *Nature Medicine,* **14**: 213-221.

Owens CD. 2010, Adaptive changes in autogenous vein grafts for arterial reconstruction: clinical implications, *J Vasc Surg,* **51**: 736-46.

Parang P, Arora R. 2009, Coronary vein graft disease: pathogenesis and prevention, *Can J Cardiol,* **25**: 57-62.

Pellegata AF, Asnaghi MA, Zonta S, Zerbini G, Mantero S. 2012, A novel device for the automatic decellularization of biological tissues, *Int J Artif Organs,* **35**: 191-8.

Pennati G, Fiore GB, Lagana K, Fumero R. 2004, Mathematical modeling of fluid dynamics in pulsatile cardiopulmonary bypass, *Artif Organs,* **28**: 196-209.

Pesce M, Orlandi A, Iachininoto MG, Straino S, Torella AR, Rizzuti V, Pompilio G, Bonanno G, Scambia G, Capogrossi MC. 2003, Myoendothelial differentiation of human umbilical cord blood-derived stem cells in ischemic limb tissues, *Circ Res,* **93**: e51-62.

Piola M, Soncini M, Prandi F, Polvani G, Beniamino Fiore G, Pesce M. 2012, Tools and procedures for ex vivo vein arterialization, preconditioning and tissue engineering: a step forward to translation to combat the consequences of vascular graft remodeling, *Recent Pat Cardiovasc Drug Discov,* **7**: 186-95.

Porter KE, Nydahl S, Dunlop P, Varty K, Thrush AJ, London NJM. 1996, The development of an in vitro flow model of human saphenous vein graft intimal hyperplasia, *Cardiovascular Research,* **31**: 607-614.

Punchard MA, Stenson-Cox C, O'Cearbhaill ED, Lyons E, Gundy S, Murphy L, Pandit A, McHugh PE, Barron V. 2007, Endothelial cell response to biomechanical forces under simulated vascular loading conditions, *Journal of Biomechanics,* **40**: 3146-3154.

Qi YX, Qu MJ, Yan ZQ, Zhao D, Jiang XH, Shen BR, Jiang ZL. 2010, Cyclic strain modulates migration and proliferation of vascular smooth muscle cells via Rho-GDIalpha, Rac1, and p38 pathway, *Journal of cellular biochemistry,* **109**: 906-14.

Quint C, Kondo Y, Manson RJ, Lawson JH, Dardik A, Niklason LE. 2011, Decellularized tissue-engineered blood vessel as an arterial conduit, *Proceedings of the National Academy of Sciences of the United States of America,* **108**: 9214-9219.

Rey J, Probst H, Mazzolai L, Bosman FTB, Pusztaszeri M, Stergiopulos N, Ris HB, Hayoz D, Saucy F, Corpataux JM. 2004, Comparative assessment of intimal hyperplasia development after 14 days in two different experimental settings: Tissue culture versus ex vivo continuous perfusion of human saphenous vein, *Journal of Surgical Research,* **121**: 42-49.

Robb WL. 1968, Thin silicone membranes--their permeation properties and some applications, *Annals of the New York Academy of Sciences,* **146**: 119-37.

Robertson KE, McDonald RA, Oldroyd KG, Nicklin SA, Baker AH. 2012, Prevention of coronary in-stent restenosis and vein graft failure: does vascular gene therapy have a role?, *Pharmacol Ther,* **136**: 23-34.

Rueda F, Souza D, Lima Rde C, Menezes A, Johansson B, Dashwood M, The E, Gesteira M, Escobar M, Vasconcelos F. 2008, Novel no-touch technique of harvesting the saphenous vein for coronary artery bypass grafting, *Arq Bras Cardiol,* **90**: 356-62.

Sarkar S, Schmitz-Rixen T, Hamilton G, Seifalian AM. 2007, Achieving the ideal properties for vascular bypass grafts using a tissue engineered approach: a review, *Medical & Biological Engineering & Computing,* **45**: 327-336.

Sasaki N, Horinouchi H, Ushiyama A, Minamitani H. 2012, A new method for measuring the oxygen diffusion constant and oxygen consumption rate of arteriolar walls, *Keio J Med,* **61**: 57-65.

Saucy F, Probst H, Alonso F, Berard X, Deglise S, Dunoyer-Geindre S, Mazzolai L, Kruithof E, Haefliger JA, Corpataux JM. 2010, Ex vivo Pulsatile Perfusion of Human Saphenous Veins Induces Intimal Hyperplasia and Increased Levels of the Plasminogen Activator Inhibitor 1, *European Surgical Research,* **45**: 50-59.

Sauvage LR, Kaplan S; 1990. Method of making vascular prosthesis by perfusion; **US4911713**.

Schaner PJ, Martin ND, Tulenko TN, Shapiro IM, Tarola NA, Leichter RF, Carabasi RA, DiMuzio PJ. 2004, Decellularized vein as a potential scaffold for vascular tissue engineering, *Journal of Vascular Surgery,* **40**: 146-153.

Segal E, Shapira M, Regev A, Pe'er D, Botstein D, Koller D, Friedman N. 2003, Module networks: identifying regulatory modules and their condition-specific regulators from gene expression data, *Nature genetics*, **34**: 166-76.

Seifalian AM, Tiwari A, Hamilton G, Salacinski HJ. 2002, Improving the clinical patency of prosthetic vascular and coronary bypass grafts: the role of seeding and tissue engineering, *Artif Organs*, **26**: 307-20.

Seliktar D, Black RA, Vito RP, Nerem RM. 2000, Dynamic mechanical conditioning of collagen-gel blood vessel constructs induces remodeling in vitro, *Ann Biomed Eng*, **28**: 351-62.

Seliktar D, Nerem RM, Galis ZS. 2003, Mechanical strain-stimulated remodeling of tissue-engineered blood vessel constructs, *Tissue Engineering*, **9**: 657-66.

Severyn DA, Muluk SC, Vorp DA. 2004, The influence of hemodynamics and wall biomechanics on the thrombogenicity of vein segments perfused in vitro1, *Journal of Surgical Research*, **121**: 31-37.

Sharp MK, Dharmalingam RK. 1999, Development of a hydraulic model of the human systemic circulation, *ASAIO Journal*, **45**: 535-540.

Shi ZD, Tarbell JM. 2011, Fluid Flow Mechanotransduction in Vascular Smooth Muscle Cells and Fibroblasts, *Annals of Biomedical Engineering*, **39**: 1608-1619.

Shin'oka T, Imai Y, Ikada Y. 2001, Transplantation of a tissue-engineered pulmonary artery, *N Engl J Med*, **344**: 532-3.

Shin'oka T, Matsumura G, Hibino N, Naito Y, Watanabe M, Konuma T, Sakamoto T, Nagatsu M, Kurosawa H. 2005, Midterm clinical result of tissue-engineered vascular autografts seeded with autologous bone marrow cells, *The Journal of thoracic and cardiovascular surgery*, **129**: 1330-8.

Sodian R, Lemke T, Fritsche C, Hoerstrup SP, Fu P, Potapov EV, Hausmann H, Hetzer R. 2002, Tissue-engineering bioreactors: a new combined cell-seeding and perfusion system for vascular tissue engineering, *Tissue Eng*, **8**: 863-870.

Soma G, Kotturathu MC; 2009. Small diameter vascular graft from processed cadaver saphenous vein; **WO2009044407A1**.

Souza DS, Johansson B, Bojo L, Karlsson R, Geijer H, Filbey D, Bodin L, Arbeus M, Dashwood MR. 2006, Harvesting the saphenous vein with surrounding tissue for CABG provides long-term graft patency comparable to the left internal thoracic artery: results of a randomized longitudinal trial, *J Thorac Cardiovasc Surg*, **132**: 373-8.

Squillace D; 2010. Vascular graft sterilization and decellularization; **US7658706B2**.

Stigler R, Steger C, Schachner T, Holfeld J, Edlinger M, Grimm M, Semsroth S. 2012, The impact of distension pressure on acute endothelial cell loss and neointimal proliferation in saphenous vein grafts, *Eur J Cardiothorac Surg*, **42**: e74-9.

Stooker W, Gök M, Sipkema P, Niessen HWM, Baidoshvili A, Westerhof N, Jansen EK, Wildevuur CRH, Eijsman L. 2003, Pressure-diameter relationship in the human greater saphenous vein, *The Annals of Thoracic Surgery*, **76**: 1533-1538.

Surowiec SM, Conklin BS, Li JS, Lin PH, Weiss VJ, Lumsden AB, Chen CY. 2000, A new perfusion culture system used to study human vein, *Journal of Surgical Research*, **88**: 34-41.

Tanaka K, Nagata D, Hirata Y, Tabata Y, Nagai R, Sata M. 2011, Augmented angiogenesis in adventitia promotes growth of atherosclerotic plaque in apolipoprotein E-deficient mice, *Atherosclerosis*, **215**: 366-73.

Teebken OE, Puschmann C, Breitenbach I, Rohde B, Burgwitz K, Haverich A. 2009, Preclinical Development of Tissue-Engineered Vein Valves and Venous Substitutes using Re-Endothelialised Human Vein Matrix, *European Journal of Vascular and Endovascular Surgery*, **37**: 92-102.

Thomas A. 2003, Advances in vascular tissue engineering, *Cardiovascular Pathology*, **12**: 271-276.

Thomas AC. 2012, Animal models for studying vein graft failure and therapeutic interventions, *Current Opinion in Pharmacology*.

Thompson CA, Colon-Hernandez P, Pomerantseva I, MacNeil BD, Nasseri B, Vacanti JP, Oesterle SN. 2002, A novel pulsatile, laminar flow bioreactor for the development of tissue-engineered vascular structures, *Tissue Eng*, **8**: 1083-8.

Torsney E, Hu Y, Xu Q. 2005, Adventitial progenitor cells contribute to arteriosclerosis, *Trends in cardiovascular medicine*, **15**: 64-8.

Torsney E, Xu Q. 2011, Resident vascular progenitor cells, *Journal of molecular and cellular cardiology*, **50**: 304-11.

Tran-Son-Tay R, Hwang M, Garbey M, Jiang Z, Ozaki CK, Berceli SA. 2008, An Experiment-Based Model of Vein Graft Remodeling Induced by Shear Stress, *Annals of Biomedical Engineering*, **36**: 1083-1091.

Tranquillo RT, Ross J, Reyes M; 2007. Engineered blood vessels; **US20070128171**.

Tschoeke B, Flanagan TC, Cornelissen A, Koch S, Roehl A, Sriharwoko M, Sachweh JS, Gries T, Schmitz-Rode T, Jockenhoevel S. 2008, Development of a Composite Degradable/Nondegradable Tissue-engineered Vascular Graft, *Artificial Organs*, **32**: 800-809.

Tsui JC, Dashwood MR. 2002, Recent strategies to reduce vein graft occlusion: a need to limit the effect of vascular damage, *Eur J Vasc Endovasc Surg*, **23**: 202-8.

Uygun BE, Soto-Gutierrez A, Yagi H, Izamis ML, Guzzardi MA, Shulman C, Milwid J, Kobayashi N, Tilles A, Berthiaume F and others. 2010, Organ reengineering through

development of a transplantable recellularized liver graft using decellularized liver matrix, *Nature Medicine,* **16**: 814-U120.

Vilender K, Nickel T; 2008. Bioreactor with plurality of chambers for conditioning intravascular tissue engineered medical products; **US7348175B2**.

Villalona GA, Udelsman B, Duncan DR, McGillicuddy E, Sawh-Martinez RF, Hibino N, Painter C, Mirensky T, Erickson B, Shinoka T and others. 2010, Cell-seeding techniques in vascular tissue engineering, *Tissue Eng Part B Rev*, **16**: 341-50.

Vismara R, Soncini M, Talò G, Dainese L, Guarino A, Redaelli A, Fiore GB. 2009, A Bioreactor with Compliance Monitoring for Heart Valve Grafts, *Annals of Biomedical Engineering,* **38**: 100-108.

Voisard R, Ramiz E, Baur R, Gastrock-Balitsch I, Siebeneich H, Frank O, Hombach V, Hannekum A, Schumacher B. 2010, Pulsed perfusion in a venous human organ culture model with a Windkessel function (pulsed perfusion venous HOC-model), *Med Sci Monit,* **16**: 523-9.

Wallitt EJ, Jevon M, Hornick PI. 2007, Therapeutics of vein graft intimal hyperplasia: 100 years on, *Ann Thorac Surg*, **84**: 317-23.

Wang C, Cen L, Yin S, Liu Q, Liu W, Cao Y, Cui L. 2010, A small diameter elastic blood vessel wall prepared under pulsatile conditions from polyglycolic acid mesh and smooth muscle cells differentiated from adipose-derived stem cells, *Biomaterials,* **31**: 621-630.

Weinberg CB, Bell E. 1986, A blood vessel model constructed from collagen and cultured vascular cells, *Science,* **231**: 397-400.

Wiedemann D, Kocher A, Bonaros N, Semsroth S, Laufer G, Grimm M, Schachner T. 2012, Perivascular administration of drugs and genes as a means of reducing vein graft failure, *Current Opinion in Pharmacology,* **12**: 203-16.

Williams C, Wick TM. 2004, Perfusion bioreactor for small diameter tissue-engineered arteries, *Tissue Eng,* **10**: 930-41.

Wolfinbarger L; 2003. Bioreactor mediated recellularization of natural and tissue engineered vascular grafts; **US20030219417A1**.

Zhang L, Freedman NJ, Brian L, Peppel K. 2004, Graft-extrinsic cells predominate in vein graft arterialization, *Arteriosclerosis, Thrombosis, and Vascular Biology,* **24**: 470-6.

Zhu S, Malhotra A, Zhang L, Deng S, Zhang T, Freedman NJ, Storms R, Peppel K, Goldschmidt-Clermont PJ, Dong C. 2010, Human umbilical cord blood endothelial progenitor cells decrease vein graft neointimal hyperplasia in SCID mice, *Atherosclerosis,* **212**: 63-9.